UNIVERSITY OF SOUTHAMPTON

FACULTY OF PHYSICAL AND APPLIED SCIENCES

Optoelectronics Research Centre

Tantalum Pentoxide Waveguide Amplfier and Laser for Planar Lightwave Circuits

by

Ananth Subramanian

Thesis for the degree of Doctor of Philosophy

February 2011

UNIVERSITY OF SOUTHAMPTON

ABSTRACT

FACULTY OF PHYSICAL AND APPLIED SCIENCES
OPTOELECTRONICS RESEARCH CENTRE

Doctor of Philosophy

by Ananth Subramanian

A planar lightwave circuit (PLC) has been envisioned to provide a new generation of optical networks capable of delivering signal at high speed and bandwidth to the household. High index contrast (HIC) and optical gain in the same material system would substantially enhance integration of different optical devices in a small area and compensate for the losses in the system to realise low cost, dense multi-functional PLCs. This thesis investigates the use of tantala as a HIC material system for realising gain efficient Erbium doped waveguide amplifiers (EDWAs) and lasers to be used at 1.5 μm wavelength, towards realising dense multi-functional PLCs.

Slab waveguides were fabricated by magnetron sputter deposition under optimised conditions of a powder pressed, Er:Ta_2O_5 target onto an oxidized silicon substrate. Optimised sputtering process yielded a Er:Ta_2O_5 thin film with a refractive index of 2.105 @ 1550 nm and a maximum erbium lifetime of 2.3 ms. Single mode rib waveguides were designed and the fabricated using photolithography and argon ion beam milling. A maximum propagation loss of 0.65 $\pm$ 0.05 dB/cm at 1600 nm was measured, the peak erbium absorption and emission cross-section was determined to be 4.8 $\pm$ 0.2 $\times$ 10^{-21} cm^2 and 4.4 $\pm$ 0.2 $\times$ $10^{-21}cm^2$ respectively.

Numerical modeling of Er:Ta_2O_5 based EDWA predicted a maximum gain of 4 dB/cm at 200 mW pump power, in a 5.4 cm long waveguide with an erbium concentration of 5.4 $\times$ 10^{20} ions/cm^3. Gain measurements were performed on a 2.3 cm long rib waveguide with a erbium concentration of 2.7 $\times$ 10^{20} ions/cm^3, at a pump power of 200 mW, and a net optical gain of 2.25 dB/cm peaking at 1531.5 nm was measured in a 2 μm wide waveguide. The pump threshold with respect to the launched pump power was measured to be as low as 4.5 mW. The cavity was formed by affixing two mirrors at the end facets of the waveguides. Lasing was observed in a single longitudinal and transverse mode peaking between 1556 and 1560 nm. The lasing threshold of 14 mW with a slope efficiency of 0.3% was measured with respect to the launched power.

Finally, a feasibility study for inscribing sub-micron grating structures on the Er:Ta_2O_5 waveguides were carried out using interferometric ablation. Gratings inscribed with 23 mJ/cm^2 energy density and 1000 pulses yielded a maximum reflectivity of 11 dB for TE polarisation at 1505 nm. This feasibility study shows potential to realise integrated cavity line narrowed lasers and filters. Tantala has long been used for different photonic applications but gain at 1.5 μm is demonstrated for the first time. The results presented in the thesis demonstrate that tantala due to its HIC, net optical gain and other inherent properties that it possesses have the potential to realise low cost, compact PLCs for the short haul networks.

Contents

List of Figures

List of Tables

Declaration Of Authorship

I, Ananth Subramanian declare that the thesis entitled

"Tantalum Pentoxide Waveguide Amplfier and Laser for Planar Lightwave Circuits"

and the work presented in it are my own. I confirm that:

1. This work was done wholly or mainly while in candidature for a research degree at this University;
2. Where any part of this thesis has previously been submitted for a degree or any other qualification at this University or any other institution, this has been clearly stated;
3. Where I have consulted the published work of others, this is always clearly attributed;
4. Where I have quoted from the work of others, the source is always given. With the exception of such quotations, this thesis is entirely my own work;
5. I have acknowledged all main sources of help;
6. Where the thesis is based on work done by myself jointly with others, I have made clear exactly what was done by others and what I have contributed myself;
7. Either none of this work has been published before submission, or parts of this work have been published as [please see List of Publications]:

Signed: .....

Date: .....

Acknowledgements

I crossed the borders of my homeland India for the first time and reached ORC in 2006, and it has been a fulfilling and challenging time. It has been a journey and I have enjoyed every bit of it, no regrets. There are many people who made this work possible and I would like to thank every one of them.

I am deeply indebted to my supervisor, Prof. James S Wilkinson who has been my inspiration and without whose support and guidance this work would have not been possible. He helped me settle down nicely both in and outside ORC during my early days. He has always been very supportive and available for a chat, sometimes even during the weekends. I would never forget his advise "never rely on others for your work" which helped me in learning and enhancing my skills. He also helped me in establishing good collaborations that enabled me to go to places like Tromso and Crete. Thank you for driving me around Crete, buying me wonderful lunch and dinner, and all those drinks on various occasions. Finally, I would like to thank him for providing me with so many opportunities to help me become a better researcher.

I would then like to thank two people- Dr. Senthil G Murugan and Dr. Claudio J Oton, who have been my unofficial co-supervisors and helped me immensely in completing my PhD. I would like to thank Claudio for helping me with waveguide characterisation, erbium spectroscopy and numerical modeling of EDWA. I would like to thank him for spending many hours with me inside and outside the lab. Senthil has been my go-to man for any problem and his contribution in completing my PhD has been phenomenal. I would like to thank him for helping me solve issues with the fabrication in the cleanroom, experiments (especially the gain measurement) and lending any component I needed from his "secret storehouse". I would like to thank him for being always available even outside ORC for any other problems and for so many wonderful get togethers and food at his place.

I cannot imagine my PhD without thanking Neil Sessions and David Sager for their incredible support inside the cleanroom. I would like to thank them for enduring me all these years for obliging my requests time and again, and training me on different machines in the cleanroom that has helped me become a better researcher in the area of fabrication and process engineering. I would like to thank Dr Stavros Pissadakis for helping me inscribe gratings in the waveguides in Crete and for making my stay at Crete a memorable one. I would like to thank Prof. David P Shepherd for teaching me how to attach mirrors to the waveguide and for useful tips for achieving lasing. I would like to thank Prof. Michalis N Zervas for so many stimulating discussions on EDWA, gratings and lasers which helped me a lot in interpreting the results. I would also like to thank Dr. Olav H Gaute and Dr. Balpreet S Ahluwalia for their wonderful hospitality in Tromso that included excellent cakes, northern lights, cricket, squash and long drives along the coastline and of course learnt a lot about particle/cells trapping and propulsion using tantala waveguides.

I would like to thank Jaclyn for her tireless help to solve my numerous latex problems while writing this thesis. I would like to thank Luis for teaching me the game of squash and for playing with me even during weekends which at times really helped me releasing my frustration. I would like to thank Hamish for many stimulating discussions, Dr. James Gates for pigtailing my devices, and Ping for teaching me waveguides end-polishing. I would like to thank Eve Smith for solving my all the bureaucratic issues like

countless visa letters, visa extension and all kind of forms. I would like to thank all my other friends at ORC for their help and support during the last 4 years in one way or other that made my stay here in ORC a memorable one.

No amount of words is enough to thank my wife Kamal who was not only instrumental in convincing me to do a PhD but also stood by me during the highs and lows during my PhD. She endured my erratic lifestyle towards the end of my PhD, constantly motivated me, and in-spite of her own PhD work fed me with splendid food and shared bulk of the household work. So thanks a lot for being there. I love you. I would like to thank my parents without whose support, I would not have made it this far. I can never forget the sacrifices they made and would like to thank them for their encouragement and prayers. Finally, I would like to thank god for giving me the strength and opportunity to realise my dream. Namaste.

Nomenclature

AFM	Atomic force microscopy
ASE	Amplified spontaneous emission
CMOS	Complementary metal oxide semiconductors
CUC	Co-operative upconversion
CVD	Chemical vapour deposition
DI	Deionised
EDFA	Erbium doped fibre amplifiers
EDWA	Erbium doped waveguide amplifiers
ESA	Excited State Absorption
FFT	Fast fourier transformation
FIB	Focussed ion beam
FP	Fabry-Perot
FSR	Free spectral range
FTTH	Fibre to the home
HIC	High index contrast
HUC	Homogeneous upconversion
IBM	Ion beam milling
IC	Integrated circuits
ICP	Inductively coupled plasma
IO	Integrated optics
IR	Iinfrared
KOH	Potassium hydroxide
LPCVD	Low pressure chemical vapour deposition
MAN	Metropolitan access network

NA	Numerical aperture
NF	Noise figure
OSA	Optical spectrm analyser
PECVD	Plasma enhanced chemical vapour deposition
PIQ	Pair induced quenching
PL	Photoluminescence
PLC	Planar lightwave circuit
PR	Positive resist
RF	Radio frequency
RIE	Reactive ion etching
SEM	Scanning Electron Microscope
SM	Single mode
SMF	Single mode fibre
SOA	Semiconductor optical amplfiers
TE	Transverse electric
TIR	Total internal reflection
TM	Transverse magnetic
UV	Ultraviolet
WDM	Wavelength division multiplexing
XRD	X-ray diffraction
Yb	Ytterbium

Dedicated to my parents and wife

Chapter 1

Introduction

1.1 Light confinement in waveguides

Electronics refers to the control of flow of the electrons and *photonics* involves all those processes that enable the control of the flow of photons (in vacuum and matter) for different applications such as light signal processing and transmission, sensing, data storage etc. Photonics also encompasses materials research for developing superior light transmission and confinement technology and devices. The phenomenon of total internal reflection (TIR) led to a new technology of transmitting light through dielectric conduits or waveguides called $guided - wave$ optics. Perhaps the most important example of such waveguides was the development of fibre optic communications, where the light travels down the long lengths of low-loss optical silica fibres carrying the bulk of the information such as telephone signals, video etc with minimal delay across continents. Optical waveguides may also be formed on a planar substrate by depositing a thin film of higher index on top of a lower index substrate such as oxidised silicon, leading to 1-D confinement of light. 2-D confinement can be achieved by fabricating different waveguiding geometries in these thin films such as strip, rib and diffused waveguides. However, the basic principle of light guidance and confinement remains the same in all the waveguiding configurations- TIR.

Integrated optics (IO) is the technology of integrating various optical devices on a single substrate. IO takes advantage of the advanced silicon processing technology to achieve miniaturisation of photonic devices just like integrated circuits (IC) miniaturised electronic devices. It is hard to achieve dense integration with conventional IO due to the small index contrast between waveguide core and cladding which leads to larger optical mode dimension and therefore larger devices. Increasing the index contrast between the core and cladding leads to strong confinement of the optical mode inside the small cross-sectional area of the waveguide (few μm^2). This helps in negotiating the tight bends in a device leading to smaller footprint area of the device or high density packing of optical devices. Smaller dimensions lead to higher intensity inside the waveguide allowing

efficient exploitation of nonlinear optical interactions such as Raman and Kerr effects, in chip scale devices at lower power levels.

Silicon technology revolutionised the electronics industry by shrinking the device dimensions and obtaining higher speed and functionality at lower cost. The photonics industry requires such a universal material for competing and ultimately achieving a uniform convergence with the electronics industry. High index contrast (HIC) materials with gain would help in monolithic integration and all optical processing in very compact sizes to achieve true compatibility with IC processing and even supersede them. Ultra-compact optical devices [1–3] with low loss can be achieved by constructing photonic bandgaps or photonic crystals, which also require HIC for best performance.

1.2 Planar lightwave circuits

In the current world, discrete photonic components are interconnected by fibre which works well in the long haul networks where the emphasis is on low loss components and dispersion management and the cost is secondary. But it is space consuming and does not allow for the integration of several functions on a single chip. The smaller network within a city such as the metropolitan access network (MAN), suffers a significant drop in the transmission rate due to the lack of sufficient fibre optic architecture and return to electronic technology within the city which creates a bottleneck between the user and long haul network. A MAN involves transmission of signals over small distances (at the most a few km) and the gain requirement is generally less than in long haul erbium doped fibre amplifiers (EDFAs) and the integration density of optical components on a single substrate and cost are of prime importance whereas loss requirements are relaxed. With unrelenting growth in the data communication traffic and demand for faster information processing, newer architectures that take advantage of compact, low cost, and more functional optical devices including amplifiers are being developed. Advancement in IO technology based on waveguides present a fantastic opportunity to meet these demands and are specially well suited for MAN applications. Nodal losses increase the need for a large number of optical amplifiers in the network and erbium doped waveguide amplifiers (EDWAs) are expected to becomes important for regenerating degraded signals in these systems. Such amplifiers would compensate for the losses in components and to achieve integration of many optical devices on a single planar substrate to produce low cost, compact integrated devices. This could possibly open the door for realising *fibre to the home* (FTTH) systems capable of delivering high speed and high transmission bandwidth signal to the household for intensive audio-video and internet applications. The current metallic interconnect technology induces line delay in ICs due to constant miniaturisation and line densification and replacing the metallic interconnect lines with optical waveguides would be able to solve the interconnect bottleneck problem [4]. The

solution would also require an interface of optical waveguides and a light source/modulator/detector that would transduce electronic signal into optical signal and back. The solution to the interconnect bottleneck problem and FTTH requires integration of various optical functions on a single substrate that takes advantage of existing IC and the telecommunications technology to form a planar lightwave circuit (PLC).

1.3 Erbium doped amplifiers

High quality optical amplifiers are key components of any telecommunications and integrated optical system. In this context, erbium doped materials are of great importance in optical communications technology, for their ability to act as gain media for broadband amplifiers and lasers at the standard telecommunications wavelength of 1.5 μm with low noise and no crosstalk between adjacent channels. Optical fibre networks were built as an alternative to the copper telephone lines that were lossy and had low bandwidth. The revolution in the communication technology that we see today can be attributed to the overlap of the low loss window of silica and one of the intra 4f- level transitions in the erbium ion at 1.5μm. The transmission of the signal through thousands of kilometres in a long haul network without significant degradation of the signal was made possible by the advent of the EDFA. EDFA provided amplification of light through stimulated emission between the three level energy system within the erbium ion. EDFA obviated the time consuming and costly process of taking the optical signal out of the fibre for regenerating the original signal and thus, EDFA brought speed and efficiency to the network system. The success of optical amplification at 1.5 μm has set the standard of optical communications at this wavelength [5, 6]. The advent of wavelength division multiplexing (WDM) produced the capability of simultaneous transmission of multiple channels in a single optical fibre link. The compatibility of EDFA with WDM enabled simultaneous amplification and negligible cross-talk between the adjacent channels in a long distance telecommunications network, giving rise to the enormous data rate ($\sim$200 Gbit/s and rising) and handling the huge demands of internet and other communication applications. The EDFA is an optical fibre whose core has been doped with erbium and is typically a few metres long with slightly higher numerical aperture. EDFA is an amplifier that is optically pumped with diode lasers (980 nm or 1480 nm) and at sufficient pump power population inversion of erbium ions is achieved that leads to the amplification at the signal wavelength ($\sim$1.5 μm).

Semiconductor optical amplifiers (SOA) have risen as a competitive amplifier for the long and short haul networks capable of supplying 20-25 dB gain [7]. In SOA, the gain is achieved by the energy bands of the active semiconductor crystal (e.g. InGaAsP) instead of erbium ion in EDFA. The population inversion is achieved by electrically pumping the crystal and populating the bands with electrons and holes. An optical

signal passing through the crystal in such a state experiences amplification because of stimulated emission. SOA are cheaper than EDFA and are very compact (∼few mm in length) and can be integrated with other devices but they suffer from some intrinsic issues such as low lifetime (ns), temperature and polarisation dependence. The Low lifetime of SOA leads to a higher noise figure (NF) and significant WDM channel interference at higher gain modulation in a SOA.

Advances in the integrated optics technology based on planar waveguides have provided an opportunity to merge the advantages of EDFA and SOA to enable high quality, cheap, multifunctional integrated waveguide amplifiers and devices. These waveguide amplifiers are the miniature planar version of the EDFA, fabricated using the well developed silicon technology, with much higher erbium concentration forming lower cost optical amplifier known as EDWA. The high erbium concentration in the waveguides leads to concentration dependent gain coefficients limiting the gain to ~ 3 dB/cm and it also puts extra pressure on the fabrication for producing low loss planar waveguides with homogeneous erbium distribution. Several methods and materials have been used to successfully realise EDWAs such as sputtering, ion implantation, plasma enhanced chemical vapour deposition (PECVD), ion exchange etc showcasing the versatility of these amplifiers. The EDWA inherits the fundamental qualities of the EDFA such as low noise figure, negligible polarisation dependence, and no cross-talk between adjacent channels and provides amplifiers with lower cost and integration of optical functions on the same chip. However, there are some key issues and limitations in this technology that need to be addressed. High erbium content in the device leads to high upconversion effects leading to lower gain and pump efficiency. Another limitation of the waveguide technology is the absence of integrated isolators to avoid back-reflections and lasing effects and this requires external bulk isolators that makes the product slightly bigger. But waveguide technology is maturing at a rapid rate and in conjunction with EDWA should be able to address the demands of MAN for more functionality and lower cost.

1.4 Aim and material selection

Circuit elements with gain are ubiquitous in electronics and required to achieve many functions, but gain in a small space is much harder to obtain in optical circuitry. Gain in optical circuits is necessary to compensate for the losses encountered and to achieve "lossless" optical circuits. Gain can be introduced in the material by doping with elements such as erbium, especially for working in the C-band telecom wavelength band. It was found that for ICs, gain efficiency increases as $\sim\Delta n^{0.93}$ (with upconversion) and footprint area of the device decreases as $\sim\Delta n^{1.4}$, where Δn is the index contrast [8], as compared to conventional EDFA. The integration of waveguide as optical interconnects in an existing IC technology requires the deposition of waveguide core material onto the IC surface.

A feasible material choice would be the integration of silicon technology compatible dielectric material with refractive index in the range of 1.6 - 2.2 [9]. The ability to make single mode (SM) optical waveguides with tight bends to fit in small area ($\sim$100 μm^2) to replace metal interconnects requires HIC material system. HIC in conjunction with net optical gain, silicon processing compatibility and other inherent material property is also important to realise dense PLCs comprising of active and passive devices that are compact and low cost. Smaller dimensions EDWA would lead to lower pump threshold due to higher intensity inside the waveguide and hence low power consumption devices.

The challenge ahead is therefore to explore possible material systems with sufficient index contrast that are compatible with the existing silicon processing technology to fabricate efficient EDWAs and other passive devices to realise a compact multifunctional PLCs. Tantalum pentoxide (Ta_2O_5) or tantala is under active exploration for several photonic applications. Tantala has a high refractive index of $\sim$2.1 corresponding to an index contrast of $\sim$0.65 and is transparent over a wide wavelength range (300-8000 nm) and therefore useful for optical applications. It has been used extensively used as a dielectric material in microelectronics industry for many years and is thus compatible with almost all the silicon processing techniques [10]. The HIC of tantala has been exploited to make evanescent field based biological and chemical sensors [11]. The HIC of tantala has also been utilised for making reflectors [12] and photonic crystals [13]. Tantala also possesses additional inherent properties such high third order non-linearity [14] and photosensitivity [15]. Gain in tantala was achieved for the first time by our group by doping Neodymium (Nd) in tantala and Nd:Ta_2O_5 rib waveguide lasers were realised [16]. But gain in Er:Ta_2O_5 has not been demonstrated so far. There have been few photoluminescence (PL) studies based on Er:Ta_2O_5 [17–19] but none have reported any gain in this material system. It is believed to have a large fraction of edge sharing non-bridging oxygen atoms that could be helpful in attaining high erbium solubility [17–19] and moderate phonon energy (< 900 cm^{-1}) that could prove to be useful for lower threshold [20] EDWA. This thesis therefore continues the research on EDWA based on Ta_2O_5 and its process engineering for achieving low loss waveguides and high gain EDWA. The thesis focuses on the clear advantage of gain (at 1.5 μm) and HIC of Er:Ta_2O_5 enabling the possibility of fabricating more complex, integrated photonic devices in a compact way that could be assembled on a low cost planar substrate and/or to achieve monolithic integration of electro-optical components.

1.5 Achievements and structure of the thesis

The thesis explores the implication of different fabrication process on the waveguide loss and erbium spectroscopy of Ta_2O_5. It also adds substantially to the study of erbium

spectroscopy and gain in tantala waveguides. The achievements of the thesis can be summarised as below

- A comprehensive process engineering and optimisation program was undertaken for the fabrication of Er:Ta_2O_5 rib waveguides using magnetron sputtering on oxidised silicon substrates to yield low loss waveguides ($\sim$ 0.6 dB/cm). The fabrication parameters were optimised to yield low loss and maximum PL intensity.
- Numerical modelling for an Er:Ta_2O_5 based EDWA with and without upconversion process for studying the gain dynamics was successfully carried out based on the erbium spectroscopic parameters such as absorption and emission cross sections and lifetime determined experimentally for the first time in this material.
- Optical net gain was achieved for the first time in Er:Ta_2O_5 material system doped with a high erbium concentration of 2.7 $\times$ 10^{20} ions/cm^3. An EDWA with maximum gain of 2.25 dB/cm was realised with a rib waveguide geometry.
- An Er:Ta_2O_5 waveguide laser was realised for the first time in this material system. The lasing was single mode and the cavity was realised by affixing two mirrors at the ends of the waveguide.
- Lastly, to realise an integrated line narrowed laser, a feasibility study of inscribing gratings was carried out in different waveguides using two different mechanisms-interferometric ablation and photolithography. Sub-micron grating structures with reflectivity of 11 dB peaking at 1505 nm were achieved using the interferometric ablation method.

Chapter 2 deals with fundamental aspects of the EDWA. It briefly discusses the main principles and factors affecting the working of the EDWA and steps to improve them. It then discusses different concentration quenching mechanisms especially upconversion processes and their effect on rare-earth doped devices. The chapter finally presents the literature review on different host materials that have shown net optical gain so far and compare their performance.

Chapter 3 presents the gain dynamics in Er:Ta_2O_5 material through numerical modelling of the rate equations of a three level system. It then presents the effect of different parameters such as pump power, concentration of erbium ions, length of the waveguide, and signal power on the gain of the material system. Finally, based on the results obtained it predicts the best performance of the Er:Ta_2O_5 amplifier and the required optimum value of different material properties.

Chapter 4 investigates the entire process engineering adopted to obtain low loss waveguides based on Er:Ta_2O_5. It discusses in detail the optimisation process undertaken to achieve high quality optical thin film and rib waveguides of Er:Ta_2O_5 on oxidised silicon substrates. It then presents the qualitative and quantitative results on the various characterisation processes and erbium spectroscopy results of the waveguides fabricated.

Chapter 5 presents the experimental results of the gain and lasing action in the Er:Ta_2O_5 material system. The first half of the chapter presents the experimental set up and the net gain obtained during the measurement. The experimental results were fitted to the model described in the second chapter and the gain is compared to other HIC materials. The second half of the chapter presents the experimental details of the waveguide lasing action in Er:Ta_2O_5 material system.

Chapter 6 presents the feasibility study of the sub-micron structures inscription on Er:Ta_2O_5 waveguides using two different techniques- interferometric ablation and photolithography. It discusses the steps undertaken to inscribe these structures, their advantages and the results obtained during the experiments.

Finally, in chapter 7 conclusions and suggestions for further work to build on the results obtained in this thesis are presented.

Bibliography

[1] P. Dumon, W. Bogaerts, V. Wiaux, J. Wouters, S. Beckx, J. Van Campenhout, D. Taillaert, B. Luyssaert, P. Bienstman, D. Van Thourhout, and R. Baets. *Low-loss SOI photonic wires and ring resonators fabricated with deep UV lithography. Photon Tech Lett*, **16**:1328, 2004.

[2] H. Kosaka, T. Kawashima, A. Tomita, M. Notomi, T. Tamamura, T. Sato, and S. Kawakami. *Superprism phenomena in photonic crystals: Toward microscale lightwave circuits. J Lightwave Technol*, **17**:2032, 1999.

[3] J. Ouellette. *Seeing the future in photonic crystals. The Industrial Physicist*, (12): 14, 2002.

[4] ITRS(2009). International technology roadmap for semiconductors:2009. Technical report, 2009.

[5] A. Ghatak and K. Thyagarajan. Introduction to Fibre Optics. Cambridge University Press, Cambridge, 1999.

[6] E. Desurvire. Erbium-Doped Fibre Amplfiers:Principles and Applications. John Wiley & Sons, New York, 1994.

[7] D. R. Zimmerman and L. H. Spiekman. *Amplifiers for the masses: EDFA, EDWA, and SOA amplets for metro and access applications. J Lightwave Technol*, **22**:63, 2004.

[8] S. Saini, J. Michel, and L. C. Kimerling. *Index contrast scaling for optical amplifiers. J Lightwave Technol*, **21**:2368, 2003.

[9] S. Saini. Gain Efficient Waveguide Optical Amplfiers for Si Microphotonics. PhD thesis, 2004.

[10] C. Chaneliere, J. L. Autran, R. A. B. Devine, and B. Balland. *Tantalum pentoxide (Ta_2O_5) thin films for advanced dielectric applications. Mat Sci Eng R*, **22**:269, 1998.

[11] K. Schmitt, K. Oehse, G. Sulz, and C. Hoffmann. *Evanescent field sensors based on tantalum pentoxide waveguides - A review. Sensors-Basel*, **8**:711, 2008.

[12] S. Pissadakis, M. N. Zervas, L. Reekie, and J. S. Wilkinson. *High-reflectivity Bragg gratings fabricated by 248-nm excimer laser holographic ablation in thin Ta_2O_5 films overlaid on glass waveguides. Appl Phys a-Mater*, **79**:1093, 2004.

[13] U. Huebner, R. Boucher, W. Morgenroth, J. Kunert, H. Roth, H. G. Meyer, T. Glaser, and S. Schroeter. *Fabrication of photonic crystals in tantalum pentoxide films. Microelectron Eng*, **78-79**:422, 2005.

[14] C. Y. Tai, C. Grivas, and J. S. Wilkinson. *UV photosensitivity in a Ta_2O_5 rib waveguide Mach-Zehnder interferometer. Photon Tech Lett*, **16**:1522, 2004.

[15] C. Y. Tai, J. S. Wilkinson, N. M. B. Perney, M. C. Netti, F. Cattaneo, C. E. Finlayson, and J. J. Baumberg. *Determination of nonlinear refractive index in a Ta_2O_5 rib waveguide using self-phase modulation. Opt Exp*, **12**:5110, 2004.

[16] B. Unal, M. C. Netti, M. A. Hassan, P. J. Ayliffe, M. D. B. Charlton, F. Lahoz, N. M. B. Perney, D. P. Shepherd, C. Y. Tai, J. S. Wilkinson, and G. J. Parker. *Neodymium-doped tantalum pentoxide waveguide lasers. J Quant Electron*, **41**:1565, 2005.

[17] K. Kojima, S. Yoshida, and H. Shiraishi. *Green upconversion fluorescence in Er^{3+}-doped Ta_2O_5 heated gel. Appl. Phys. Lett.*, **67**:3423, 1995.

[18] N. Maeda, N. Wada, H. Onoda, A. Maegawa, and K. Kojima. *Preparation and optical properties of sol-gel derived Er^{3+}-doped Al_2O_3-Ta_2O_5 films. Opt Mater*, **27**: 1851, 2005.

[19] H. Rigneault, F. Flory, S. Monneret, S. Robert, and L. Roux. *Fluorescence of Ta_2O_5 thin films doped by kilo-electron-volt Er implantation: Application to microcavities. Appl Optics*, **35**:5005, 1996.

[20] P. S. Dobal, R. S. Katiyar, Y. Jiang, R. Guo, and A. S. Bhalla. *Raman scattering study of a phase transition in tantalum pentoxide. J Raman Spectrosc*, **31**:1061, 2000.

Chapter 2

Basic Concepts and Review of Erbium Doped Waveguide Amplifiers

High quality optical amplifiers are key components of any telecommunications and integrated optical system. In this context, erbium doped materials are of great importance in optical communications technology, for their ability to act as gain media for broadband amplifiers and lasers at the standard telecommunications wavelength of 1.5 μm with low noise and no crosstalk between adjacent channels. It might seem straightforward to translate the concepts of EDFAs to EDWAs, but when scaling down the amplifier's dimension from a few metres for EDFAs to few centimetres or less for EDWAs, the concentration of erbium has to be increased to achieve the same optical gain. In doing so, many of the physical processes that were unimportant in EDFAs play an important role in determining the net optical gain in EDWAs. Towards this goal, several erbium doped materials have been explored and net optical gain has also been demonstrated [1–11]. But an important challenge is to understand the physical processes and factors that affect the optical gain and to find materials, structures and fabrication techniques that can realise the best performance from EDWAs. This chapter discusses important principles and obstacles in the realisation of efficient high gain in EDWAs and finally presents a review on the performance of EDWAs realised so far in different materials.

2.1 Fundamental Properties and Factors Affecting the EDWA

2.1.1 Energy levels

The lanthanides and actinides are generally classified as rare earth (RE) materials with each group consisting of 14 elements. Erbium is the 11^{th} element in the lanthanide series of elements. In most host materials, erbium ions usually take a trivalent charge state with the electronic configuration of [Xe] $4f^{11}$ with the xenon electronic configuration ($1s^2 2s^2 2p^6 3s^2 3p^6 3d^{10} 4s^2 4p^6 4d^{10} 5s^2 5p^6$) common to all the RE ions and the electrons in the 4f-shell remain shielded from any outside effect by the $5s^2 5p^6$ closed shells of the [Xe]. When the erbium ion is incorporated in a solid host such as glass, then the crystal field of the host material interacts with the erbium ion and perturbs the 4f wave function and each degenerate level is Stark- split into a manifold of levels. There are several discrete energy states available within the 4f-shell which results in numerous optical transitions as shown in Fig 2.1a. Because of the shielding of the inner 4f-shell, the position of energy levels and the transitions are barely dependent on the host materials in which the erbium ions are incorporated but the lifetime, decay rates, absorption and emission cross-sections are highly dependent on the host [12–14]. In an EDWA, erbium is doped in the core of the waveguide and, a source of pump radiation usually at a wavelength of 980 nm or 1480 nm, erbium ions are excited to one of its higher lying energy levels. From there, the ions rapidly relax to the first excited level ($^4I_{13/2}$) as shown in Fig 2.1a. When sufficient pump power is applied, ions reaches the state of population inversion. A signal (at 1.5 μm) travelling through such a waveguide will induce stimulated emission from the $^4I_{13/2}$ level to $^4I_{15/2}$ level and hence experience amplification.

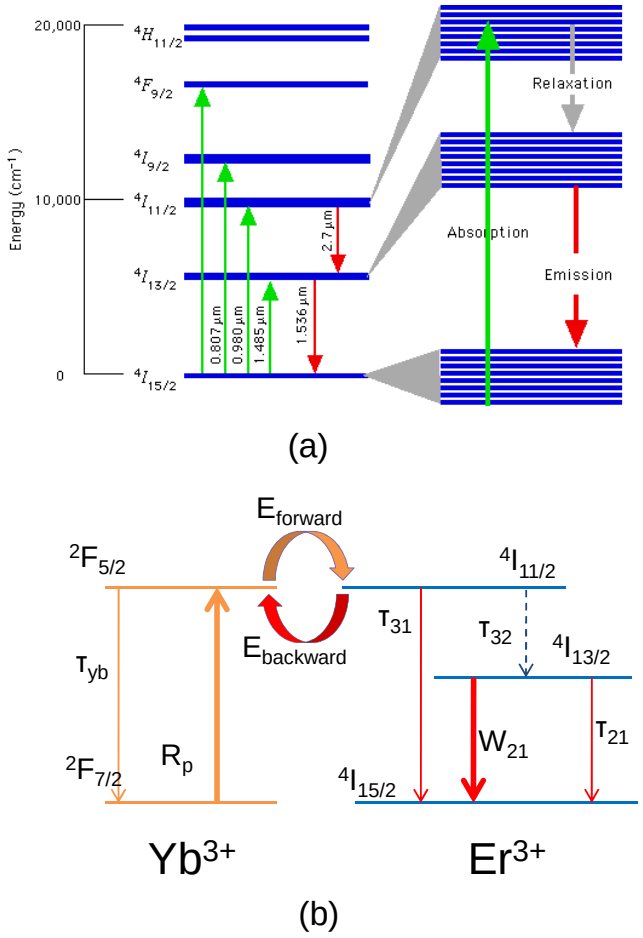

FIGURE 2.1: a) Some of the spectroscopically important energy levels of an Er^{+3} ion. The green lines show the absorption lines whereas the red lines show the emission lines. b) shows the energy levels of Yb^{+3} ion and its resonance with the Er^{+3}energy levels. The orange arrow denotes the forward energy transfer from Yb^{+3} to Er^{+3} when pumped at 980 nm (R_p). Depending on the phonon energy of the host material there is a possibility of backward energy transfer from Er^{+3} to Yb^{+3} ion denoted by the red arrow.

2.1.2 Emission and absorption cross sections

The gain of an EDWA is mainly determined by absorption (σ_a) and emission cross-sections (σ_e). The absorption cross-section determines the ability of an erbium ion to absorb light (pump and signal) and the emission cross section quantifies the ability of an erbium ion to emit light. These quantities are among the most fundamental features of an erbium ion and are dependent on the host material. σ_a (cm^2) can be determined by measuring the decrease in the optical intensity travelling through a "loss-less" material

of length L at a wavelength λ

$$I(\lambda) = I_0(\lambda)\, e^{-\alpha L} \tag{2.1}$$

where I is the intensity measured after length L , I_0 the incident intensity on the sample, and α is the absorption (cm^{-1}) at wavelength λ. Then σ_a can be calculated as

$$\sigma_a(\lambda) = \alpha(\lambda)/N \tag{2.2}$$

where N is the total number of ions in cm^{-3} unit. σ_e (cm^2) can be determined using σ_a by McCumber relationship [15] and Fuchtbauer-Ladenburg method [16]. Once the cross-sections have been determined then the gain of the system is given by

$$G_{dB}(\lambda) = 10 \times log_{10}\left((\sigma_e N_2 - \sigma_a N_1)\right) L \tag{2.3}$$

where both the emission and absorption cross-sections are calculated at the signal wavelength.

2.1.3 Lifetime

The lifetime of a level is inversely proportional to the probability per unit time that an ion will vacate that particular level in the absence of stimulated emission. Thus, the population of erbium ions from an excited level decays exponentially with a time constant equal to the lifetime. However, due to defects in the host composition there may be several channels available for the population to decay, in which case the total probability is the sum of the individual probability for each pathway. Broadly, the decay channels can be classified into radiative and non-radiative , and the total lifetime of a level is given by [17]

$$1/\tau = 1/\tau_r + 1/\tau_{nr} \tag{2.4}$$

where τ is the total lifetime, τ_r is the radiative lifetime, and τ_{nr} is the non-radiative lifetime. The radiative lifetime arises from the fluorescence from the higher to lower energy levels. The non-radiative lifetime largely depends on the host composition and the coupling between the phonon and erbium energy levels [18] .

2.1.4 Solubility

The EDWA is advantageous because of its short length (compact size) and integrability. To achieve net gain over a few centimetres a high concentration of erbium ions is required. At such high concentrations, erbium ions are very close to each other and, as a result, they start interacting and exchanging energy with each other and can form clusters as well [19–24]. As a result, the erbium ions lose their efficiency to provide gain. In the absence of ion-ion interactions, the gain in the system is proportional to the erbium concentration therefore, the high solubility of optically active erbium ions in the host

material is one of the main criteria that determine the efficiency of an EDWA. Rare-earth ions are bound to the non-bridging oxygen atoms within the host matrix as shown in Fig.2.2a. The solubility of erbium ions can be improved by using network modifiers such as aluminium and phosphorus which help in enhancing the fraction of non-bridging oxygen atoms and hence the solubility of rare-earth ions in the host as shown in Fig. 2.2b. The exact mechanism by which the modifiers increase the solubility is not completely known but both Al and P the modifiers have been found to be efficient in increasing the solubility [25–32].

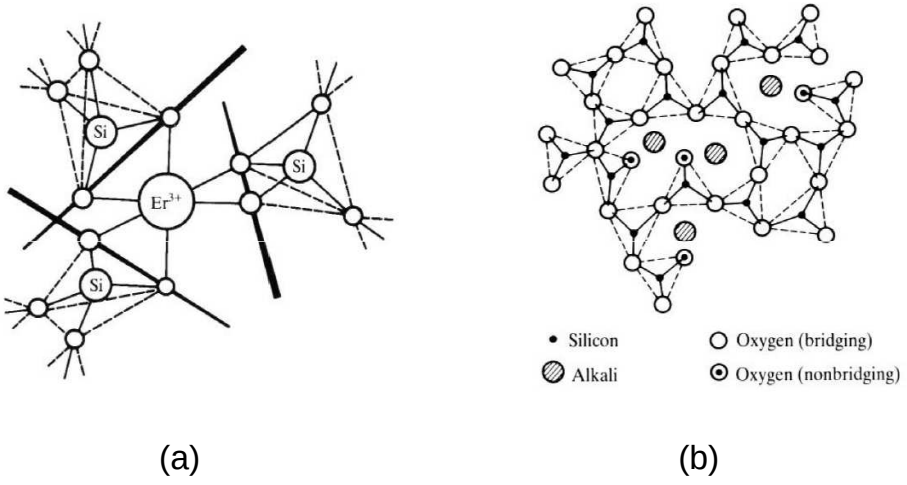

FIGURE 2.2: Incorporation of erbium ion in (a) host (silica) showing the erbium ion bound to non-bridging oxygen atoms and (b) impact of modifiers on the host and erbium ion bonds [33]

2.1.5 Phonon interactions

Phonon interactions are involved in the non-radiative transitions that takes place in the various higher energy erbium ions levels. They are necessary in depopulating the higher energy levels and populating the metastable level ($^4I_{13/2}$) of the erbium ion and hence achieve population inversion. But these processes are significant when the energy gap to bridge is small and, as a rule of thumb [33], if the phonon cut-off energy of the material is greater than 25% of the energy gap then the ions will be de-excited or in other words the luminescence will be quenched. For phonon cut-off energies between 10% and 25% of energy gap, quenching will result in a temperature dependent luminescence lifetime and for phonon cut-off energies smaller than this the multi-phonon relaxation is negligible. The phonon relaxation or interaction is thus strongly dependent on material (host) and rare-earth doped in the host. For erbium ions, for example, selection of a

low phonon energy host such as a tellurite glass [34, 35] will allow much more efficient radiative transition from higher levels that would otherwise be quenched. But for an Er/Ytterbium (Yb) co-doped system (2.1b) a higher phonon energy host is needed to prevent the back-coupling of energy transfer from Er ion to Yb ion [36].

2.1.6 Concentration Quenching

Any process other than stimulated emission that removes ions from the excited state necessarily reduces the efficiency of the amplifier. High concentrations of erbium ions reduce the luminescence efficiency of the system due to processes such as concentration quenching. Such quenching processes convert the useful pump photons into heat and are deleterious to the EDWA system. In this section we will discuss about various quenching mechanisms associated with erbium doped materials and devices.

2.1.6.1 Co-operative upconversion and clustering

The most common process for luminescence inefficiency in the erbium doped devices is co-operative upconversion (CUC) process [20, 37]. The CUC process will occur when two ions interact and exchange energy if a higher energy level is present in the system that is resonant with this energy exchange. In an EDWA, CUC occurs due to the interaction between two excited erbium ions ($^4I_{13/2}$) resulting in the non-radiative transfer of one ion to the ground state ($^4I_{15/2}$) and the other ion to higher energy level ($^4I_{9/2}$). The excited ion then quickly relaxes to the metastable state through multi-phonon relaxation and subsequently relaxes to the ground state radiatively or non-radiatively as shown in Fig. 2.3.

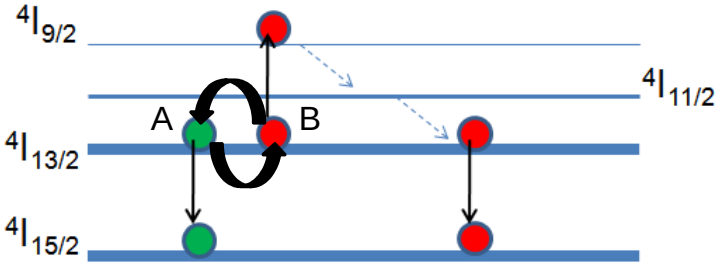

FIGURE 2.3: Homogeneous upconversion in erbium doped host. Green (A) and red (B) coloured balls represents two erbium ions in metastable state exchanging energy and promoting B to $^4I_{9/2}$ and A to $^4I_{15/2}$. The dashed arrow shows the non-radiative transition from higher level to metastable level

CUC process reduces the population of the excited erbium ions and puts extra pressure on the pump to achieve a required population inversion as at least one signal photon

is wasted because of upconversion process thereby reducing the gain of the system. To understand the process of upconversion more clearly, the material matrix where the erbium ions are doped must be studied (Fig. 2.4). When the concentration levels are such that the separation between two erbium ions is greater than the diameter of an individual erbium ion then the upconversion process is called "homogeneous upconversion (HUC)". But with the increase in the concentration the inter-ionic distance between two erbium ions becomes less and they come much closer to each other so as to form "clusters" and most commonly form "pairs". The interaction between the pairs upon pumping is called "inhomogeneous upconversion" or "pair induced quenching (PIQ)" [20, 27, 30, 31, 38–41]. HUC occurs for all concentrations but the PIQ starts to occur and dominate over HUC only at high concentrations [39–43] as the upconversion is largely dependent on the inter-ionic distance between erbium ions [20, 40, 42]. The upconversion also increases at high pump power because of increased number of ions at the excited state which tend to interact at a faster rate. This puts an upper limit on the concentration of the erbium ions that one can dope in the host material to extract maximum gain from the system. Thus a combination of high concentration and high pump power leads to faster quenching of luminescence intensity leading to a decline in the gain and efficiency of the EDWA [42–48].

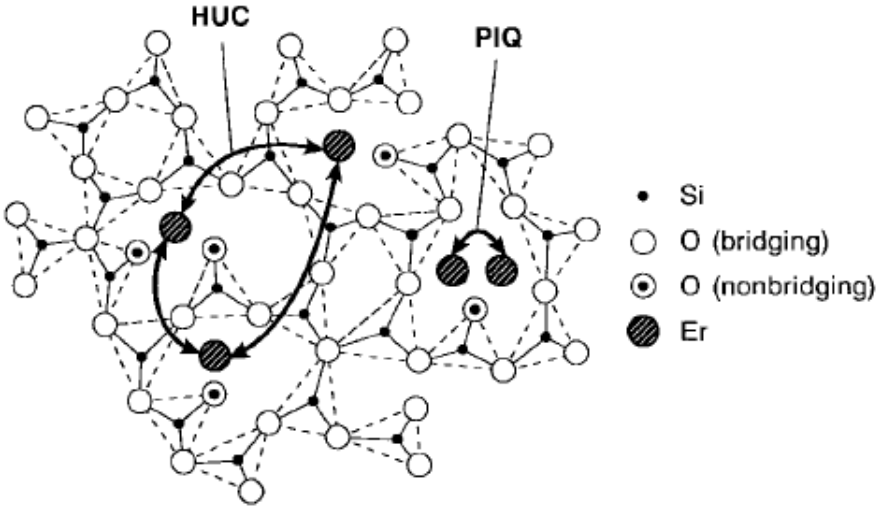

FIGURE 2.4: Two dimensional schematic representation of HUC and PIQ [44]. HUC takes place between erbium ions that are separated by a distance that is more than the diameter of an erbium ion. Whereas PIQ occurs at high concentrations, when the ions form clusters as they are separated by a distance that is equal or less than the diameter of an individual ion.

Apart from quenching the $^4I_{13/2}$ luminescence intensity, emission of other radiative transition is also observed. For example, upconversion leads to emission of green light that occurs via second order upconversion process, where two ions in the $^4I_{13/2}$ level interact,

promoting one ion to the ground level and other to the $^4I_{9/2}$ level. The ion from the $^4I_{9/2}$ relaxes back to the $^4I_{11/2}$ level, where again two ions interact to yield an ion in the $^2H_{11/2}$ level, which relaxes to the $^2S_{3/2}$ level. There is a green emission when the ions relaxes back to the ground level ($^4I_{15/2}$) from either $^2H_{11/2}$ or $^2S_{3/2}$ level emitting in the range of 530-565 nm (green). The key difference between the HUC and higher order upconversion is highlighted in Fig. 2.5. Almost all the medium to highly doped erbium waveguides emit bright green light when pumped at 980 nm or 1480 nm, which is generally considered as the sign of upconversion or clustering. The measurement and analysis of the green and 980 nm emission is quite helpful in determining the HUC coefficient and degree of clustering. This is done by performing "from the top" measurement of the fluorescence and fitting it to the 3-level rate equations to determine upconversion coefficient and degree of clustering [24, 38, 39, 45–48] . The other common method to measure the upconversion in a material is to measure the lifetime of the the $^4I_{13/2}$ level for different concentration and pump power and fit it to the 3-level erbium rate equations [24, 44, 48–51]. There have also been other methods proposed to study the clustering and upconversion coefficients [52–54].

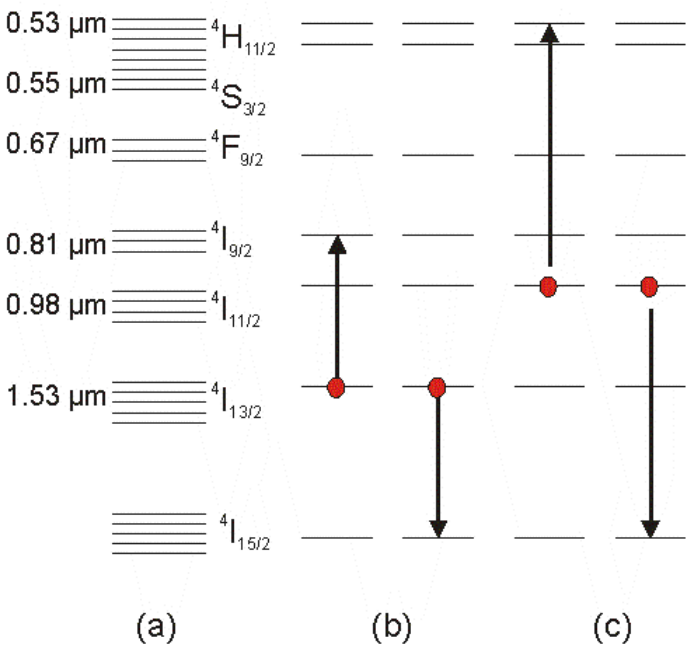

FIGURE 2.5: Schematic representation of upconversion process in an erbium ion. (a) shows the stark split energy levels and corresponding emission wavelength (b) HUC from the $^4I_{13/2}$ level and (c) One possible route for second order upconversion from $^4I_{11/2}$ leading to 980 nm and 535 nm (green) luminescence.

The upconversion process is a material property as it depends on the location of energy levels, phonon energy spectrum and cross-sections. The upconversion coefficient can be altered to a certain extent by better controlled fabrication process that can ensure a

homogeneous distribution of erbium ions without clustering. For example, in alumina [45], it was found that amplifiers fabricated using ion-implantation led to net optical gain whereas amplifiers prepared by co-sputtering led to stronger upconversion and no optical gain. The reason was attributed to the fact that the implantation technique led to a more homogeneous erbium ion distribution than co-sputtering resulting in lower upconversion. But recently with proper optimsation of co-sputtering technique net optical gain was reported in co-sputtered alumina waveguides as well [2]. Although the upconversion process reduces the efficiency of lasers and amplifiers, it can be useful for visible wavelength lasers and is an interesting area of research among spectroscopists and physicists around the world [55–58] . Materials with low phonon energy and high concentrations of rare-earth ions are used to make the upconversion process more prominent resulting in higher frequency (shorter wavelengths) that can then be used to make visible lasers. The other advantage of this process is that the readily available diode lasers at near and mid IR wavelenghts used for EDWA can be used as a pump for visible lasers. Different rare-earth ions can be doped in the suitable host material for different visible wavelength luminescence. For example, erbium for green [55, 56], praseodymium for green, blue and red [59, 60], Holmium for green [61]and thulium for blue lasers with high quantum efficiency [57, 58].

2.1.6.2 Excited state absorption (ESA)

The next main gain limiting effect seen in erbium ions is ESA. In this process, the excited ion ($^4I_{11/2}$) absorbs a signal or pump photon and is excited to even higher levels and from there it either decays non-radiatively down to the metastable state, or radiatively at a higher frequency (Fig. 2.6). Since this process involves both signal and pump photons it affects both the pump efficiency and the maximum gain. If the higher levels have an appreciable lifetime, generally due to low phonon energy of the material then it leads to significant build up of photons at that level, thereby reducing the population inversion at the main lasing level and the pump becomes inefficient [24, 51, 62, 63] especially at high pump powers. Generally, in erbium doped materials, ESA is insignificant at 1480 nm and quite low at 980 nm. But at shorter wavelengths, such as 800 nm ESA is very strong leading to poor gain and pump efficiency, therefore 800 nm is not a preferred pump choice for EDWA applications [33].

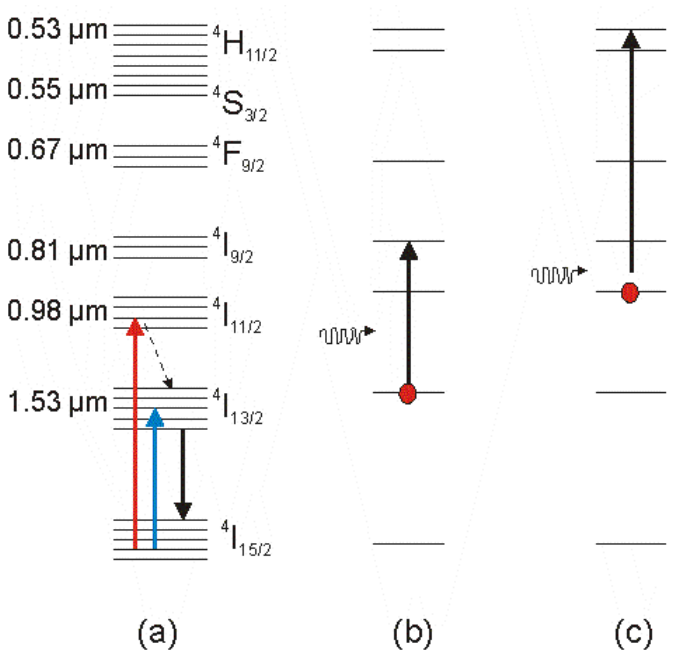

FIGURE 2.6: Schematic of ESA process in an erbium ion showing the ESA process. a) shows the 1.53 μm transition (black arrow) and the red and blue arrows indicate the excitation using 980 nm and 1480 nm pump light respectively. b) & c) represents the ESA process corresponding to 1480 nm and 980 nm pump photon respectively.

2.1.6.3 Energy migration and quenching centres

An excited erbium ion can transfer energy to an unexcited ion causing the excitation energy to diffuse through the system. This does not reduce the population but can be detrimental to the optical gain if it strongly couples to non-radiative quenching sites such as the hydroxyl group (OH^-) or irradiation damage areas in the material system. The phonon assisted activity is greater at this ion-OH^- junction that leads to loss of energy and hence decreases the luminescence efficiency. This occurs because the second overtone of the stretch vibration of the OH^- ion is resonant with the first excited level of erbium ion. Therefore, it is imperative that the material is as pure as possible and free of OH^-or any other defect sites that are resonant with erbium luminescence [64].

2.1.7 Waveguide Loss

Waveguide loss is highly dependent on the choice of material and fabrication technique and therefore directly impacts the effective gain of an EDWA. Loss in a waveguide occurs through absorption and scattering of the guided light in the waveguide. This is also known as passive or propagation loss. To achieve net gain in the amplifier, stimulated

emission has to compensate for both the active (erbium absorption) and the passive losses suffered by the signal. Scattering is induced by the irregularities, both physical and in refractive index on the scale of wavelength. This becomes more important for HIC structures because at a HIC interface scattering becomes more pronounced leading to higher loss. The loss in the waveguide is also influenced by the fabrication method adopted. For example, roughness is one of the major reasons for scattering losses and it is induced in the waveguide during fabrication steps like etching. It has also been found that waveguides made using the sol-gel method retain water, which is a quenching centre for $1.5\mu m$ and leads to losses, as it has been observed that two O-H vibrations are enough to reduce the quantum efficiency of the $^4I_{13/2}$ level [14]. Thus, careful choice of material and proper optimized fabrication techniques can help in minimizing losses in a waveguide.

2.1.8 Mode confinement

For maximising gain in an EDWA, the signal and pump should be well confined so that there is maximum overlap of the optical mode and erbium ion concentration profile. Refractive index contrast plays an important role because in HIC waveguides, the optical mode can be much tightly confined inside the core of the waveguide as compared to a low index waveguide of similar dimensions. Therefore, high pump intensities can be achieved inside the waveguide at low power decreasing the pump threshold for amplification. HIC waveguides also help in fabricating small structures, confining light in tighter bends and hence are important in achieving dense circuitry [65–69].

2.1.9 Pumping Mechanisms

The EDWA uses two main pumping schemes- 980 nm and 1480 nm and both fall under the three level system regime as shown in Fig. 2.1. The 1480 nm pump results in a quasi three level system, with a good overlap between the signal and pump mode due to the similar mode sizes at these wavelengths. Also, the scattering losses are less at longer wavelengths thus favouring long wavelength pumping. At 1480 nm, both the absorption and stimulated emission cross-sections are large for the same spectrum, which induces stimulated emission at the pump wavelength as well and that reduces the pump absorption. This also puts an upper limit on the population inversion that can be obtained at this wavelength, even at high pump powers. The absorption cross section at 980 nm is less than at 1480 nm and also the internal relaxation from higher levels heats up the system and hence the pump threshold increases [33]. But because of an almost complete absence of stimulated emission at the pump wavelength, this pump is the most preferred choice (theoretically inversion can reach a value of 1). The higher inversion level at 980 nm also leads to lower noise in the system. The pump performance can be improved by using Yb as sensitizer, which has a larger cross-section at the pump wavelength, a broader absorption band and has its upper energy level in resonance with

the of erbium ion, which enables it to transfer most of the energy non-radiatively to this level as shown in Fig. 2.1b. There is a possibility of back transfer of the energy from Er to Yb if the phonon energy of the host material is low enough for increasing the probability of this transition. On the other hand if the phonon energy is very high then that leads to reduction in the radiative lifetime of the metastable state. Therefore, there is an optimum phonon energy requirement of the host material to be used as efficient amplifier. The higher inversion level also helps in reducing the noise behavior in an amplifier. The Er-Yb combination has been found to improve the pump threshold and efficiency in EDWAs [70–73].

2.2 The state of the art in EDWA

There has been tremendous research activity in the past few years to realise an EDWA in different material systems, that could satisfy the need of low threshold (when net gain = 0 dB), high broadband gain, and low cost for ever expanding metro networks. But only few material systems have demonstrated successful devices capable of net on-chip gain that are compatible with the existing silicon technology. In this section, state of the art in EDWA is discussed and compared.

Table 2.1 highlights some of the salient characteristics of an EDWA based on different host materials. These host materials have been researched for many years and net gain reported by several groups over the years. But this table only reports the best results obtained in these materials. The salient features listed in Table 2.1 includes properties like- the index difference between core and cladding (Δn), propagation loss, erbium concentration (N_t), device length (L), luminescence lifetime (τ), luminescence bandwidth (BW), pump power threshold (P_{th}), and net optical gain (G_{net}) achieved by the device. Net optical gain is calculated as (signal enhancement - propagation loss-erbium absorption)/length of the waveguide.

Property	Al_2O_3[2]	Si-nc[74]	Polymer		Glasses	
			ENR[10]	PMMA[1]	Phosphate[75]	Borosilicate[76]
Δn	0.2	0.095	0.123	0.079	0.02	NA
Loss (dB/cm)	0.35	<2	NA	1.35	0.4	0.2
Fabrication	sputter	sputter	UV write	spin coat	ion exchange	ion exchange
Dimension (μm^2)	~4	~10	~40	~17.5	~20	~14
N_t ($10^{20} cm^{-3}$)	2.70	4.0	0.41*	0.36	2.3wt%*	3 wt%*
L (cm)	5.4	3.0	2.0	1.6	3.1	3.9
τ (ms)	7.6	NA	11-15	NA	NA	NA
BW (nm)	80	NA	70	NA	> 35 nm	20
P_{th}(mW)	4.0	NA	NA	~7.0	160	~45
$I_{th}(10^5$ W/cm$^2)$	1.75	NA	NR	0.34	8.0	3.25
G_{net} (dB/cm)	2.0	NR	1.60	0.84	4.8	2.5
Year published	2010	2005	2005	2006	2006	1996

* co-doped with Yb NR- not reported NA- not available

TABLE 2.1: Characteristics of the some of the best EDWA till date on different hosts.

Glasses have been known to be a good host for RE ions for a long time due to high erbium solubility and luminescence lifetime. There has been a lot of interest generated in erbium doped glasses for fabricating integrated amplifiers and lasers for optical communications [13, 14]. An EDWA based on borosilicate glass [76] was one of the first reported EDWA

with net optical gain as high as 2.5 dB/cm in a 3.9 cm long device. This result was published soon after reporting the first Er/Yb doped planar waveguide lasers by the same group [77]. The waveguides were fabricated by the ion exchange method and the waveguide loss was reported to be as low as 0.2 dB/cm. The actual device was the first successful demonstration of lossless planar splitting (1 $\times$2) at 1.5 μm wavelength band. The entire device was patterned on an Er/Yb doped substrate with an erbium concentration of 3 wt% and 5 wt% Yb concentration. The maximum gain (2.5 dB/cm) was achieved at an input pump power of 115 mW from a 980 nm laser diode. The pump threshold was $\sim$ 45 mW of the incident power, the actual power inside the waveguide was not provided.

A commercially available Er/Yb co-doped phosphate glass substrate (from Schott glass technologies) is reported to have achieved the highest gain per unit length (4.8 dB/cm) to date [75]. The 3.1 cm long waveguide was fabricated by Ag-Na ion exchange method that lead to a refractive index change of 0.02 with a propagation loss of 0.4 dB/cm. A 975 nm diode laser in a counter-propagation scheme was used for pumping the erbium ions, where pumping was achieved from both ends of the waveguides. At a 460 mW pump power, a maximum net optical gain of 4.8 dB/cm was obtained. A noise figure of 5 dB for the entire C band was achieved for this device. Phosphate glass have been used for a long time for making amplifiers and have been providing the highest gain for a long time. Before this result, the highest gain reported for an EDWA was 4.1 dB/cm in another phosphate glass based EDWA [11]. The reason for the high gain reported in these glasses is attributed to the low loss and the favourable environment for erbium ions in the glass matrix that leads to lower clustering and upconversion effects.

Alumina (Al_2O_3) is another material that has been used extensively as a host for erbium in making both active and passive devices at 1.5 μm. Alumina has been used as a gain medium for erbium because of the similarity in the valency and lattice constants with Er_2O_3 that has allowed for higher concentrations of erbium in the alumina crystal structure. Alumina has also been used as a modifier in other material systems for enabling higher doping of erbium concentration [25–27]. The refractive index of alumina is higher than most glasses ($\sim$1.65) leading to relatively high index difference which allowed the fabrication of a spiral ridge amplifier [78] with a net optical gain of 0.58 dB/cm and an interaction length of 4 cm that fitted into an area of 1 mm^2, making it the smallest EDWA to date. The pump threshold was as low as 3 mW in the waveguide. However, the best results obtained in alumina were reported very recently [2] when a net optical gain of 2 dB/cm was reported with a pump threshold of just 4 mW. The waveguide used for this demonstration was 5.4 cm long and was fabricated by sputter deposition on an oxidised silicon substrate. The alumina waveguide was doped with erbium ions with a concentration as high as 2.7 $\times 10^{20}$ ions/cm^3. The other important result demonstrated by this device was the gain bandwidth of 80 nm making it suitable for broadband amplification.

Other glasses have also demonstrated net optical gain in the past and many research groups are still actively engaged in improving the results. Recently a net gain was demonstrated in Al/P co-doped silica glass (1.15 dB/cm) [6] and in sodalime glass (1.96 dB/cm)[79]. The Al/P co-doped silicate glass was fabricated using the sol-gel method whereas the sodalime waveguides were fabricated using ion exchange method.

Polymers have always been considered to be very promising materials for integrated optical devices due the their easy fabrication methods but they have a poor solubility for RE ions. Recently, two different groups [1, 10] demonstrated net optical gain with two different polymers, Polymethyl Methacrylate (PMMA) and Epoxy Novolak Resin (ENR), using sol gel techniques. Erbium was dissolved in the host by using a ligand which forms a solvation shell around the ions that helped in achieving the desired erbium solubility. PMMA achieved an optical gain of 0.84 dB/cm over a length of 1.6 cm and with a pump threshold of only 7 mW. ENR demonstrated twice as much gain, 1.6 dB/cm, in a 2 cm long device. The waveguide using ENR was fabricated by direct UV writing technique that induced an index change of 0.123 and had a high luminescence lifetime of 11-15 ms which is comparable to glass making it a very promising material for active and passive photonic devices. But polymers have to address the issue of aging before they can be fully adopted as a material for planar photonics.

Technically, from the point of view of fabrication, silica based waveguides would be the best material to make an EDWA because of the well developed Si microelectronics and fibre technology. Low loss waveguides are possible with silica but, unfortunately silica has high phonon energy and poor solubility for erbium. However with the addition of co-dopants such as phosphorus net gain was achieved in silica based waveguide amplifier [80] . Intense research is underway in the area of silicon nanocrystals (Si-nc) to achieve better luminescence and net gain [74]. So far, many groups have performed luminescence studies on erbium doped silicon nanocrystals but net gain is yet to be reported. Nonetheless this is one of the most exciting new directions for future generation active waveguide devices.

For implementing planar devices in the networks, dense integration, low power and cost are important issues that need to be addressed. In all the materials discussed above, there has not been a single material that has demonstrated high gain, low threshold, and HIC simultaneously. In this regard, Table 2.2 lists some of the candidate materials with higher index contrast than the materials discussed in Table 2.1, and that have shown net optical gain or have the potential to be used for EDWAs and other active devices. One of the most promising materials that has come out of recent research activities on RE doped materials is tellurite glass. It is attractive compared to other glasses because it has tuneable phonon energy, high linear and non-linear refractive index, broad emission bandwidth, and most importantly it has a large absorption and emission cross-sections at 980/1550nm, which makes it an ideal candidate for EDWA. These properties can be tailored and improved by adding dopants such as tungsten, borate and phosphate. Until

recently, many groups had done spectroscopic studies on tellurite based erbium doped waveguides but none had reported any net optical gain. But very recently, net optical gain as high as 2.2 dB/cm was reported in a 5 cm long tellurite waveguide based EDWA [81]. The waveguide was prepared by co-sputtering tellurite glass and erbium on a silicon substrate. The maximum erbium concentration in the sample that demonstrated gain was 2.2 $\times 10^{20}$ ions/cm^3. The waveguide loss was measured to be 0.6 dB/cm and a pump threshold ~25 mW, which was slightly on the higher side and the reason could be attributed to the low lifetime of the metastable level (1.3 ms). The index contrast (0.63) of this device is by far the highest when compared to other materials that have reported net gain. HIC is necessary to realise dense and compact planar devices and amplifiers to be used in the planar lightwave circuits.

The other relatively HIC materials that have been pursued for achieving gain are zirconia (ZrO_2) [9] and zinc-silicate-germanate (ZSG) [3]. Zirconia had a index difference of 0.170 which is greater than most glasses but much lower to telluride and even alumina whereas ZSG had a higher index contrast of 0.30. For both the materials, the waveguides were prepared by co-sputtering process of core material and erbium. Schermer et al. managed to overcome the the total losses in the zirconia based EDWA and demonstrated a gain of just 0.005 dB/cm but no other work has been reported on this material. ZSG on the other hand, demonstrated a net optical gain of 0.4 dB/cm but just like zirconia no other work has been reported on this material.

Property	Tellurite[81]	ZrO_2[9]	ZSG[3]	SiON[82, 83]	Ta_2O_5[84, 85]
Δn	0.63	0.170	0.30	0.1-0.85	0.65
Loss (dB/cm)	0.6	0.45	0.32	0.1	0.7
Fabrication	sputter	sputter	sputter	CVD	sputter
Dimension (μm^2)	~2.8	~10.5	~3	slab (1.18 μm)	slab (1.36 μm)
N_t (10^{20}cm^{-3})	2.2	0.88	0.80	4-5	NA
L (cm)	5	6.5	3.7	7	NA
τ (ms)	1.3	1.77	2.8	3-7	NA
BW (nm)	40	54	NA	NR	NR
P_{th}(mW)	~25.0	36.0	~ 12.0	NR	NR
I_{th}(10^5 W/cm^2)	9.26	3.43	4.0	NR	NR
G_{net} (dB/cm)	2.2	0.005	0.4	NR	NR
Year published	2010	2003	2004	1996-2005	1995-2005

* co-doped with Yb NR- not reported NA- not available

TABLE 2.2: Characteristics of the some of the recent material systems used for realising EDWA.

Silicon oxynitride (SiON) is a versatile material for integrated optics applications because SiON is compatible with the silicon processing techniques but SiON layers contains a significant amount of N-H bonds, and the N-H stretching vibration has its first overtone at 1.5 μm that causes absorption losses in the wavelength range 1529-1590 nm. High temperature annealing has been found to suppress the hydrogen content and hence the absorption loss in the SiON layer and waveguides with low loss ($<$ 0.2 dB/cm) have been realised [82, 86]. Erbium doped SiON waveguides have been realised but so far they have been restricted to photoluminescence studies only [82, 87, 88] and a metastable lifetime as high as 7 ms have been calculated in one of the erbium doped SiON waveguides [87]. One of the reasons for no gain in the sputtered material have been attributed to the silicon dangling bonds that have been shown to contribute both to the losses in the waveguide and to the non-radiative energy transfer in the erbium doped material [88]. But they have already been used to fabricate filters [86], dynamic gain equaliser, dispersion compensator and other passive devices [89]. The best performance from SiON waveguides have been mainly restricted to the fabrication using PECVD and low pressure chemical vapour deposition (LPCVD) techniques but SiON is one of the few materials that provides with a flexibility of changing the refractive index of the material from silica ($\sim$1.46) to silicon-rich silicon nitride ($\sim$2.3). This flexibility offer the advantages of utilising the benefits of both low and high index contrast of the system with gain and cost efficient photonic devices [83].

Tantalum pentoxide (Ta_2O_5) or tantala is under active exploration for several photonic applications. Tantala has a high refractive index of $\sim$2.1 corresponding to an index contrast of $\sim$0.65 and is transparent over a wide wavelength range (300-8000 nm) and therefore useful for optical applications. Erbium doped tantala waveguides have been limited to fluorescence studies only [84, 85, 90] therefore, the behavior of erbium ions in tantala is still relatively unknown and so far only Nd doped tantala systems have been studied in detail and gain in tantala was demonstrated by in Nd:Ta_2O_5 rib waveguides [91].

The results discussed in both the tables indicate that a lot of progress has been made in the EDWA, and much research is still being carried out to improve the gain in existing systems and to find new alternative material systems with low loss and high gain for realising efficient planar devices. The current trend of photonic integration is to fabricate photonic devices compatible with complementary metal oxide semiconductors (CMOS) technology. Most photonic materials are not CMOS compatible therefore it is difficult to achieve monolithic integration of photonics on Si platform using Si CMOS technology. One approach to overcome this problem is to find Si CMOS compatible material that is capable of delivering various optical functionality and gain. In this context, Si CMOS compatible HIC materials are important materials for achieving low threshold, low power, and compact EDWA and other planar devices that could ultimately lead to low cost and efficient future generation PLC. However, there have been very few HIC

material systems ($\Delta n > 0.3$) that have demonstrated net gain, so there is much scope for the study of novel HIC material systems with gain. All the previous results suggests that tantala could serve as an excellent host for erbium ions which could lead to potential gain in the system at the telecom wavelength. The other inherent properties and results based on tantala waveguides demonstrate the versatility of tantala for integrated photonics devices and applications. This thesis explores the routes to achieve low loss waveguides in Er:Ta_2O_5 and achieve high gain amplifiers and lasers from the Ta_2O_5 material system.

2.3 Conclusions

In this chapter, the fundamentals behind gain mechanism in an erbium ion was described. The limiting factor in the efficient use of the pump power for high gain were discussed and methods to overcome problems such as CUC and ESA were presented. The important factors for an efficient EDWA, is the ability to yield low loss waveguides and incorporate high concentrations of optical active erbium ions (without clustering effects) leading to better use of the pump power and high gain. Finally, a review on the state of the art on EDWA was presented where the performance of different materials as EDWA were compared. For the work presented in this thesis tantala was selected as the HIC host material for achieving low threshold, and high gain for realising dense PLC.

Bibliography

[1] J. Zyss I. Ledoux. G. Cusmai R. Costa. A. Barberis A.Q.L. Quang, R. Hierle and S.M. Piertralunga. *Demonstration of net gain at 1550 nm in an erbium doped polymer single mode rib waveguide. Appl Phys Lett*, **89**:141124, 2006.

[2] J. D. B. Bradley, L. Agazzi, D. Geskus, F. Ay, K. Worhoff, and M. Pollnau. *Gain bandwidth of 80 nm and 2 dB/cm peak gain in Al_2O_3:Er^{3+} optical amplifiers on silicon. J Opt Soc Am B*, **27**:187, 2010.

[3] C. C. Baker, J. Heikenfeld, Z. Yu, and A. J. Steckl. *Optical amplification and electroluminescence at 1.54 μm in Er-doped zinc silicate germanate on silicon. Appl Phys Lett*, **84**:1462, 2004.

[4] R. N. Ghosh, J. Shmulovich, C. F. Kane, M. R. X. deBarros, G. Nykolak, A. J. Bruce, and P. C. Becker. *8-mW threshold Er^{3+}-doped planar waveguide amplifier. Photon Tech Lett*, **8**:518, 1996.

[5] K. Hattori, T. Kitagawa, M. Oguma, Y. Ohmori, and M. Horiguchi. *Erbium-Doped Silica-Based Wave-Guide Amplifier Integrated with a 980/1530nm WDM Coupler. Electron Lett*, **30**:856, 1994.

[6] W. Huang and R. R. A. Syms. *Sol-gel silica-on-silicon buried-channel EDWAs. J Lightwave Technol*, **21**:1339, 2003.

[7] T. Kitagawa, K. Hattori, K. Shuto, M. Yasu, M. Kobayashi, and M. Horiguchi. Amplification in erbium-doped silica-based planar lightwave circuits. *Electron Lett*, **28**:1818, 1992.

[8] S. Kogahara, S. Shinada, S. Nakajima, T. Kawanishi, H. Nakajima, and M. Izutsu. *Optical amplification characteristics of Ti-diffused waveguides on Erbium-doped $LiNbO_3$ crystal. IEICE Electron Expr*, **4**:134, 2007.

[9] R. Schermer, W. Berglund, C. Ford, R. Ramberg, and A. Gopinath. *Optical amplification at 1534 nm in erbium-doped zirconia waveguides. J Quant Elect*, **39**:154, 2003.

[10] W. H. Wong, E. Y. B. Pun, and K. S. Chan. *Er^{3+}-Yb^{3+} codoped polymeric optical waveguide amplifiers. Appl Phys Lett*, **84**:176, 2004.

[11] Y. C. Yan, A. J. Faber, H. deWaal, P. G. Kik, and A. Polman. *Erbium-doped phosphate glass waveguide on silicon with 4.1 dB/cm gain at 1.535 μm. Appl Phys Lett*, **71**:2922, 1997.

[12] H. Ebendorff-Heidepriem, D. Ehrt, M. Bettinelli, and A. Speghini. *Effect of glass composition on Judd-Ofelt parameters and radiative decay rates of Er^{3+} fluoride phosphate and phosphate glasses. J Non-Cryst Solids*, **240**:66, 1998.

[13] A. J. Kenyon. *Recent developments in rare-earth doped materials for optoelectronics. Prog Quant Electron*, **26**:225, 2002.

[14] G. C. Righini and M. Ferrari. *Photoluminescence of rare-earth-doped glasses. Riv Nuovo Cimento*, **28**:1, 2005.

[15] W. J. Miniscalco and R. S. Quimby. *General Procedure for the Analysis of Er^{3+} Cross-Sections. Opt Lett*, **16**:258, 1991.

[16] X. L. Zou and H. Toratani. *Evaluation of spectroscopic properties of Yb^{3+}-doped glasses. Phys Rev B*, **52**:15889, 1995.

[17] E Desurvire. Erbium doped fibre amplfier:principles and applications. John Wiley & Sons, Inc, 1995.

[18] A. Lidgard, A. Polman, D. C. Jacobsen, G. E. Blonder, R. Kistler, J. M. Poate, and P. C. Becker. *Fluorescence Lifetime Studies of Mev Erbium Implanted Silica Glass. Electron Lett*, **27**:993, 1991.

[19] F. Auzel and P. Goldner. *Towards rare-earth clustering control in doped glasses. Opt Mater*, **16**:93, 2001.

[20] F. Auzel. *Upconversion and anti-stokes processes with f and d ions in solids. Chem Rev*, **104**:139, 2004.

[21] C. Y. Chen, R. R. Petrin, D. C. Yeh, W. A. Sibley, and J. L. Adam. *Concentration-Dependent Energy-Transfer Processes in Er^{3+}-Doped and Tm^{3+}-Doped Heavy-Metal Fluoride Glass. Opt Lett*, **14**:432, 1989.

[22] M. Federighi and F. Dipasquale. *The Effect of Pair-Induced Energy-Transfer on the Performance of Silica Wave-Guide Amplifiers with High Er^{3+}/Yb^{3+} Concentrations. Photon Tech Lett.*, **7**:303, 1995.

[23] W. Q. Shi, M. Bass, and M. Birnbaum. *Effects of Energy-Transfer among Er^{+3} Ions on the Fluorescence Decay and Lasing Properties of Heavily Doped Er-$Y_3Al_5O_{12}$. J Opt Soc Am B*, **7**:1456, 1990.

[24] G. N. vandenHoven, E. Snoeks, A. Polman, C. vanDam, J. W. M. vanUffelen, and M. K. Smit. *Upconversion in Er-implanted Al_2O_3 waveguides. J Appl Phys*, **79**: 1258, 1996.

[25] K. Arai, H. Namikawa, K. Kumata, T. Honda, Y. Ishii, and T. Handa. Aluminum or phosphorus co-doping effects on the fluorescence and structural-properties of neodymium-doped silica glass. *J Appl Phys*, **59**:3430, 1986.

[26] S. Berneschi, M. Bettinelli, M. Brenci, G. N. Conti, S. Pelli, S. Sebastiani, C. Siligardi, A. Speghini, and G. C. Righini. *Aluminum co-doping of soda-lime silicate glasses: Effect on optical and spectroscopic properties. J Non-Cryst Solids*, **351**: 1747, 2005.

[27] A. Monteil, S. Chaussedent, G. Alombert-Goget, N. Gaumer, J. Obriot, S. J. L. Ribeiro, Y. Messaddeq, A. Chiasera, and M. Ferrari. *Clustering of rare earth in glasses, aluminum effect: experiments and modeling. J Non-Cryst Solids*, **348**:44, 2004.

[28] A. Polman and F. C. J. M. van Veggel. *Broadband sensitizers for erbium-doped planar optical amplifiers: review. J Opt Soc Am B*, **21**:871, 2004.

[29] M. J. Lochhead and K. L. Bray. *Rare-Earth Clustering and Aluminum Codoping in Sol-Gel Silica - Investigation Using Europium(Iii) Fluorescence Spectroscopy. Chem Mater*, **7**:572, 1995.

[30] P. Goldner, B. Schaudel, M. Prassas, and F. Auzel. *Influence of the host structure and doping precursors on rare earth clustering in phosphate glasses analysed by co-operative luminescence. J Lumin*, **87-89**:688, 2000.

[31] F. Rocca, M. Ferrari, A. Kuzmin, N. Daldosso, C. Duverger, and F. Monti. *EXAFS studies of the local structure of Er^{3+} ions in silica xerogels co-doped with aluminium. J Non-Cryst Solids*, **293**:112, 2001.

[32] K. Hattori, T. Kitagawa, M. Oguma, H. Okazaki, and Y. Ohmori. *Optical amplification in Er^{3+}-doped P_2O_5-SiO_2 planar waveguides. J Appl Phys*, **80**:5301, 1996.

[33] W. J. Miniscalco. *Erbium-Doped Glasses for Fiber Amplifiers at 1500 nm. J Lightwave Technol*, **9**:234, 1991.

[34] H. Yamauchi, G. S. Murugan, and Y. Ohishi. *Optical properties of Er^{3+} and Tm^{3+} ions in a tellurite glass. J Appl Phys*, **97**:043505, 2005.

[35] S. Shen, A. Jha, E. Zhang, and S. J. Wilson. *Compositional effects and spectroscopy of rare earths (Er^{3+}, Tm^{3+}, and Nd^{3+}) in tellurite glasses. Cr Chim*, **5**:921, 2002.

[36] J. F. Philipps, T. Topfer, H. Ebendorff-Heidepriem, D. Ehrt, and R. Sauerbrey. *Energy transfer and upconversion in erbium-ytterbium-doped fluoride phosphate glasses. Appl Phys B*, **74**:233, 2002.

[37] J. C. Wright. *Up-conversion and excited-state energy transfer in rare-earth doped materials.* In F. K. Fong, editor, *Topics in Applied Physics*, volume **15**, page 239. Springer, New York, 1976.

[38] R. S. Quimby, W. J. Miniscalco, and B. Thompson. *Clustering in Erbium-Doped Silica Glass-Fibers Analyzed Using 980 nm Excited-State Absorption. J Appl Phys*, **76**:4472, 1994.

[39] M. P. Hehlen, N. J. Cockroft, T. R. Gosnell, A. J. Bruce, G. Nykolak, and J. Shmulovich. *Uniform upconversion in high-concentration Er^{3+}-doped soda lime silicate and aluminosilicate glasses. Opt Lett*, **22**:772, 1997.

[40] F. Dipasquale and M. Federighi. *Modeling of Uniform and Pair-Induced up-Conversion Mechanisms in High-Concentration Erbium-Doped Silica Wave-Guides. J Lightwave Technol*, **13**:1858, 1995.

[41] J. Nilsson, B. Jaskorzynska, and P. Blixt. *Performance Reduction and Design Modification of Erbium-Doped Fiber Amplifiers Resulting from Pair-Induced Quenching. Photon Tech Lett*, **5**:1427, 1993.

[42] H. Masuda, A. Takada, and K. Aida. *Modeling the Gain Degradation of High-Concentration Erbium-Doped Fiber Amplifiers by Introducing Inhomogeneous Cooperative up-Conversion. J Lightwave Technol*, **10**:1789, 1992.

[43] P. Myslinski, D. Nguyen, and J. Chrostowski. *Effects of concentration on the performance of erbium-doped fiber amplifiers. J Lightwave Technol*, **15**:112, 1997.

[44] T. Ohtsuki, S. Honkanen, S. I. Najafi, and N. Peyghambarian. *Cooperative upconversion effects on the performance of Er^{3+}-doped phosphate glass waveguide amplifiers. J Opt Soc Am B*, **14**:1838, 1997.

[45] P. G. Kik and A. Polman. *Cooperative upconversion as the gain-limiting factor in Er doped miniature Al_2O_3 optical waveguide amplifiers. J Appl Phys*, **93**:5008, 2003.

[46] J. L. Philipsen, J. Broeng, A. Bjarklev, S. Helmfrid, D. Bremberg, B. Jaskorzynska, and B. Palsdottir. *Observation of strongly nonquadratic homogeneous upconversion in Er^{3+}-doped silica fibers and reevaluation of the degree of clustering. J Quant Electron*, **35**:1741, 1999.

[47] K. Suh, M. Lee, J. S. Chang, H. Lee, N. Park, G. Y. Sung, and J. H. Shin. *Cooperative upconversion and optical gain in ion-beam sputter-deposited $Er_xY_{2-x}SiO_5$ waveguides. Opt Exp*, **18**:7724, 2010.

[48] E. Snoeks, G. N. Vandenhoven, A. Polman, B. Hendriksen, M. B. J. Diemeer, and F. Priolo. *Cooperative up-Conversion in Erbium-Implanted Soda-Lime Silicate Glass Optical Wave-Guides. J Opt Soc Am B*, **12**:1468, 1995.

[49] Y. D. Hu, S. B. Jiang, G. Sorbello, T. Luo, Y. Ding, B. C. Hwang, J. H. Kim, H. J. Seo, and N. Peyghambarian. *Numerical analyses of the population dynamics and determination of the upconversion coefficients in a new high erbium-doped tellurite glass. J Opt Soc Am B*, **18**:1928, 2001.

[50] G. C. Jones and S. N. Houde-Walter. *Determination of the macroscopic upconversion parameter in Er^{3+}-doped transparent glass ceramics. J Opt Soc Am B*, **23**: 1600, 2006.

[51] R. S. Quimby. *Output Saturation in a 980 nm Pumped Erbium-Doped Fiber Amplifier. Appl Opt*, **30**:2546, 1991.

[52] S. V. Sergeyev and B. Jaskorzynska. *Statistical model for energy-transfer-induced up-conversion in Er^{3+}-doped glasses. Phys Rev B*, **62**:15628, 2000.

[53] D. A. Zubenko, M. A. Noginov, V. A. Smirnov, and I. A. Shcherbakov. *Different mechanisms of nonlinear quenching of luminescence. Phys Rev B*, **55**:8881, 1997.

[54] N. Nikonorov, A. Przhevuskii, M. Prassas, and D. Jacob. *Experimental determination of the upconversion rate in erbium-doped silicate glasses. Appl Opt*, **38**:6284, 1999.

[55] A. J. Silversmith, W. Lenth, and R. M. Macfarlane. *Green Infrared-Pumped Erbium Upconversion Laser. Appl Phys Lett*, **51**:1977, 1987.

[56] T. J. Whitley, C. A. Millar, R. Wyatt, M. C. Brierley, and D. Szebesta. *Upconversion Pumped Green Lasing in Erbium Doped Fluorozirconate Fiber. Electron Lett*, **27**:1785, 1991.

[57] R. Paschotta, P. R. Barber, A. C. Tropper, and D. C. Hanna. *Characterization and modeling of thulium:ZBLAN blue upconversion fiber lasers. J Opt Soc Am B*, **14**: 1213, 1997.

[58] R. Paschotta, N. Moore, W. A. Clarkson, A. C. Tropper, D. C. Hanna, and G. Maze. *230 mW of blue light from a thulium-doped upconversion fiber laser. J Sel Top Quant*, **3**:1100, 1997.

[59] A. C. Tropper, J. N. Carter, R. D. T. Lauder, D. C. Hanna, S. T. Davey, and D. Szebesta. *Analysis of Blue and Red Laser Performance of the Infrared-Pumped Praseodymium-Doped Fluoride Fiber Laser. J Opt Soc Am B*, **11**:886, 1994.

[60] P. Xie and T. R. Gosnell. *Room-Temperature up-Conversion Fiber Laser Tunable in the Red, Orange, Green, and Blue Spectral Regions. Opt Lett*, **20**:1014, 1995.

[61] J. Y. Allain, M. Monerie, and H. Poignant. *Room-Temperature CW Tunable Green Upconversion Holmium Fiber Laser. Electron Lett*, **26**:261, 1990.

[62] P. G. Kik and A. Polman. *Erbium doped optical-waveguide amplifiers on silicon. Mrs Bull*, **23**:48, 1998.

[63] J. E. Roman, M. Hempstead, C. C. Ye, S. Nouh, P. Camy, P. Laborde, and C. Lerminiaux. *1.7 μm Excited-State Absorption Measurement in Erbium-Doped Glasses. Appl Phys Lett*, **67**:470, 1995.

[64] A. Polman. *Erbium implanted thin film photonic materials. J Appl Phys*, **82**:1, 1997.

[65] M. Lipson. *Guiding, modulating, and emitting light on silicon - Challenges and opportunities. J Lightwave Technol*, **23**:4222, 2005.

[66] G. L. Bona. *Integrated optical planar waveguide components. Microsyst Technol*, **9**: 291, 2003.

[67] R. L. Espinola, R. U. Ahmad, F. Pizzuto, M. J. Steel, and R. M. Osgood. *A study of high-index-contrast 90 degrees waveguide bend structures. Opt Exp*, **8**:517, 2001.

[68] D. Liang, J. S. Wang, and D. C. Hall. *Single-facet folded-cavity diode laser with ultrasmall bend radius high-index-contrast oxidized AlGaAs ridge waveguide. Photon Tech Lett*, **19**:598, 2007.

[69] A. S. Liu and M. Paniccia. *Advances in silicon photonic devices for silicon-based optoelectronic applications. Physica E*, **35**:223, 2006.

[70] C. Strohhofer and A. Polman. *Relationship between gain and Yb^{3+} concentration in Er^{3+}-Yb^{3+} doped waveguide amplifiers. J Appl Phys*, **90**:4314, 2001.

[71] C. Strohhofer and A. Polman. *Absorption and emission spectroscopy in Er^{3+}-Yb^{3+} doped aluminum oxide waveguides. Opt Mater*, **21**:705, 2003.

[72] R. Osellame, S. Taccheo, G. Cerullo, M. Marangoni, D. Polli, R. Ramponi, P. Laporta, and S. De Silvestri. *Optical gain in Er-Yb doped waveguides fabricated by femtosecond laser pulses. Electron Lett*, **38**:964, 2002.

[73] D. L. Veasey, D. S. Funk, P. M. Peters, N. A. Sanford, G. E. Obarski, N. Fontaine, M. Young, A. P. Peskin, W. C. Liu, S. N. Houde-Walter, and J. S. Hayden. *Yb/Er-codoped and Yb-doped waveguide lasers in phosphate glass. J Non-Cryst Solids*, **263**: 369, 2000.

[74] N. Daldosso, D. Navarro-Urrios, M. Melchiorri, L. Pavesi, F. Gourbilleau, M. Carrada, R. Rizk, C. Garcia, P. Pellegrino, B. Garrido, and L. Cognolato. *Absorption cross section and signal enhancement in Er-doped Si nanocluster rib-loaded waveguides. Appl Phys Lett*, **86**, 2005.

[75] G. Della Valle, S. Taccheo, G. Sorbello, E. Cianci, V. Foglietti, and R. Laporta. *Compact high gain erbium-ytterbium doped waveguide amplifier fabricated by Ag-Na ion exchange. Electron Lett*, **42**:632, 2006.

[76] P. Camy, J. E. Roman, F. W. Willems, M. Hempstead, J. C. vanderPlaats, C. Prel, A. Beguin, A. M. J. Koonen, J. S. Wilkinson, and C. Lerminiaux. *Ion-exchanged planar lossless splitter at 1.5 μm. Electron Lett*, **32**:321, 1996.

[77] J. E. Roman, P. Camy, M. Hempstead, W. S. Brocklesby, S. Nouh, A. Beguin, C. Lerminiaux, and J. S. Wilkinson. *Ion-Exchanged Er/Yb Wave-Guide Laser at 1.5 μm Pumped by Laser-Diode. Electron Lett*, **31**:1345, 1995.

[78] G. N. vandenHoven, R. J. I. M. Koper, A. Polman, C. vanDam, J. W. M. vanUffelen, and M. K. Smit. *Net optical gain at 1.53 μm in Er-doped Al_2O_3 waveguides on silicon. Appl Phys Lett*, **68**:1886, 1996.

[79] F. Ondracek, J. Jagerska, L. Salavcova, M. Mika, J. Spirkova, and J. Ctyroky. *Er-Yb waveguide amplifiers in novel silicate glasses. J Quant Elect*, **44**:536, 2008.

[80] K. Hattori, T. Kitagawa, M. Oguma, M. Wada, J. Temmyo, and M. Horiguchi. *Erbium-Doped Silica-Based Planar Wave-Guide Amplifier Pumped by 0.98 μm Laser-Diodes. Electron Lett*, **29**:357, 1993.

[81] K. Vu and S. Madden. *Tellurium dioxide Erbium doped planar rib waveguide amplifiers with net gain and 2.8dB/cm internal gain. Opt Exp*, **18**:19192, 2010.

[82] A. V. Chelnokov, J. M. Lourtioz, P. Boucaud, H. Bernas, J. Chaumont, and T. Plowman. *Deep High-Dose Erbium Implantation of Low-Loss Silicon Oxynitride Wave-Guides. Electron Lett*, **30**:1850, 1994.

[83] S. Saini. Gain efficient waveguide optical amplfiers for Si microphotonics. PhD thesis, 2004.

[84] N. Maeda, N. Wada, H. Onoda, A. Maegawa, and K. Kojima. *Preparation and optical properties of sol-gel derived Er^{3+}-doped Al_2O_3-Ta_2O_5 films. Opt Mater*, **27**: 1851, 2005.

[85] H. Rigneault, F. Flory, S. Monneret, S. Robert, and L. Roux. *Fluorescence of Ta_2O_5 thin films doped by kilo-electron-volt Er implantation: Application to microcavities. Appl Opt*, **35**:5005, 1996.

[86] R. Germann, H. W. M. Salemink, R. Beyeler, G. L. Bona, F. Horst, I. Massarek, and B. J. Offrein. *Silicon oxynitride layers for optical waveguide applications. J Electrochem Soc*, **147**:2237, 2000.

[87] O. Lumholt, H. Bernas, A. Chabli, J. Chaumont, G. Grand, and S. Valette. *Low-Energy Erbium Implanted $Si_3N_4/SiO_2/Si$ Wave-Guides. Electron Lett*, **28**:2242, 1992.

[88] J.G. Sandland. Sputtered silicon oxynitride for microphotonics: A materials study. PhD thesis, 2005.

[89] G. L. Bona, R. Germann, and B. J. Offrein. *SiON high-refractive-index waveguide and planar lightwave circuits. IBM J Res Dev*, **47**:239, 2003.

[90] K. Kojima, S. Yoshida, and H. Shiraishi. *Green upconversion fluorescence in Er^{3+}-doped Ta_2O_5 heated gel. Appl Phys Lett*, **67**, 1995.

[91] B. Unal, M. C. Netti, M. A. Hassan, P. J. Ayliffe, M. D. B. Charlton, F. Lahoz, N. M. B. Perney, D. P. Shepherd, C. Y. Tai, J. S. Wilkinson, and G. J. Parker. *Neodymium-doped tantalum pentoxide waveguide lasers. J Quant Electron*, **41**:1565, 2005.

Chapter 3

Numerical Modelling and Analysis of Gain in Er:Ta_2O_5 Waveguides

EDWAs are increasingly becoming important components for metro networks and FTTHs. EDWAs can provide high gain over a small length, low noise and can be easily integrated with other optical devices such as waveguides, fibres, light sources etc. EDWAs have been realised in many host materials [1–11] in the past but recently there has been a surge of interest in erbium doped HIC materials [8–18] as they can provide high gain with low pump threshold due to tight mode confinement that can also lead to compact photonic devices. Gain in an EDWA is dependent on the concentration of the erbium ions but, due to small length of the device, erbium ions interact with each other through processes like CUC [19–23] and PIQ [24–27], resulting in the reduction of the gain and increase in the pump threshold. EDWAs have been studied for a long time and using many theoretical models - finite element [28–30], beam propagation [31], numerical integration [32–39] and analytical solutions [40–44] in the past to improve and analyse the EDWA's performance. In this chapter, the gain of a tantala based EDWA is analysed using numerical integration along the waveguide. The effect of parameters such as pump power, length of the device, ion concentration and co-operative upconversion, on the performance of EDWA is derived and analysed.

3.1 The Amplifier Model and Theory

The erbium ions participating in process of amplification can be described by the energy level diagram shown in Fig 3.1. For the experiments, 977 nm pump wavelength was used and from here on this pump wavelength will be used for all calculations. When pumped at 977 nm, the erbium ions in the $^4I_{15/2}$ level are pumped to the $^4I_{11/2}$ level, with a pumping rate W_{13} and from here the ions rapidly decay non-radiatively (A_{32}=$1/\tau_{32}$) to the metastable state $^4I_{13/2}$ where the erbium ions starts to build up because the lifetime of this level is typically long (few ms). τ_{32} is typically few to hundreds of μs and depends on the phonon spectrum of the host material. The lifetime of higher lying levels is very short ($< 1\mu s$) [33, 45] and the ions non-radiatively decay to one these three levels and the present discussion was limited to a 3-level erbium system only.

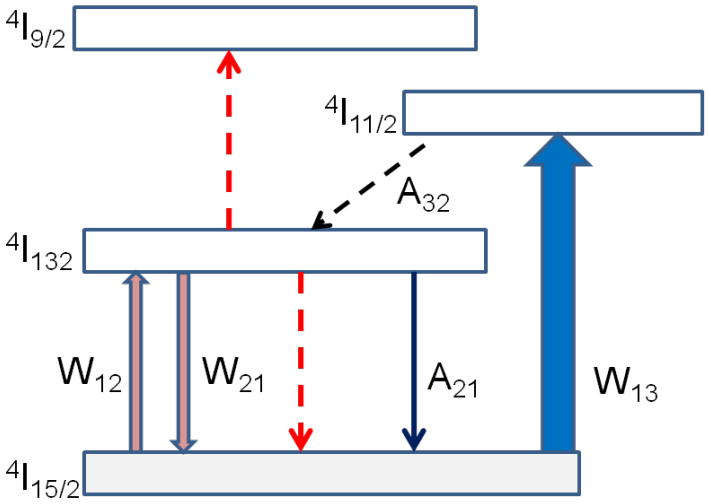

FIGURE 3.1: Typical pump and signal transitions in an erbium ion. The red arrows indicate the cooperative upconversion process.

In order to describe the amplification process, the interaction between the light and erbium ions must be described. This can be done by writing the rate equations for the erbium ion at different participating levels, that describe the change in the population of the ions due to different excitations. Let n_1, n_2, n_3 be the fractions of population of the erbium ions in $^4I_{15/2}$, $^4I_{13/2}$, $^4I_{11/2}$ levels respectively and N_t be the total erbium concentration. Then the following can be written [33]

$$\frac{dn_1}{dt} = -W_{13}n_1 + W_{21}n_2 - W_{12}n_1 + \frac{n_2}{\tau_{21}} + N_t C_{up} n_2^2 \tag{3.1}$$

$$\frac{dn_2}{dt} = W_{12}n_1 - W_{21}n_2 - \frac{n_2}{\tau_{21}} - 2N_tC_{up}n_2^2 + \frac{n_3}{\tau_{32}} \tag{3.2}$$

$$\frac{dn_3}{dt} = W_{13}n_1 + N_tC_{up}n_2^2 - \frac{n_3}{\tau_{32}} \tag{3.3}$$

where the symbols have the following definitions

$$W_{13} = I_p\sigma_{13}^p/h\nu_p \tag{3.4}$$

W_{13} is the pumping rate at the pump wavelength;

I_p is the pump intensity

h is the Planck's constant; σ_{13}^p is the absorption cross section at the pump wavelength and ν_p is the pump frequency

$$W_{12} = I_s\sigma_{12}^s/h\nu_s \tag{3.5}$$

W_{12} is the absorption rate at the signal wavelength;

I_s is the signal intensity

σ_{12}^s is the absorption cross section at the signal wavelength & ν_s is the signal frequency

$$W_{21} = I_s\sigma_{21}^s/h\nu_s \tag{3.6}$$

W_{21} is the stimulated emission rate at signal wavelength and σ_{21}^s is the emission cross section at signal wavelength. τ_{21} & τ_{32} are the lifetimes of the excited erbium ions in $^4I_{13/2}$ and $^4I_{11/2}$ levels respectively. C_{up} is the up-conversion coefficient of erbium ions in the host material.

The upconversion process is indicated by the red arrows in Fig 3.1. It involves two erbium ions in the $^4I_{13/2}$ level interacting with each other, forcing one to drop down to the $^4I_{15/2}$ level and while the other is excited to the $^4I_{9/2}$ level, from where it non-radiatively decays to $^4I_{11/2}$ or $^4I_{13/2}$. In the present model only uniform upconversion is considered. Other quenching effects such as higher order co-operative upconversion and clustering [24–27, 46, 47], which leads to pairing of erbium ions, are not taken into account. Further, the intensities (pump and signal) change along the length of waveguide (in z direction) according to the absorption and emission of pump and signal at those wavelengths. $N_t(x, y)$ is the total erbium population and is not dependent on z but $N_1(x, y, z)$, $N_2(x, y, z)$, $N_3(x, y, z)$ are z dependent quantities such that in steady state

$$N_t(x, y) = N_1(x, y, z) + N_2(x, y, z) + N_3(x, y, z) \tag{3.7}$$

$\mathrm{n}_i = \dfrac{N_i(x, y, z)}{N_t(x, y)}$, such that

$$\sum_i n_i = 1 \tag{3.8}$$

where i = 1, 2, 3.

For a given pump and signal intensity, Eq. (3.1 - 3.4) & Eq. (3.8) can be solved in steady state ($dn_i/dt = 0$) to calculate the population of erbium ions in different energy levels. The fraction of erbium ions in different energy level changes only along the length of the waveguide (z) according to the change in the pump and signal intensities. In the steady state, the rate equations above reduces to the following

$$(2C_{up}N_t)n_2^2 + (W_{12} + W_{21} + (1/\tau_{21}) + (W_{13}\,(1 - W_{12}\tau_{32}))\,/\,(1 + W_{13}\tau_{32}))\,n_2 - \frac{W_{12} + W_{13}}{1 + W_{13}\tau_{32}} = 0 \tag{3.9}$$

If the following substitutions are used:

$$a = 2C_{up}N_t \tag{3.10}$$

$$b = W_{12} + W_{21} + \frac{1}{\tau_{21}} + \frac{W_{13}(1 - W_{12}\tau_{32})}{1 + W_{13}\tau_{32}} \tag{3.11}$$

$$c = -\frac{W_{12} + W_{13}}{1 + W_{13}\tau_{32}} \tag{3.12}$$

Eq. (3.9) is found to be a standard quadratic equation and its roots can be found by finding the discriminant (D) of the equation that is given by the following relation

$$D = b^2 - 4ac \tag{3.13}$$

The real roots or the solution for the above quadratic equation is given by the following relation

$$n_2 = \frac{-b + \sqrt{D}}{2a} \tag{3.14}$$

Substituting the values of a,b, and c yields the following equation for $n_2(z)$

$$n_2 = -\frac{W_{12} + W_{21} + \frac{1}{\tau_{21}} + \frac{W_{13}(1 - W_{12}\tau_{32})}{1 + W_{13}\tau_{32}}}{4C_{up}N_t} + \frac{\sqrt{\left(W_{12} + W_{21} + \frac{1}{\tau_{21}} + \frac{W_{13}(1 - W_{12}\tau_{32})}{1 + W_{13}\tau_{32}}\right)^2 + 8C_{up}N_t\frac{W_{12} + W_{13}}{1 + W_{13}\tau_{32}}}}{4C_{up}N_t} \tag{3.15}$$

From Eq. (3.3) & Eq. (3.9) n_3 can be written as

$$n_3 = W_{13}\tau_{32}\frac{(1 - n_2)}{1 + W_{13}\tau_{32}} \tag{3.16}$$

& from Eq. (3.8)

$$n_1 = 1 - n_2 - n_3 \tag{3.17}$$

n_1, n_2, & n_3 varies along the length of the waveguide. The light propagation in the waveguide can be analysed by calculating the evolution of pump and signal power along the length of the waveguide. If P_p and P_s are the pump and signal power inside the waveguide then [28, 33]

$$dP_p\left(z\right)/dz = \left(-\alpha_p + \left(\sigma_{31}n_3\left(z\right) - \sigma_{13}n_1\left(z\right)\right)\Gamma_p N_t\right)P_p\left(z,\nu_p\right) \tag{3.18}$$

$$dP_s\left(z\right)/dz = \left(-\alpha_s + \left(\sigma^s_{21}n_2\left(z\right) - \sigma^s_{12}n_1\left(z\right)\right)\Gamma_s N_t\right)P_s\left(z,\nu_s\right) \tag{3.19}$$

$$g(z) = \left(dP_s/dz\right)/P_s\left(z\right) = \left(-\alpha_s + \left(\sigma^s_{21}n_2\left(z\right) - \sigma^s_{12}n_1\left(z\right)\right)\Gamma_s N_t\right) \tag{3.20}$$

$\alpha_{p,s}$:Propagation loss of the waveguide at pump and signal wavelength

$\Gamma_{p,s}$: Overlap factor of pump and signal intensity with erbium ion distribution

$g\left(z\right)$: Gain of the amplifier

The evolution of amplified spontaneous emission (ASE) may also be included along with the pump and signal power to calculate the noise in the amplifier. In order to do that the evolution of P_{ASE} needs to be calculated for each Δz, for each spectral component of the ASE on the entire ASE spectrum. This calculation usually takes long and for all practical purposes, for small signal gain ($<$ 20 dB) amplifiers ASE can be neglected [11, 39, 41, 48–50] and the pump and signal evolution along the length of the waveguide is sufficient to understand the gain dynamics of the amplifier to design the amplifier with optimum performance.

To evaluate the gain the pump and signal power evolution is calculated. The evolution of pump and signal depends on the excited erbium ion distribution which in turn depends on the pump and signal intensities at particular z, therefore to calculate gain the equations were solved numerically and the following steps were followed to solve the equations Eq. (3.18 - 3.20)

- Initial values were attributed to pump ($P_p(0)$) , signal ($P_s(0)$) power at the start of the waveguide ($z = 0$)
- The total length of the waveguide was broken into small segments of Δz, i.e. from $z = 0$ to $z = L$ in steps of Δz
- The initial erbium population in different levels ($n_i(z)$) were determined at $z = 0$ for P_{p0} and P_{s0} using Eq. (3.15, 3.16, 3.17)

- Using COMSOL, mode profile at signal and pump wavelength and the overlap with the active region was calculated. This mode profile is not dependent on z.
- Eq. (3.18 - 3.20) were solved at z=0 with initial values $P_p(0)$, $P_s(0)$, and n_i along the waveguide length leading to new value of $P_p(z+\Delta z)$, $P_s(z+\Delta z)$ & $g(z+\Delta z)$ at each interval of Δz

$$P_p(z+\Delta z) = P_p(z) + (-\alpha_p + (\sigma_{31} n_3(z) - \sigma_{13} n_1(z))\,\Gamma_p N_t)\,P_p(z,\nu_p)\,.\Delta z \quad (3.21)$$

$$P_s(z+\Delta z) = P_s(z) + (-\alpha_s + (\sigma^s_{21} n_2(z) - \sigma^s_{12} n_1(z))\,\Gamma_s N_t)\,P_s(z,\nu_s)\,.\Delta z \quad (3.22)$$

$$g(z+\Delta z) = g(z) + (-\alpha_s + (\sigma^s_{21} n_2(z) - \sigma^s_{12} n_1(z))\,\Gamma_s N_t)\,.\Delta z \quad (3.23)$$

- Once $P_p(z+\Delta z)$ & $P_s(z+\Delta z)$ are calculated then the new values of $n_i(z+\Delta z)$ were calculated which were then used to calculate new $P_p(z)$, $P_s(z)$ & $g(z)$. These steps were repeated until $z = L$, the end of the waveguide was reached.
- Finally, the whole sequence of equations was iterated for number of times until the difference between the two successive iterations, for the gain was less than 10^{-8} nepers/cm.

3.2 Simulations

The parameters used for the simulation are shown in the Table 3.1. A rib waveguide of cross section $\left(2 \times 2\mu m^2\right)$ was used for the simulation as shown in Fig 3.2a. The signal and pump intensity profile, and their overlap was calculated with the help of commercially available *COMSOL* software and is shown in Fig 3.2(b). The HIC between the core and cladding (~ 0.65) renders $> 95\%$ overlap between the pump and signal mode in the doped region of the waveguide. Based on the overlap ($> 95\%$) between pump and signal mode and the rib waveguide design, $\Gamma_{p,s}$ was estimated to be $> 85\%$ with power propagating in SiO_2 being ignored.

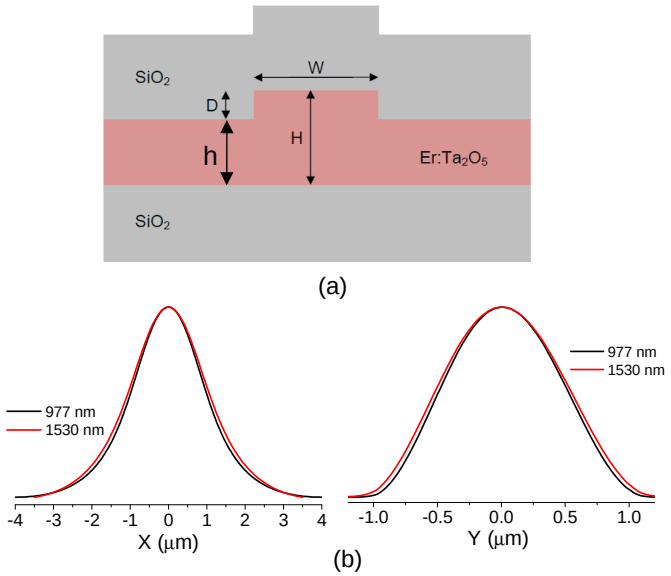

FIGURE 3.2: a) Schematic of the rib waveguide used for simulation. H (2 μm) is the rib height, W (2 μm) is the width of the waveguide, D (400 nm) is the etch depth. b) Shows the simulated mode intensity profile for a rib waveguide shown in (a) along with the simulated mode profile at 977 nm (black) and 1530 nm (red) in X and Y direction respectively.

Fig 3.3 shows the measured absorption cross-section of the erbium ions along with the calculated emission cross-sections over a wavelength range of 1460-1580 nm. The emission cross-section was calculated using McCumber theory [51] as discussed in chapter 4.

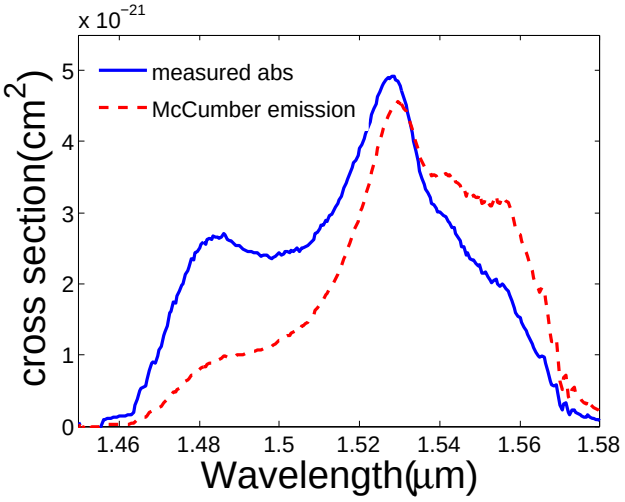

FIGURE 3.3: Absorption and emission cross-sections of erbium ions in Ta_2O_5 waveguide. The emission cross-section was calculated from absorption cross-section using McCumber theory.

Parameter	Value
signal absorption cross section at 1527 nm (σ^s_{12})	$4.8\times10^{-21}cm^2$
signal emission cross section at 1527 nm (σ^s_{21})	$4.4\times10^{-21}cm^2$
pump absorption cross section at 977 nm (σ^p_{13})	$2.1\times10^{-21}cm^2$
$^4I_{13/2}$ lifetime (τ_{21})	2.3 ms
$^4I_{11/2}$ lifetime (τ_{32})	30 μs [52]
Waveguide loss at pump (α_p)	0.23 cm^{-1}
Waveguide loss at signal wavelength(α_s)	0.15 cm^{-1}
Active region- core cross-section	$2\times2\mu m^2$
Overlap factor ($\Gamma_{p,s}$)	0.85
Co-operative upconversion (C_{up})	10^{-18}- $10^{-17}cm^3s^{-1}$

TABLE 3.1: Physical parameters used in the simulation of signal gain in Er:Ta_2O_5 waveguides.

The step size (Δz) used for the simulation was 100 μm. The parameters that were kept as design variables were the total erbium concentration (N_t), length of the waveguide (L), input pump power ($P_p(0)$), and input signal power ($P_s(0)$). The EDWA can be optimised for best performance by studying the effect of these design parameters on the gain of the system. The other parameters given in table 2.1 were determined experimentally on the Er:Ta_2O_5waveguides, except for $\tau_{32}(30\mu s)$ and C_{up} values varying between 10^{-18} cm^3s^{-1} and 10^{-17} cm^3s^{-1} were used in this model as fitting parameters and for comparison. The value for τ_{32} which was measured in alumina [52] was used for the model because the phonon energy of alumina [53] and tantala [54] are similar ($\sim$900 cm^{-1}) therefore the erbium ions are expected to be in a similar host environment leading to comparable τ_{32}. There is a linear model for the calculation of upconversion for different erbium concentration [26, 55, 56] that has been used for optimising EDWAs and lasers. To understand the effect of upconversion on gain and lack of experimental or theoretical values of upconversion coefficient for Er:Ta_2O_5 the value of C_{up} was kept constant here for all the concentrations of the erbium ions [25, 33, 57].

3.2.1 Results and Discussion

3.2.1.1 Pump power (P_p)

Fig 3.4a shows the pump power evolution as a function of the propagation length of the

waveguide for different concentration of the total erbium ions, N_t ($\times 10^{20}$ ions/cm^3)= 0.1, 2, 10. As an example to illustrate the effect of erbium concentration on the pump evolution along the length of the waveguide, the pump power was fixed at 1 mW and signal power at $1\mu W$. As the pump light propagates along the waveguide it is continually absorbed leading to reduction in the available pump power for each subsequent distance it covers. With the increase in the erbium concentration, the absorption increases and becomes much stronger as there are more number of erbium ions present in the ground state and therefore for each concentration there is an optimum length of the waveguide to achieve maximum gain from the amplifier. Fig 3.4b demonstrates the pump power evolution for a fixed concentration $\left(N_t = 2.0 \times 10^{20}/cm^3\right)$ and different incident pump power (0.5, 50 and 200 mW). For the sake of clear comparison, the pump power at each propagation length is normalised with respect to the maximum incident pump power. At very low pump power levels (0.5 mW), there is an almost exponential decay of the pump power mainly resulting from the propagation loss at pump wavelength resulting from the unbleached erbium absorption. But with increase in the pump power levels, the bleaching of the erbium absorption increases leading to non-exponential decay of the pump power which also leads to the gain of the signal. In the above illustrations, to keep things simple and to understand the effect of erbium ions on pump power evolution, the effect of upconversion was not taken into consideration.

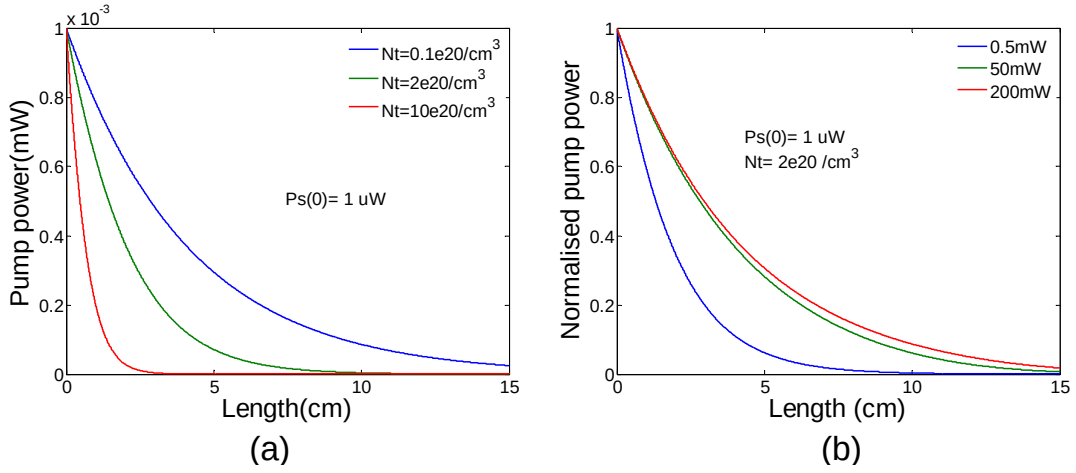

FIGURE 3.4: Evolution of pump power along the length of the waveguide for (a) different erbium concentration $\left(10^{20}cm^{-3}\right)$ with constant pump 1 mW & (b) different pump power with constant erbium concentration $\left(2.0 \times 10^{20}cm^{-3}\right)$. $C_{up} = 0$ & P_s=1 μW are held constant for both calculations.

3.2.1.2 Population inversion fraction (n_2)

The fraction of erbium ions in the $^4I_{13/2}$ level (n_2) plotted as a function of length of the waveguide for different pump powers (0.5, 50 & 200 mW) and fixed total erbium

concentration of 2.0 $\times 10^{20}$ ions/cm^3, is shown in the Fig 3.5. The injected signal power at $z = 0$ was fixed at $1\mu W$. For a fixed pump power, n_2 decreases along the length of the waveguide as the pump is absorbed by erbium ions. At low pump power, n_2 is very low but as the input pump power is increased, the fraction of ions inverted increases as there are more pump photons available for inverting the same population of the erbium ions. Upconversion effects were not taken into consideration for this example but will be discussed later on in this section.

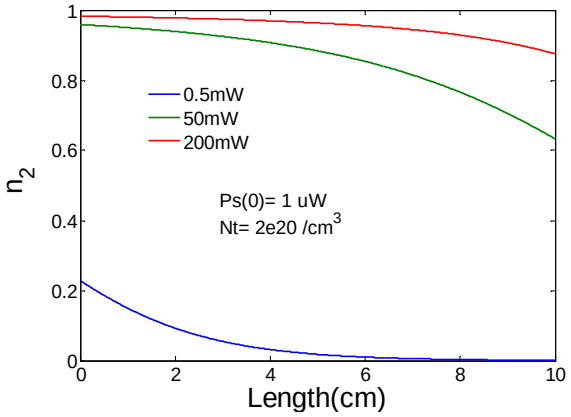

FIGURE 3.5: Variation of population inversion (n_2) with length for different pump power. The erbium concentration was fixed at $2.0\times10^{20}cm^{-3}$,signal power at $1\mu W$ & $C_{up} = 0$

In Fig 3.6, n_2 is plotted as a function of length of the waveguide for different erbium concentrations for a fixed pump power of 50 mW. For a given concentration, the fraction of inverted population decreases along the length of the waveguide as the pump is absorbed so there are fewer pump photons available for each subsequent length of the waveguide to maintain the inversion level . For a low concentration (N_t= 0.1 $\times 10^{20}$/cm^3), the inversion falls from $\sim$ 0.97 the start of the waveguide to $\sim$0.73 over a length of 10 cm. But at higher concentration (N_t= 5 $\times 10^{20}$/cm^3) and the same pump power (50 mW), the n_2 decreases from $\sim$ 0.97 the start of the waveguide to $\sim$0.44 at L= 10 cm. The reason for this can be attributed to the significantly greater number of erbium ions present in the ground state for N_t= 5 $\times 10^{20}$/cm^3 that leads to stronger pump absorption leading to lower inversion fraction values at longer distances.

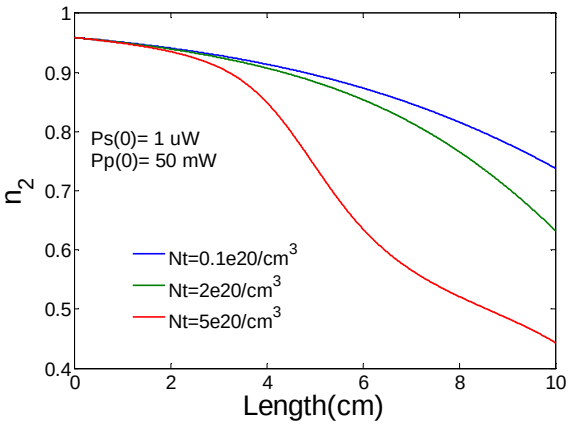

FIGURE 3.6: Variation of population inversion (n_2) along the waveguide for different erbium concentration (0.1, 2, 5 $\times 10^{20}$ions/cm^3) with pump and signal power fixed at 50 mW and 1μW, C_{up}= 0.

So far, in all the results discussed, the effect of upconversion was not considered. In Fig 3.7, to illustrate the effect of upconversion on the inversion level n_2 is plotted versus the length of the waveguide for a fixed N_t (2×10^{20}ions/cm^3), pump power (50 mW), and signal power (1 μW) but different cooperative upconversion coefficients $C_{up}(\times 10^{-18}$ cm^3/s)= 0, 0.1, 1, 10 respectively. The effect of upconversion can be readily seen by comparing Fig 3.6 and Fig 3.7. In Fig 3.6, then n_2 at the start for all concentrations of erbium ions was the same whereas due to the upconversion n_2 decreases with the increase in the C_{up}. For C_{up}= 0, n_2 decreases from ~0.97 at the start of the waveguide to ~ 0.62 at L=10 cm but for C_{up}= 1 $\times 10^{-18}$ cm^3/s, the inversion decreases to less than 0.5 at the end of the waveguide. For higher values of C_{up}= 10 $\times 10^{-18}$ cm^3/s, the n_2 decreases more dramatically to ~0.18 implying that no gain is possible with this length, N_t and pump power in this waveguide. The reason for the decrease is because of the upconversion effects, where two erbium ions exchange energy with each other promoting one of the ions to higher energy levels and the other to the ground level (non-radiatively) thereby decreasing inversion and making pumping inefficient. With an increase in the value of N_t or C_{up}, this interaction increases further leading to further degradation in the inversion levels. In order to achieve net gain in this waveguide with the same N_t and C_{up}, either the length of the waveguide would have to be reduced (n_2(L) > 0.5) or pump power needs to be increased to achieve higher inversion level. The other way would be to reduce N_t so that the upconversion effects reduces which would lead to efficient use of the pump power and therefore higher inversion of erbium ions.

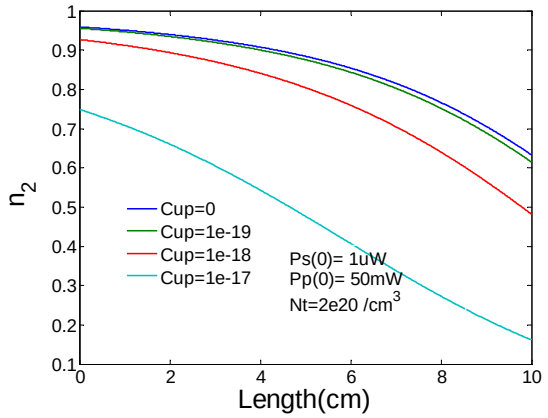

FIGURE 3.7: Variation of population inversion (n_2) along the waveguide for different erbium concentration with different upconversion coefficient values $C_{up}(\times 10^{-18}\text{cm}^3/\text{s})$ = 0, 0.1, 1, 10. The pump power was fixed at 50 mW, N_t= 2 $\times 10^{20}$ ions/cm^3 and the signal power at 1μW.

3.2.1.3 Gain figure (g)

Fig 3.8 shows the gain versus the length of the waveguide for different erbium concentration at a constant pump power of 200 mW, and no upconversion. For N_t=0.1 $\times 10^{20}$ ions/cm^3, no gain is achieved as the concentration is too low to provide any gain for any length of the waveguide. For higher concentration, N_t=2 $\times 10^{20}$ ions/cm^3, a maximum gain of 22 dB is achieved for a 10 cm long waveguide without any sign of saturation because at this concentration the pump power is strong enough to maintain the inversion level to yield signal gain. But for even higher concentration, N_t=5 $\times 10^{20}$ ions/cm^3, gain achieved is much higher at 40 dB for a 9 cm long waveguide. At this length, the system has already achieved the maximum inversion level and any excess pump energy will not increase the gain any further therefore the gain saturates as shown by the red curve in Fig 3.8 . But for longer lengths (not shown in the figure) the gain will then start to decrease as the erbium ions will start to re-absorb the pump leading to loss rather than gain.

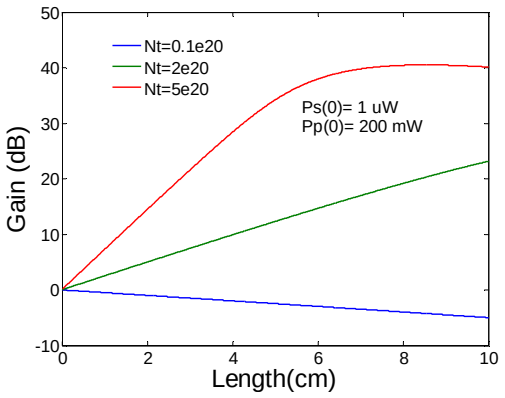

FIGURE 3.8: Gain variation along the waveguide length for different erbium concentration but fixed pump power ($200mW$) & C_{up}= 0. The signal power was fixed at $1\mu W$.

The gain as a function of the propagation length for different pump powers is shown in Fig 3.9a. The erbium concentration was kept constant at 2.0×10^{20} ions/cm^3 and the signal power at 1 μW. If the pump power is sufficient the gain initially grows along the waveguide and reaches its maximum at a certain length and then drops. At higher pump power, higher gain is achieved and is maintained over a longer length of the waveguide. This can be explained by variation of inversion level along the length of the waveguide with the pump power as explained in Fig 3.5. At higher pump powers, higher inversion is achieved and maintained over longer distance and as consequence gain increases with the length and at certain length reaches the saturation. With further increase in the length the inversion level drops and is not enough to provide sufficient gain for amplification. A similar trend is seen when lower pump power is used as shown in Fig 3.9a. For a pump power of 10 mW, the maximum gain and the length for which net gain is obtained is low whereas for higher pump power (200 mW) much higher gain is achieved and the gain does not saturate over a length of 10 cm. Fig 3.9b shows the effect of upconversion on the gain along the length of the waveguide at constant power 200 mW and erbium concentration N_t= 2×10^{20} ions/cm^3, and different C_{up}. At 200 mW with no upconversion, a high level of inversion is achieved as discussed for Fig 3.9a, leading to higher gain (23 dB) over the length of 10 cm as shown by the blue line in Fig 3.9b. As the upconversion increases the the gain starts to saturate at shorter lengths and lower values and any further increase in the length reduces the gain. For example, in Fig 3.9b for C_{up}= 10 $\times10^{-18}$ cm^3/s the maximum gain dramatically reduces from 23 dB (C_{up}= 0) to ~10 dB for a 8 cm long sample and the gain starts to reduce for longer lengths. The reason is again attributed to the energy exchange between the erbium ions at higher upconversion values or higher concentration leading to inefficient use of pump. Thus, it can be concluded that there is an optimal length of the amplifier for each concentration to achieve maximum gain from the amplifier.

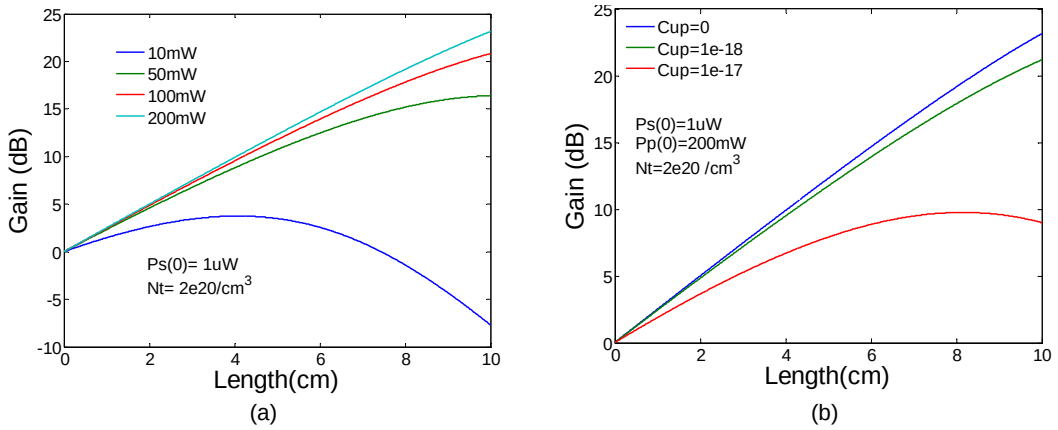

FIGURE 3.9: Gain variation along the waveguide length for (a) different pump powers with fixed erbium concentration $\left(2.0 \times 10^{20} cm^{-3}\right)$ and $C_{up} = 0$ & (b) different $C_{up}(\times 10^{-18} cm^3/s)$= 0, 1, 10 but fixed pump power ($200mW$) & N_t= 2×10^{20} ions/cm^3. The signal power was fixed at $1\mu W$ for both the cases.

Fig 3.10 shows the plot of signal gain versus pump power for different erbium concentrations and optimum length of the waveguide with C_{up}= 5 $\times 10^{-18}$ cm^3/s. The gain in Fig 3.10 was calculated at the optimum length of the waveguide for each concentration (at which gain is maximum). The result depicted in 3.10 shows that higher gain can be achieved for higher concentration but the pump threshold increases with the concentration. For example, for the five different concentrations, the maximum gain of $\sim$ 32 dB is achieved for a waveguide with highest N_t= 10×10^{20} cm^{-3} at 350 mW pump power but it also has the highest pump threshold of $\sim$ 35 mW. This is because for a lower concentration, there are fewer of erbium ions to be inverted along the length of the waveguide so lower pump power is sufficient but with the higher concentration there are more number of erbium ions that requires higher pump power. Another important result that can be deduced from the plot is that of the gain saturation- for a particular concentration one cannot keep increasing the gain by pumping harder as gain saturates after attaining a maximum value. The saturation pump power increases with the increase in the erbium concentration.

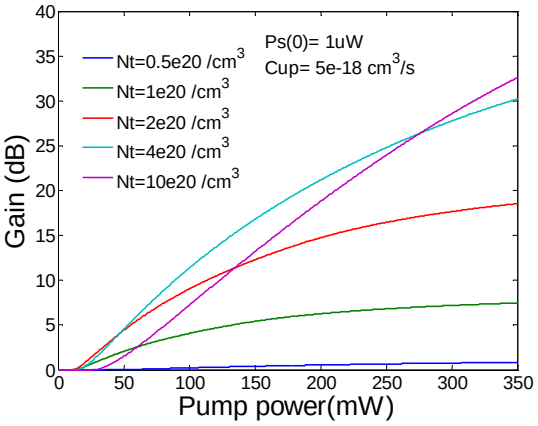

FIGURE 3.10: Dependence of gain on the pump power for different erbium concentration. Signal power and upconversion was fixed at 1 μW and 5 $\times$ 10^{-18} cm^3/s.

Fig 3.11(a, b) shows the gain as a function of erbium concentration with and without upconversion. In order to plot this curve, first the optimum amplifier length for each concentration was evaluated in order to maximise the gain for that concentration. This gain was then plotted against the erbium concentration at different pump powers (10, 100 and 200 mW) as shown in Fig 3.11a. It can be seen from this plot that there does not exist any optimum concentration for any of the three pump powers for maximising the signal gain from the amplifier. This is because the upconversion factor has not been taken into account resulting in the increase in the gain with the erbium concentration. In Fig 3.11b, the same result is plotted with three different C_{up} and the effect of upconversion can be immediately seen as there is an optimum concentration for achieving maximum gain.

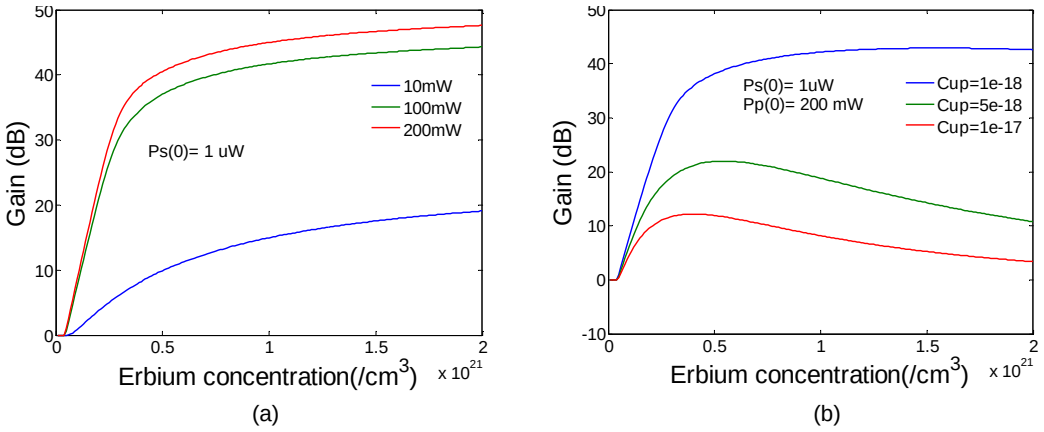

FIGURE 3.11: Signal gain variation with pump power for different erbium concentrations a) without upconversion & b) with different upconversion coefficients C_{up} ($\times 10^{-18}$ cm^3/s) = 1, 5, 10 respectively. The maximum gain at each concentration was calculated at the optimum length of the amplifier.

This result presented in Fig 3.11 is the last and the most important of the performance maps for extracting the optimum performance from the EDWA. The results can be used to predict the erbium concentration and the length of the waveguide for a given pump power and upconversion coefficient that should be used to extract maximum gain from the amplifier. For Er:Ta_2O_5, for a pump power of 200 mW, and signal power of 1 μW, the maximum gain that can be extracted is summarised in Table 3.2 and is extracted from Fig 3.11b. Thus, for the typical upconversion value of 5 $\times 10^{-18}$ cm^3/s as measured in other material [52], a maximum gain of 21.9 dB can be achieved for a waveguide of length 5.8 cm and erbium concentration 5.4 $\times 10^{20}$ $ions/cm^3$. For a reduced upconversion of 1 $\times 10^{-18}$ cm^3/s, the maximum gain that can be achieved dramatically increases to 42.9 dB for a waveguide of length 3.5 cm and erbium concentration as high as 15.5 $\times 10^{20}$ $ions/cm^3$ whereas for a very high value of 10×10^{-18} cm^3/s, the gain reduces to a modest 12.2 dB at a reduced concentration of 4.0 $\times 10^{20}$ $ions/cm^3$.

$C_{up}(\times 10^{-18}$ $cm^3/s)$	$N_t^{opt}(\times 10^{20}$ $ions/cm^3)$	L_{opt} (cm)	G_{max} (dB)
1	15.5	3.5	42.9
5	5.4	5.8	21.9
10	4.0	5.3	12.2

TABLE 3.2: Maximum gain achievable in Er:Ta_2O_5 for a pump power of 200 mW for different cooperative upconversion coefficient

Gain as a function of wavelength is shown in Fig 3.12, it was produced by solving the rate equations and gain evolution for each wavelength using the corresponding absorption and emission cross-sections at those wavelengths. Fig 3.12 shows the gain as a function of wavelength for different pump powers. The maximum gain occurs at 1531 nm and it decreases on either side of it. The curve at 0 mW corresponds to unbleached erbium absorption.

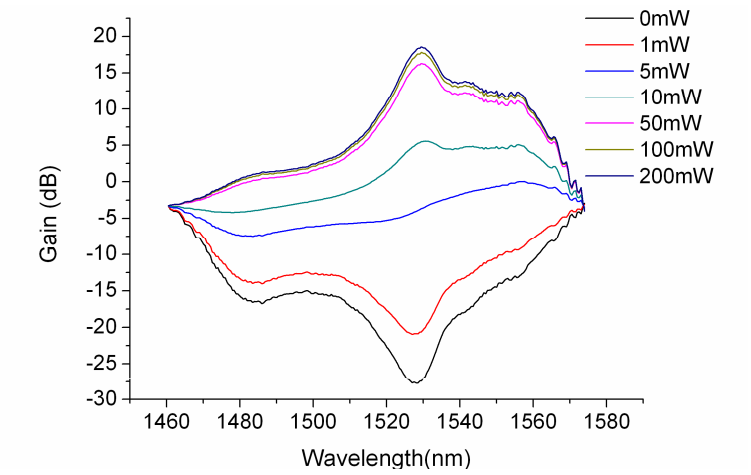

FIGURE 3.12: Variation of signal gain with the signal wavelength at different pump power

3.3 Conclusions

The three level erbium ion rate and propagation equations for analysing Er:Ta_2O_5 waveguide amplifiers pumped at 977 nm have been solved numerically and the effects of important parameters have been simulated. The effect of uniform up-conversion has been taken into account and its effect on the gain of the system has been studied. The equations were solved numerically with a step size in amplifier length of 100 μm, and the evolution of pump, signal and gain were obtained by solving the rate and propagation equations at each length interval in steady state. ASE effects were not included in the model as for all practical purposes, in amplifiers with gain $<$ 20 dB, the ASE effects can be neglected. The signal gain characteristics were analysed as a function of pump power, erbium concentration, length of the waveguide and wavelength. The population inversion and pump power evolution were also studied as function of propagation length and erbium concentration. Based on the characteristic curves of gain, a maximum gain of $\sim$ 43 dB at 1529.5 nm can be achieved for an Er:Ta_2O_5 waveguide of 3.5 cm length, with a concentration of 15.5×10^{20} ions/cm^3 pumped at 977 nm with a power of 200 mW with low upconversion coefficient (C_{up}= 1×10^{-18} cm^3/s). This gain value drops down to $\sim$ 22 dB for a higher C_{up}= 5×10^{-18} cm^3/s and for a very high value of C_{up}= 10×10^{-18} cm^3/s the gain drops down further to a modest 12.2 dB. The results produced in this chapter do not include the effects of clustering. Nevertheless, the model presented demonstrates that Er:Ta_2O_5 is a promising material for making an efficient EDWA and the added advantage of HIC will enable realisation of dense photonic lightwave circuits with gain.

Bibliography

[1] K. Hattori, T. Kitagawa, M. Oguma, Y. Ohmori, and M. Horiguchi. *Erbium-Doped Silica-Based Wave-Guide Amplifier Integrated with a 980/1530nm WDM Coupler. Electron Lett*, **30**:856, 1994.

[2] R. N. Ghosh, J. Shmulovich, C. F. Kane, M. R. X. deBarros, G. Nykolak, A. J. Bruce, and P. C. Becker. *8-mW threshold Er^{3+}-doped planar waveguide amplifier. Photon Tech Lett*, **8**:518, 1996.

[3] T. Kitagawa, K. Hattori, K. Shuto, M. Yasu, M. Kobayashi, and M. Horiguchi. *Amplification in Erbium-Doped Silica-Based Planar Lightwave Circuits. Electron Lett*, **28**:1818, 1992.

[4] Y. C. Yan, A. J. Faber, H. deWaal, P. G. Kik, and A. Polman. *Erbium-doped phosphate glass waveguide on silicon with 4.1 dB/cm gain at 1.535 μm. Appl Phys Lett*, **71**:2922, 1997.

[5] J. Zyss I. Ledoux. G. Cusmai R. Costa. A. Barberis A.Q.L. Quang, R. Hierle and S.M. Piertralunga. *Demonstration of net gain at 1550 nm in an erbium doped polymer single mode rib waveguide. Appl Phys Lett*, **89**:141124, 2006.

[6] W. H. Wong, E. Y. B. Pun, and K. S. Chan. *Er^{3+}-Yb^{3+} codoped polymeric optical waveguide amplifiers. Appl Phys Lett*, **84**:176, 2004.

[7] W. Huang and R. R. A. Syms. *Sol-gel silica-on-silicon buried-channel EDWAs. J Lightwave Technol*, **21**:1339, 2003.

[8] R. Schermer, W. Berglund, C. Ford, R. Ramberg, and A. Gopinath. *Optical amplification at 1534 nm in erbium-doped zirconia waveguides. J Quant Electron*, **39**: 154, 2003.

[9] C. C. Baker, J. Heikenfeld, Z. Yu, and A. J. Steckl. *Optical amplification and electroluminescence at 1.54 μm in Er-doped zinc silicate germanate on silicon. Appl Phys Lett*, **84**:1462, 2004.

[10] J. D. B. Bradley, L. Agazzi, D. Geskus, F. Ay, K. Worhoff, and M. Pollnau. *Gain bandwidth of 80 nm and 2 dB/cm peak gain in Al_2O_3:Er^{3+} optical amplifiers on silicon. J Opt Soc Am B*, **27**:187, 2010.

[11] S. Kogahara, S. Shinada, S. Nakajima, T. Kawanishi, H. Nakajima, and M. Izutsu. *Optical amplification characteristics of Ti-diffused waveguides on Erbium-doped $LiNbO_3$ crystal. IEICE Electron Expr*, textbf4:134, 2007.

[12] A. Z. Subramanian, C. J. Oton, J. S. Wilkinson, and R. Greef. *Waveguiding and photoluminescence in Er^{3+}-doped Ta_2O_5 planar waveguides. J Lumin*, **129**:812, 2009.

[13] H. Rigneault, F. Flory, S. Monneret, S. Robert, and L. Roux. *Fluorescence of Ta_2O_5 thin films doped by kilo-electron-volt Er implantation: Application to microcavities. Appl Opt*, **35**:5005, 1996.

[14] K. Kojima, S. Yoshida, H. Shiraishi, and A. Maegawa. *Green up-Conversion Fluorescence in Er^{3+}-Doped Ta_2O_5 Heated Gel. Appl Phys Lett*, **67**:3423, 1995.

[15] B. S. Ahluwalia, A. Z. Subramanian, O. G. Helleso, N. M. B. Perney, N. P. Sessions, and J. S. Wilkinson. *Fabrication of Submicrometer High Refractive Index Tantalum Pentoxide Waveguides for Optical Propulsion of Microparticles. Photon Tech Lett*, **21**:1408, 2009.

[16] A. Zakery and S. R. Elliott. *Optical properties and applications of chalcogenide glasses: a review. J Non-Cryst Solids*, **330**:1, 2003.

[17] J. Fick, E. J. Knystautus, A. Villeneuve, F. Schiettekatte, S. Roorda, and K. A. Richardson. *High photoluminescence in erbium-doped chalcogenide thin films. J Non-Cryst Solids*, **272**:200, 2000.

[18] G. N. Conti, V. K. Tikhomirov, M. Bettinelli, S. Berneschi, M. Brenci, B. Chen, S. Pelli, and A. Speghini. *Characterization of ion-exchanged waveguides in tungsten tellurite and zinc tellurite Er^{3+}-doped glasses. Opt Eng*, **42**:2805, 2003.

[19] I. Nusinsky and A. A. Hardy. *Analysis of the effect of upconversion on signal amplification in erbium-doped fiber amplifiers (EDFAs). J Quant Electron*, **39**:548, 2003.

[20] P. Blixt, J. Nilsson, T. Carlnas, and B. Jaskorzynska. *Concentration-Dependent Upconversion in Er^{3+}-Doped Fiber Amplifiers - Experiments and Modeling. Photon Tech Lett*, **3**:996, 1991.

[21] C. Y. Chen, R. R. Petrin, D. C. Yeh, W. A. Sibley, and J. L. Adam. *Concentration-Dependent Energy-Transfer Processes in Er^{3+}-Doped and Tm^{3+}-Doped Heavy-Metal Fluoride Glass. Opt Lett*, **14**:432, 1989.

[22] P. Myslinski, D. Nguyen, and J. Chrostowski. *Effects of concentration on the performance of erbium-doped fiber amplifiers. J Lightwave Technol*, **15**:112, 1997.

[23] P. G. Kik and A. Polman. *Cooperative upconversion as the gain-limiting factor in Er doped miniature Al_2O_3 optical waveguide amplifiers. J Appl Phys*, **93**:5008, 2003.

[24] E. Delevaque, T. Georges, M. Monerie, P. Lamouler, and J. F. Bayon. *Modeling of Pair-Induced Quenching in Erbium-Doped Silicate Fibers. Photon Tech Lett*, **5**:73, 1993.

[25] F. Dipasquale and M. Federighi. *Modeling of Uniform and Pair-Induced up-Conversion Mechanisms in High-Concentration Erbium-Doped Silica Wave-Guides. J Lightwave Technol*, **13**:1858, 1995.

[26] M. Federighi and F. Dipasquale. *The Effect of Pair-Induced Energy-Transfer on the Performance of Silica Wave-Guide Amplifiers with High Er^{3+}/Yb^{3+} Concentrations. Photon Tech Lett*, **7**:303, 1995.

[27] J. Nilsson, B. Jaskorzynska, and P. Blixt. *Performance Reduction and Design Modification of Erbium-Doped Fiber Amplifiers Resulting from Pair-Induced Quenching. Photon Tech Lett*, **5**:1427, 1993.

[28] F. Dipasquale, M. Zoboli, M. Federighi, and I. Massarek. *Finite-Element Modeling of Silica Wave-Guide Amplifiers with High Erbium Concentration. J Quant Electron*, **30**:1277, 1994.

[29] F. Dipasquale and M. Zoboli. *Analysis of Erbium-Doped Waveguide Amplifiers by a Full-Vectorial Finite-Element Method. J Lightwave Technol*, **11**:1565, 1993.

[30] D. Biallo, M. D'Orazio, A. andDe Sario, V. Petruzzelli, and F. Prudenzano. *Time domain analysis of optical amplification in Er^{3+} doped SiO_2-TiO_2 planar waveguide. Opt Exp*, **13**:4683, 2005.

[31] Z. Yu, L. M. Gao, W. Wei, and X. Hou. *Numerical analysis of amplification characteristic of erbium-doped waveguide amplifiers by FD-BPM. Opt and Quant Electron*, **36**:321, 2004.

[32] M. Federighi, I. Massarek, and P. F. Trwoga. *Optical Amplification in Thin Optical Wave-Guides with High Er Concentration. Photon Tech Lett*, **5**:227, 1993.

[33] S. F. Li, C. L. Song, Q. J. Xiong, and B. Ran. *A numerical analysis of gain characteristics of Er-doped Al_2O_3 waveguide amplifiers. Opt Quant Electron*, **34**: 859, 2002.

[34] B. Pedersen. Small-Signal Erbium-Doped Fiber Amplifiers Pumped at 980 nm - a Design Study. *Opt Quant Electron*, **26**:S273, 1994.

[35] C. R. Giles and E. Desurvire. *Modeling Erbium-Doped Fiber Amplifiers. J Lightwave Technol*, **9**:271, 1991.

[36] M. V. D. Vermelho, U. Peschel, and J. S. Aitchison. *Simple and accurate procedure for modeling erbium-doped waveguide amplifiers with high concentration. J Lightwave Technol*, **18**:401, 2000.

[37] B. Pedersen, A. Bjarklev, J. H. Povlsen, K. Dybdal, and C. C. Larsen. *The Design of Erbium-Doped Fiber Amplifiers. J Lightwave Technol*, **9**:1105, 1991.

[38] A. A. M. Saleh, R. M. Jopson, J. D. Evankow, and J. Aspell. *Modeling of Gain in Erbium-Doped Fiber Amplifiers. Photon Tech Lett*, **2**:714, 1990.

[39] E. Cantelar, R. Nevado, G. Lifante, and F. Cusso. *Modelling of 980 nm pumped EDWAs: Spectroscopic variations associated to fabrication process. Opt and Quant Electron*, **33**:561, 2001.

[40] C. Barnard, P. Myslinski, J. Chrostowski, and M. Kavehrad. *Analytical Model for Rare-Earth-Doped Fiber Amplifiers and Lasers. J Quant Electron*, **30**:1817, 1994.

[41] T. Georges and E. Delevaque. *Analytic Modeling of High-Gain Erbium-Doped Fiber Amplifiers. Opt Lett*, **17**:1113, 1992.

[42] I. M. I. Habbab, A. A. M. Saleh, and P. K. Runge. *Erbium-Doped Fiber Amplifiers - Linear-Approximations. J Lightwave Technol*, **13**:33, 1995.

[43] Y. Sun, J. L. Zyskind, and A. K. Srivastava. Average inversion level, modeling, and physics of erbium-doped fiber amplifiers. *J Sel Top Quant Electron*, **3**:991, 1997.

[44] Y. H. Wang, C. S. Ma, D. L. Li, and D. M. Zhang. *Formulized analytical technique for gain characteristics of phosphate glass Er^{3+}/Yb^{3+} co-doped waveguide amplifiers. Appl Opt*, **38**:329, 2008.

[45] A. Shooshtari, T. Touam, and S. I. Najafi. *Yb^{3+} sensitized Er^{3+}-doped waveguide amplifiers: a theoretical approach. Opt and Quant Electron*, **30**:249, 1998.

[46] A. Monteil, S. Chaussedent, G. Alombert-Goget, N. Gaumer, J. Obriot, S. J. L. Ribeiro, Y. Messaddeq, A. Chiasera, and M. Ferrari. *Clustering of rare earth in glasses, aluminum effect: experiments and modeling. J Non-Cryst Solids*, **348**:44, 2004.

[47] F. Auzel and P. Goldner. *Towards rare-earth clustering control in doped glasses. Opt Mater*, **16**:93, 2001.

[48] M. Dinand and W. Sohler. *Theoretical Modeling of Optical Amplification in Er-Doped Ti-$LiNbO_3$ Wave-Guides. J Quant Electron*, **30**:1267, 1994.

[49] C. H. Huang, L. Mccaughan, and D. M. Gill. *Evaluation of Absorption and Emission Cross-Sections of Er-Doped $LiNbO_3$ for Application to Integrated-Optic Amplifiers. J Lightwave Technol*, **12**:803, 1994.

[50] E. Desurvire. Erbium doped fiber amplifiers. John Wiley & Sons Inc., 1994.

[51] R. S. Miniscalco, W. J. Quimby. *General Procedure for the Analysis of Er^{3+} Cross-Sections. Opt Lett*, **16**:258, 1991.

[52] G. N. vandenHoven, E. Snoeks, A. Polman, C. vanDam, J. W. M. vanUffelen, and M. K. Smit. *Upconversion in Er-implanted Al_2O_3 waveguides. J Appl Phys*, **79**: 1258, 1996.

[53] M. B. Lee, J. H. Lee, B. G. Frederick, and N. V. Richardson. *Surface structure of ultra-thin Al_2O_3 films on metal substrates. Appl Surf Sci*, **448**:L207, 2000.

[54] P. S. Dobal, R. S. Katiyar, Y. Jiang, R. Guo, and A. S. Bhalla. *Raman scattering study of a phase transition in tantalum pentoxide. J Raman Spectrosc*, **31**:1061, 2000.

[55] M. Karasek. *Optimum design of Er^{3+}-Yb^{3+} codoped fibers for large-signal high-pump-power applications. J Quant Electron*, **33**:1699, 1997.

[56] K. Yelen, M. N. Zervas, and L. M. B. Hickey. *Fiber DFB lasers with ultimate efficiency. J Lightwave Technol*, **23**:32, 2005.

[57] W. Q. Shi, M. Bass, and M. Birnbaum. *Effects of Energy-Transfer among Er^{+3} Ions on the Fluorescence Decay and Lasing Properties of Heavily Doped Er-$Y_3Al_5O_{12}$. J Opt Soc Am B*, **7**:1456, 1990.

Chapter 4

Er:Ta_2O_5 waveguide fabrication & erbium spectroscopy

Optical amplifiers are key components in optical telecommunications and in fully-integrated optical systems. Erbium doped materials are of particular importance in optical communications technology, due to their excellent performance as gain media for amplifiers and lasers at the telecommunications wavelength near 1.5 μm. Low-cost, compact EDWAs are essential for local-loop optical systems, and fully-functional densely integrated PLCs will rely upon gain in much the same way as electronic integrated circuits do at present. In this chapter, the deposition and optimisation of erbium-doped Ta_2O_5 (Er:Ta_2O_5) thin films using magnetron sputtering is presented. The spectroscopic properties of Er^{3+} ions in tantala are provided through photoluminescence (PL), fluorescence lifetime, and cross-sections measurements. The effect of different annealing temperatures on the PL, lifetime, and loss measurements of Er:Ta_2O_5 films are also presented to evaluate this material's potential as a HIC host for erbium and as an EDWA.

4.1 Slab waveguide fabrication, optimisation and characterisation procedures

4.1.1 Thin film deposition

Slab waveguides were fabricated by radio frequency (RF) magnetron sputter deposition (Plasma 400 Oxford Instruments) of a powder pressed, Er:Ta_2O_5 target (150 mm diameter) onto an 1mm thick oxidized silicon substrate (oxide thickness $\sim$ 2.1 μm). The target was doped with 1 wt. % of Er_2O_3 corresponding to an erbium concentration of 2.7 x 10^{20}ions/cm^3. The deposition was carried out in a vacuum chamber pumped to a base pressure of 10^{-8} Torr and back-filled with an Ar:O_2 ambient. The flow rate for both the gases inside the chamber was separately controlled. The chamber pressure was maintained at a constant value of 10 mTorr. In order to obtain high optical quality as-deposited films, optimization of the sputter deposition parameters is very important. The parameters optimized for the deposition were substrate temperature, magnetron power and O_2 gas flow and are shown in Table 4.1.

Run #	**Substrate temp (^{0}C)**	**Magnetron power (W)**	**O_2 flow rate (sccm @ STP)**	**Thickness (nm)**	**Loss (dB/cm @ 633 nm)**
1	20	300	5	642 $\pm$ 5	3.1 $\pm$ 0.1
2	100			638 $\pm$ 5	1.6 $\pm$ 0.1
3	200			646 $\pm$ 5	0.4 $\pm$ 0.1
4	300			640 $\pm$ 5	0.9 $\pm$ 0.1
5	200	200	5	672 $\pm$ 5	3.1 $\pm$ 0.4
		300		646 $\pm$ 5	
6		400		1221 $\pm$ 5	0.5 $\pm$ 0.1
7	200	300	2	740 $\pm$ 5	4.4 $\pm$ 0.1
			5	646 $\pm$ 5	
8			10	513 $\pm$ 5	0.5 $\pm$ 0.2

TABLE 4.1: Parameters optimised for Er:Ta_2O_5 thin film deposition. The argon flow rate, chamber pressure and deposition time was maintained constant at 20 sccm, 10 m.Torr and 300 minutes respectively. The base pressure of the chamber was maintained at 10^{-8} Torr

Deposition was carried out by varying substrate temperature and setting other parameters to a reasonable value. Once the deposition was complete, optical loss was measured at 633 nm by monitoring the scattered light from the waveguide and the value that gave the lowest loss and an acceptable deposition rate was used for optimizing the next

parameter. This process was carried out until all the three sputter parameters, mentioned above, were optimized. The thickness of the thin film was measured using stylus profilometer.

4.1.2 Optical loss measurements using the prism coupling method

4.1.2.1 Prism coupling principle

In integrated optics, thin films are used as the planar light guides. For thin film characterization, refractive index, thickness and loss are the main parameters to be determined. Prism coupling is the most common and one of the best techniques available to characterize thin films [1] . It is easy to set up, fast and accurate. The working principle of a prism coupler is very simple, as shown in Fig 4.1. The laser is coupled into the waveguide, based on the incident angle (θ) on the prism base. Incidence angle θ, determines the phase velocity, $V_x = c/n_p sin\theta$ in the x-direction of the incident wave in the prism and the gap between prism and waveguide. Strong coupling of laser in the guide will occur if we choose θ such that V_x equals the phase velocity (V_m) of one of the modes of propagation of the guide (m=0,1,2..). Thus, by determining these angles of strong coupling we can experimentally determine the propagation constants or the effective indices of the modes of a given film. The experimentally determined propagation constants can then be used in the solution of the characteristic planar slab waveguide equation, to determine the thickness and the refractive index of the guide layer.

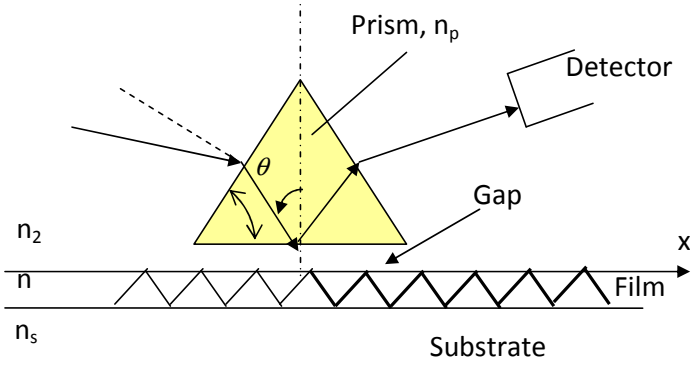

FIGURE 4.1: Schematic cross-section of a prism coupling set up. When the light energy fed from the prism is in phase with the zigzag wave inside the waveguide then coupling is effective. The amplitude inside the waveguide in this region is increased, as shown by the bold lines inside the film region

4.1.2.2 Experimental set-up

The prism coupling or the m-line set-up, used to measure losses in the waveguide, is shown in the Fig 4.2. The waveguide or the film, under test is clamped against the base of the prism through a screw. This is mounted on a rotary table or goniometer. The laser beam is linearly polarised (TE or TM) through a polariser. The beam splitter directs the incident beam onto a detector for the reference level. The laser is positioned at a point in the base of the prism where the waveguide is clamped against the prism, also called the coupling spot (visible to naked eye as black spot). This arrangement is used such that the coupling spot is stationary with respect to the rotation of the stage. The prism is rotated through a range of angles until the light is coupled to a propagating mode(s) visible as a bright streak of light along the thin film. At different angles, different modes appear as bright lines on the screen placed next to the prism. Depending on the quality of the films under observation the light coupled into the waveguide can be continuous and bright or very short and dull.

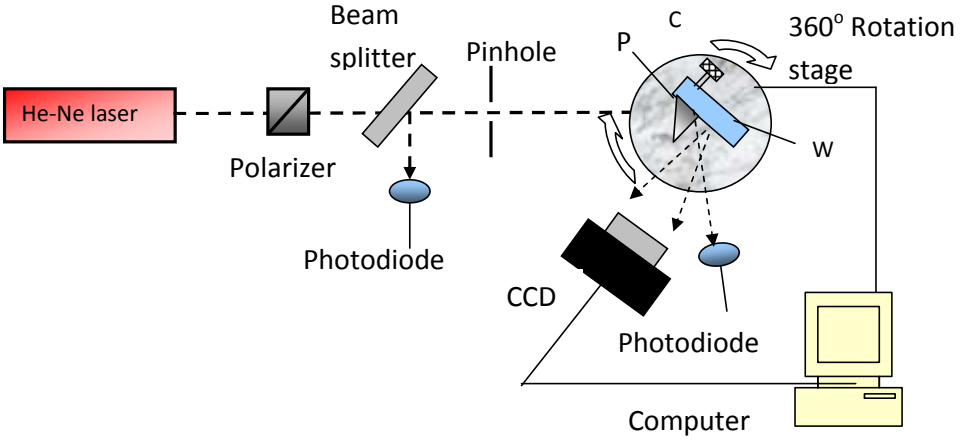

FIGURE 4.2: Schematic of prism coupling experimental set up used to measure losses, effective indices. P: Rutile prism; W: Er:Ta_2O_5 waveguide; C: clamp screw.

The slab waveguide losses were measured at 633 nm (He-Ne laser) where erbium has negligible absorption, by directly capturing and monitoring the scattered light intensity [2, 3] normal to the waveguide plane, using an imaging system (CCD). The light was coupled into the waveguide using prism coupling with a rutile prism being used to couple light into the fundamental mode of the Er:Ta_2O_5 waveguide. The propagation loss was then determined by mapping the decay of scattered light (pixels captured by the imaging system) along the propagation length of the guide. this decay should follow the Beer's law, $I_L = I_0\, exp\,(-\alpha L)$ where I_L is the scattered light intensity after length L though the waveguide, I_0 is the initial intensity at the starting point of the path and α is the loss coefficient to be determined. Taking log of both sides and multiplying by 10 will

give us the signal strength in dB and a straight line equation,

$$10Log\,(I_L) = 10Log\,(I_0) - 4.34\alpha L \tag{4.1}$$

Where a factor of 4.34 arises from Log(e). Thus, a plot of $10LogI_L$ vs. L should yield a straight line and the slope will directly yield the loss. The CCD camera and lens imaged the bright streak of light guided by the thin film, which was stored as a .BMP file as it is a non-compressed file and retains most of the information of the original image. Care was taken to avoid saturation of the CCD and the same magnification was used for all the samples. A reference image of a scale was taken to measure the length of the waveguide (light propagation length in the thin film). Fig 4.3 shows the captured image of light streak in one of the samples that was used to estimate the loss in the thin film. The losses were estimated at several different places on a sample to check the homogeneity of the sample, and averaged.

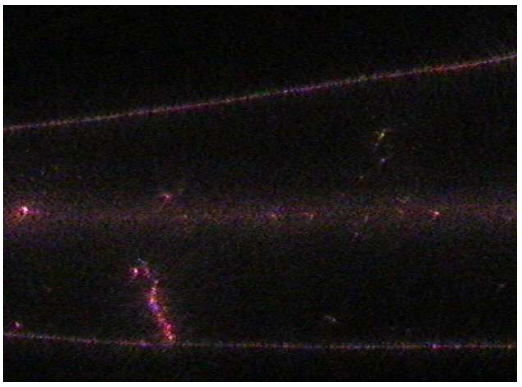

FIGURE 4.3: Image of prism coupled guided light by the Er:Ta_2O_5 waveguides

4.1.3 Optical constant measurement

4.1.3.1 Ellipsometry

The refractive index and the thickness of the sputtered tantala thin films were determined by ellipsometry [4]. The apparatus consisted of a white light source emitting in the visible region (400-1700 nm) and a detector which collects the polarized reflected light. The measurements were performed at a different angles of incidence and Tauc-Lorenz dispersion model [5] was used to fit the experimental data points. Ellipsometry is a common and versatile technique for measuring optical constants such as the refractive index and thickness of thin films. It measures the change in the polarization state upon reflection or transmission from the material under consideration. A typical experimental

set-up consists of a light source, a polariser, a sample holder, an analyzer and a detector (Fig 4.4).

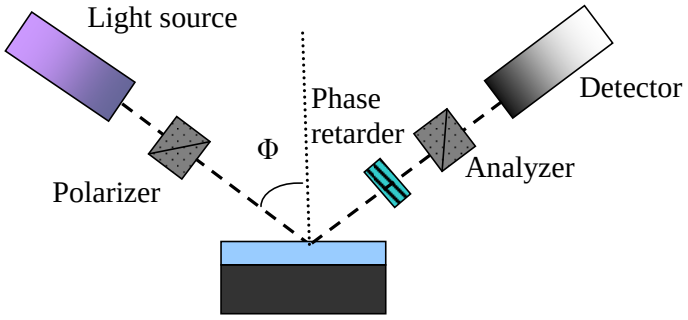

FIGURE 4.4: Schematic setup of the Ellipsometry experiment

The light passes through the polariser, which is positioned in such a way that it passes both s and p components to be incident on the surface of material under test. The elliptically polarized reflected light then passes through the analyzer and falls on the detector. The detector converts the photons falling on it into the electric signal and, using the information about the input polarization, determines the change in the polarization upon reflection. This is known as the Del (Δ) and Psi (ψ) measurement in ellipsometry. Δ is the phase change between the s and p component of the light upon reflection. Thus, Δ can vary between 0 and 360^0. ψ is the angle whose tangent is the ratio of the magnitudes of the total reflection coefficients. ψ can vary between 0 and 90^0. The step-wise procedure to perform ellipsometric measurements and data analysis is shown in a flowchart below (Fig 4.5).

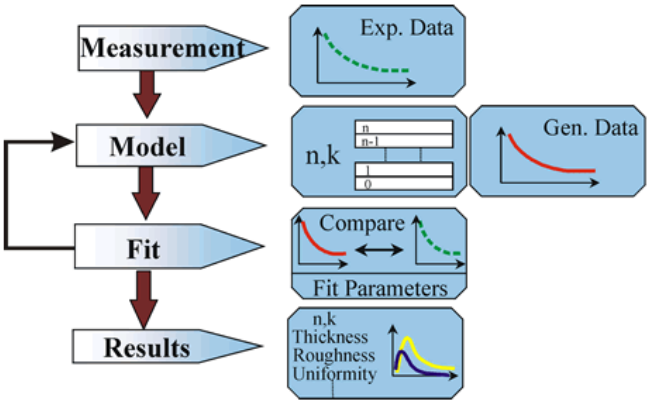

FIGURE 4.5: Flowchart for ellipsometric measurements and analysis [http://www.jawoollam.com/tutorial_5.html]

4.1.4 Photoluminescence & lifetime characterisation

PL measurements were performed at room temperature by pumping erbium ions into their $^4I_{11/2}$ level using a Ti:Sapphire laser emitting at 980 nm. The schematic of the experimental set up is shown in Fig 4.6. The thickness of the tantala thin film was approximately 2 μm. The pump was directed onto the sample at 45 degrees to the surface normal. The pump power at the surface of the sample was about 180 mW and the spot size of the pump beam was $<$ 1 mm in diameter. The pump was mechanically chopped at 25 Hz. The luminescence was analyzed using a grating monochromator normal to the sample surface, with a spectral resolution of 10 nm. A filter was used just before the monochromator to block wavelengths below 1300 nm. The signal was detected using an InGaAs detector and amplified using a lock-in amplifier. Lifetime measurements were performed with 0.2 ms resolution by monitoring the decay of the luminescence on an oscilloscope after pumping the erbium ions and mechanically chopping of the pump light source. The luminescence intensity was fitted to a single exponential decay, and the natural log of this decay, normalised with respect to the maximum intensity was plotted against time. The slope of the fit gives the luminescence decay time. PL measurements were performed on both the annealed and non-annealed samples.

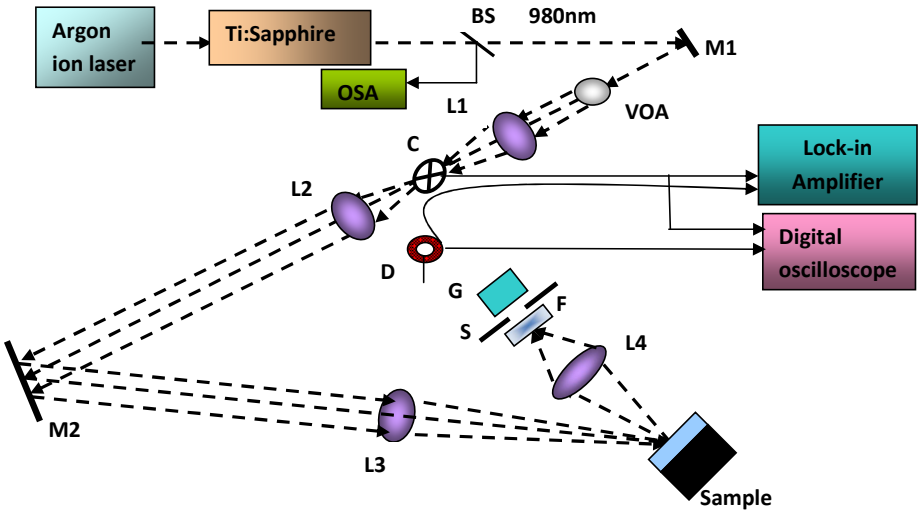

FIGURE 4.6: Schematic of the experimental setup for doing PL and lifetime measurements BS: beam splitter; M1, M2: mirrors; L1, L2, L3, L4: lenses; VOA: variable optical attenuator; C: chopper; F: filter below 1300nm; S: variable slit; GM: grating monochromator; D: InGaAs detector.

4.2 Experimental results

4.2.1 Optical loss measurements and analysis

The optical loss variation with substrate temperature is shown in Fig 4.7a. The other parameters such as magnetron power (300 W), oxygen flow rate (5 sccm), chamber pressure (10 mT) and deposition time (5 hours) were kept constant. The maximum loss of 3.1 dB/cm was measured for as-deposited sample sputtered at room temperature. With the increase in the substrate temperature for sputtering the optical loss decreased and reached a minimum of 0.4 dB/cm at 200^0C. But when the substrate temperature was increased to 300^0C the optical loss increased to 0.9 dB/cm. The variation of the scattered light intensity for the best case scenario (200^0C) and the straight line fit to this variation is shown in Fig 4.7b.

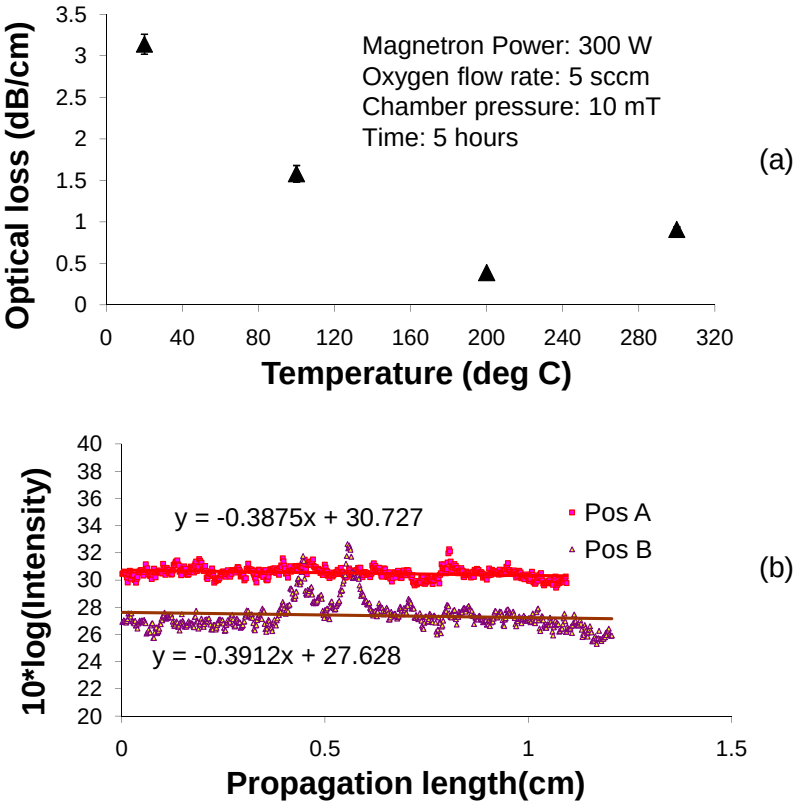

FIGURE 4.7: a) Loss for Er:Ta_2O_5 sample deposited v/s substrate temperature with other parameters held constant. b) Scattered light intensity for Er:Ta_2O_5 with fit to the straight line. The slope yields the loss in the sample. Pos (A, B) corresponds to different places on the same sample.

The substrate temperature was kept constant at the optimum 200^0C and magnetron power was varied to determine the optimum value. The other parameters such as oxygen

flow rate (5 sccm), chamber pressure (10 mT) and deposition time (5 hours) were kept constant. Fig 4.8 shows the variation of optical loss with magnetron power, and a lowest optical loss of ~ 0.4 dB/cm was achieved at both 300 W and 400 W of magnetron power whereas for lower magnetron power at 200 W the optical loss increased to 3 dB/cm. Therefore, 300 W was chosen as the optimum value for magnetron power.

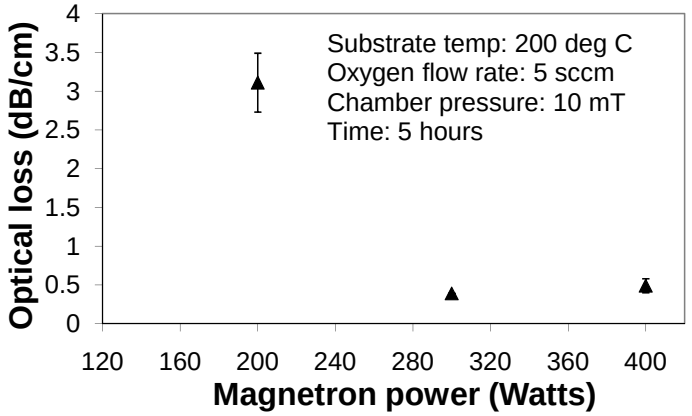

FIGURE 4.8: Optical loss at 633 nm vs. magnetron power for sputtered Er:Ta_2O_5 films

The substrate temperature and magnetron power were now kept constant at the optimum values of 200^0C and 300 W while the oxygen flow rate was varied to determine the optimum value. The other parameters such as chamber pressure (10 mT) and deposition time (5 hours) were kept constant. Argon is used to start and maintain the plasma discharge and its flow rate is not critical, but the oxygen flow rate plays an important role in achieving low loss films as shown in Fig 4.9. It was found that the optical loss decreased with the increase in the oxygen flow rate and best result was obtained for an oxygen flow rate of 5 sccm. While at higher flow rate the optical loss slightly increased and for 2 sccm the loss was as high as ~ 4.3 dB/cm.

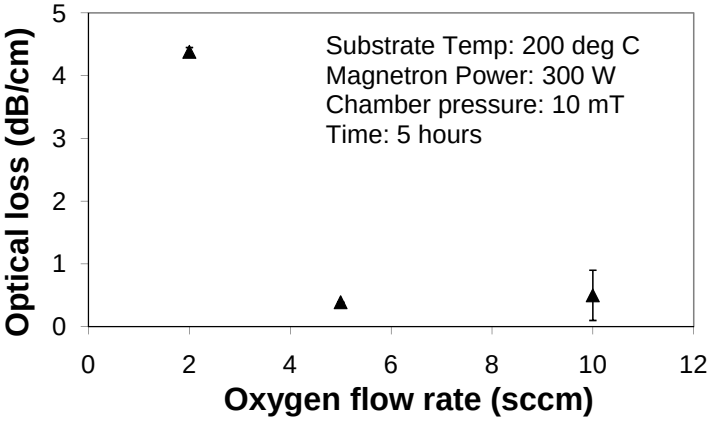

FIGURE 4.9: Optical loss at 633 nm vs. oxygen flow rate for sputtered Er:Ta_2O_5 films.

The deposition rate was determined by measuring the film thickness for various sputtering times, using a stylus profilometer. Fig 4.10 shows the thickness plotted against time, for the deposition conditions discussed in Table 4.1, with the average deposition rate found to be $\sim 2\ nm/min$ with a variation of 5-10% over the 4 inch wafer area. But over the course of the project due to wear and tear of the sputterer target the average deposition rate was found to decrease to ∼1.75 nm/min.

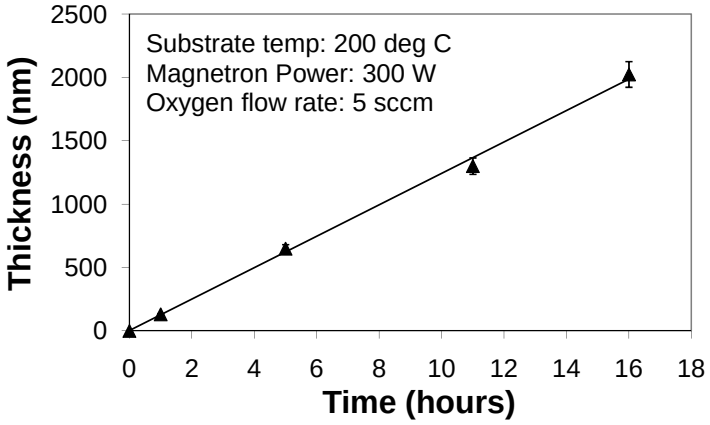

FIGURE 4.10: Deposition rate for sputtered Er:Ta_2O_5 thin film.

4.2.2 Discussion of sputtering process optimisation

The decrease in the loss with the substrate temperature can be attributed to better stoichiometry and microstructure. As the amount of oxygen in the layers increases with increasing substrate temperature, the stoichiometry improves and the microstructure of the sputtered layer becomes more regular. This in turn reduces the scattering losses [6]. The sample sputtered at 200^0C gave the lowest losses (0.40 dB/cm at 633 nm) and an acceptable deposition rate (2 nm/min), so was chosen as the optimized value for the substrate temperature. It was expected that the loss would be lower at 300^0C but the the loss increased. This increase in the loss may have been due to micro-cracking of film due to local heating and stress at that temperature, or perhaps simply due to some unwanted and un-removable scattering centres in the film. The deposition rate at 400 W was almost twice that at 300 W. However, the photoluminescence results (described in later section) showed that both luminescence intensity and lifetime were better with samples deposited at 300 W. Therefore, 300 W was chosen as the optimum magnetron power value. With the increase in the O_2 flow rate, the film approaches its stoichiometric composition and hence lowest possible loss, but a further increase will lead to increased oxidization of the target surface and an unacceptably low deposition rate. The best samples were achieved with a flow rate of 5 sccm that yielded lowest loss value

and highest deposition rate (2 nm/min) at 300 W of magnetron power. The optimized deposition parameters for achieving low loss Er:Ta_2O_5 slab waveguides determined were 200^0C substrate temperature, 300 W magnetron power and 5 sccm oxygen flow rate with argon flow rate and chamber pressure maintained at a constant value of 20 sccm and 10 mTorr respectively.

4.2.3 Annealing

In order to further improve the optical losses, the as-deposited films were annealed for an hour in oxygen ambient atmosphere at different temperatures (450, 500, 550 and 600^0C) in a tube furnace and losses were measured. The temperature ramp up and down rate was set at 3^0C/min and the oxygen flow was fixed at 2 L/min. The temperature that gave the lowest loss was taken as the optimized annealing temperature. Table 4.2 provides the results of annealing the samples. In the loss measurement for the annealed samples the losses decreased to < 0.3 dB/cm for the sample annealed at 450^0C, but it was not possible to measure losses for the samples annealed at higher temperatures because the scattered power was too low to measure, providing evidence of further reduction in the loss.

Temperature (^0C)	Time (hour)	Temp ramp ($^0C/min$)	Loss (dB/cm)
450	2	3	0.3±0.05
500	2	3	undetermined
550	2	3	undetermined
600	2	3	undetermined

TABLE 4.2: Loss values for different annealing temperatures on fully optimized as-deposited Er:Ta_2O_5 samples. The oxygen flow rate was maintained at 2 L/min . The cool down rate was also maintained at $3^0C/min$

4.2.4 Discussion

The as-deposited films are oxygen deficient and the annealing helps in enriching the film with oxygen and improve the stoichiometry. This reduces the absorptive losses in the film without increasing the scattering losses by maintaining the amorphous nature of the film. An increase in the annealing temperature continues this trend until an optimum temperature is reached when the phase change takes place and film tend to become poly-crystalline. At and beyond this temperature the scattering loss starts to dominate leading to increase in the total loss of the film. Therefore, it is imperative that the annealing temperature is kept below this transition temperature. For Er:Ta_2O_5

thin film the optical losses decreased when annealed in oxygen at 450^0C but the losses beyond this temperature could not be determined because of the experimental limitation as stated above. It is expected that optical losses would further decrease at higher temperature and the optimisation of the annealing temperature will be carried out for rib waveguides using more capable loss measuring techniques such as Fabry-Perot (FP) method discussed in a later section.

4.2.5 Refractive index measurement

Ellipsometry measurements were performed on the sputtered and annealed Er:Ta_2O_5 samples to determine the thin film refractive index especially in the infra red regime where the waveguides will be predominantly used. Fig 4.11 shows the refractive index vs. wavelength for the fully optimized Er:Ta_2O_5 film. The experimental points obtained during ellipsometry experiments were fitted using Tauc-Lorenz [5] dispersion relation which yielded a refractive index of 2.105 at 1530 nm. The thicknesses of the films were within the experimental error of the value measured by the stylus profilometer.

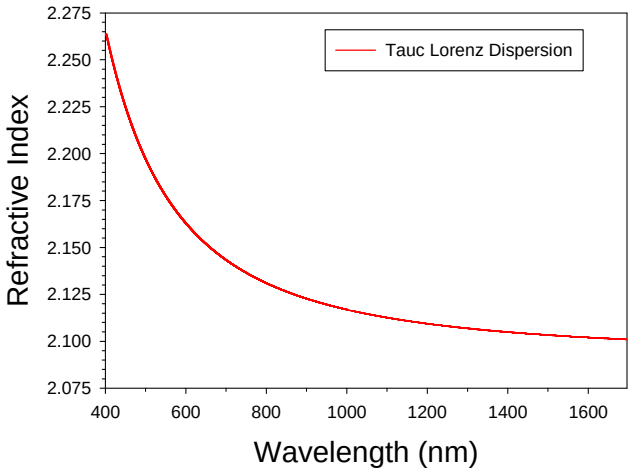

FIGURE 4.11: Refractive index of sputtered Er:Ta_2O_5 film determined by ellipsometry in the visible-mid IR wavelength region.

4.2.6 PL and lifetime results

The PL spectra of annealed and non-annealed magnetron sputtered Er:Ta_2O_5 samples are shown in Fig 4.12a. The samples were annealed at 450, 500, 550 and 600^0C, respectively but higher temperatures were not employed as annealing above 600^0C is expected to result in a lossy polycrystalline film [7]. The emission spectra correspond to the transition between the $^4I_{13/2}$- $^4I_{15/2}$ levels of the Er^{3+} ion and peak at 1534 nm. The

bandwidth of the spectrum (FWHM) was measured to be 50 nm which is substantially broader than those obtained from non-tellurite glasses (∼30 nm) [8] and comparable to HIC hosts such as tellurite glasses (n∼2.1, 65 nm) [9] and alumina (n∼1.69, 80 nm) [10] and thus shows potential for broadband applications. The PL intensity increases with annealing temperature to about 14 times that of the unannealed sample at 600^0C. Fig 4.12b shows the bandwidth of the normalised PL spectra to be constant for the annealed and unannealed Er:Ta_2O_5 samples. This suggests that there is an absence of phase change from amorphous to crystalline nature which would exhibit narrowing of bandwidth even at 600^0C. It is probable that because of the absence of phase change the losses would not increase with annealing temperatures up to 600^0C.

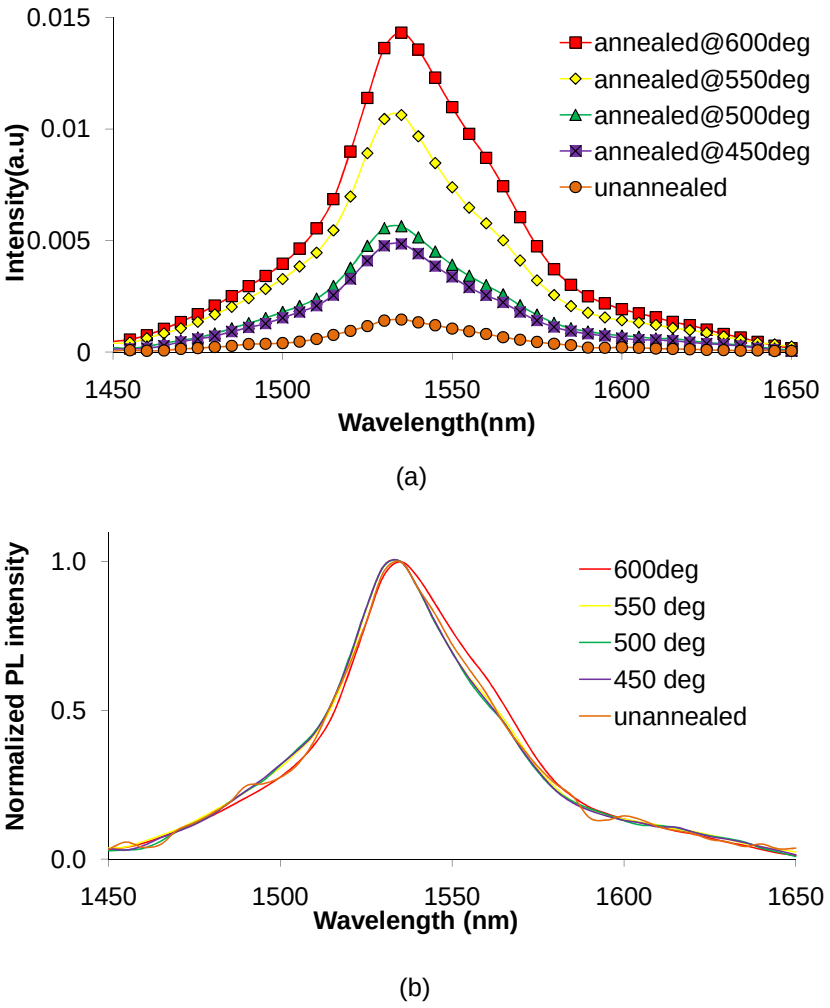

FIGURE 4.12: PL spectra for unannealed and annealed Er:Ta_2O_5 films a) The spectrum peaks at 1534 nm & b) Normalized PL spectra for annealed and unannealed Er:Ta_2O_5 films. The annealing temperatures used were 450, 500, 550 & 600^0C, respectively

The luminescence lifetime of the erbium ions is shown in Fig 4.13. It can be seen from the fit (bold dashed lines) in Fig 4.13 that the decay is almost purely single exponential,

and the result was limited by the resolution of the oscilloscope (0.2 ms) so that any faster decay component present could not be measured. The quality of the fit improves with the increasing annealing temperature so that, the luminescence decay time was found to increase from 0.53 ms for the as-deposited sample to 2.4 ms for the sample annealed at 600^0C. PL intensity and the lifetime are related to each other through the rate equations governing erbium ions transitions. The increase in the PL intensity is predominantly caused by the increase in the lifetime with the annealing temperature. The lifetime increase can be explained by the decrease in the non radiative decay centres due to annealing of sputtering induced defects in the tantala structure. The value of lifetime is smaller than those obtained from non-tellurite glasses (10-15 ms) [8] and alumina (7.6 ms) [10] but comparable to HIC hosts such as tellurite glasses (1.3 ms) [11] and zirconia (n∼2.04, 1.8 ms) [12] as shown in Table 4.3 .

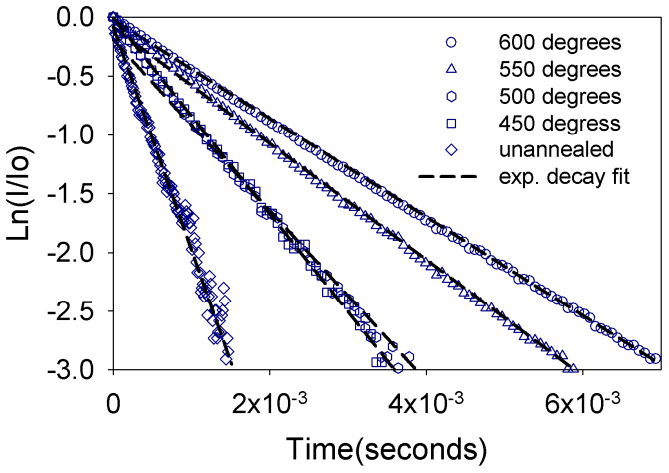

FIGURE 4.13: Comparison of luminescence decay of annealed and unannealed Er:Ta_2O_5 films. Ln(I/I_0) is the natural log of the normalized intensity of the exponential fit. Bold dashed lines show the fit to a single exponential decay

Material	Index contrast	Lifetime (ms)	Bandwidth (nm)
Hafnia [13]	0.16	6.5	45
Zirconia [12]	0.17	1.8	54
Alumina [10]	0.20	7.6	80
Zinc-silicate-germanate [14]	0.30	2.0	NA
Silicon nitride [15]	0.01-0.55	5.3	NA
Tellurite [11]	0.61	1.3	45-70
Tantala [this thesis]	0.68	2.4	50

TABLE 4.3: Comparison of lifetime and bandwidth of different HIC materials with Er:Ta_2O_5

4.2.7 XRD spectra

In the previous section, it was seen that the optical losses decreased due to annealing. The losses can be expected to decrease with the annealing temperature as long as the material remains amorphous. One way to determine the limit of annealing temperature/-time is to perform X-ray diffraction (XRD) on the thin films to check for any crystallinity in the material. Based on the results of the PL, lifetime, and loss an annealing temperature of 600^0C with different annealing time was selected for this particular experiment. Different samples - 2 μm thick undoped, and erbium doped tantala waveguides annealed for different time were prepared for the experiments. For the sake of completeness, XRD was also done on a piece of the sputtering target. The resultant spectra are shown in Fig 4.14. The presence of crystallinity would have appeared as peaks in the XRD spectra but the absence of any kind of peaks in the films reveal the amorphous nature of the material and therefore, the following conclusions can be drawn from the results

- the piece of the sputtering target show the characteristic peaks of tantala as it is essentially crystalline power fused together to form a solid target for sputtering and this serves as a good reference for the amorphous nature of the tantala thin film.
- 600^0C is a safe temperature for annealing and combined with the results of loss, PL and lifetime measurements, it is expected that the waveguides annealed at this temperature would give the best performance. Higher temperature were not employed as they have been shown to yield polycrystalline films [14].
- annealing time does not have a significant effect on the XRD spectra.
- the erbium doping does not have any significant effect on the XRD peaks

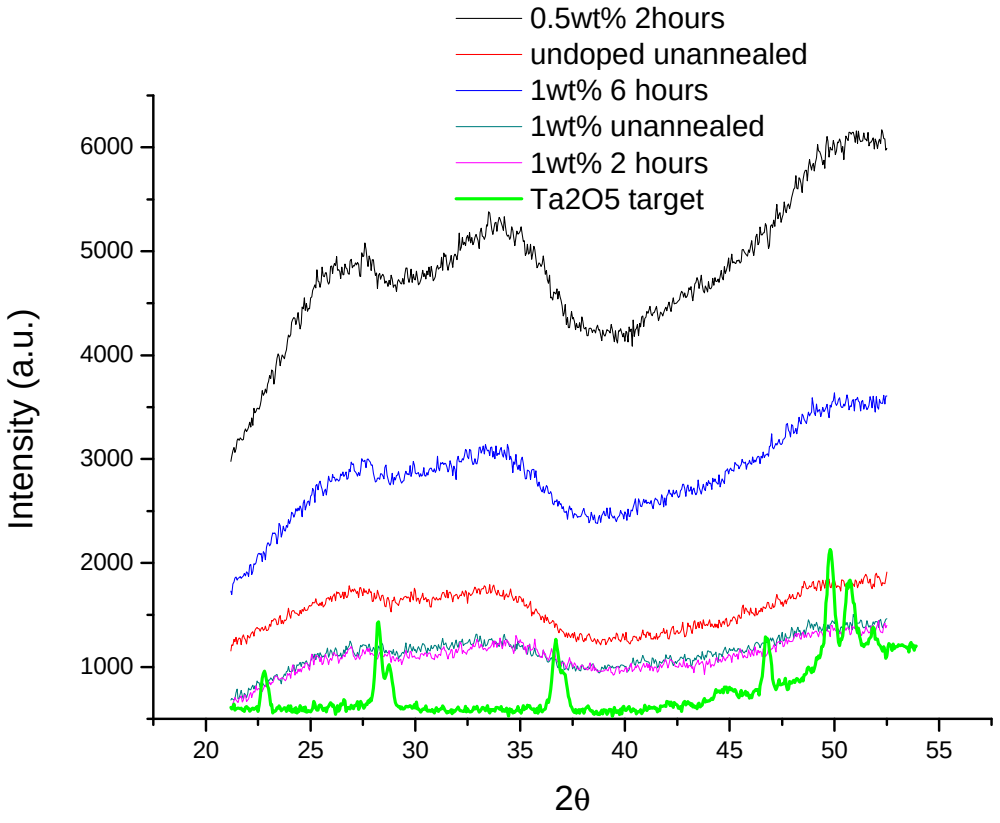

FIGURE 4.14: Comparison of XRD spectra from undoped and erbium doped tantala waveguides. The annealed samples were annealed for at 600^0C for different times with a ramp rate of 3^0C/min

4.3 Rib waveguide fabrication, optimisation and characterisation

4.3.1 Single mode condition for Er:Ta_2O_5 rib waveguides

For most planar photonic devices and applications, SM behavior is a pre-requisite. For HIC materials, such as Ta_2O_5-air or Ta_2O_5-SiO_2 if a rectangular cross-section is used then to achieve SM condition the transverse dimensions should be sub-micron which puts extra pressure on the fabrication tolerances and also leads to low coupling efficiency to standard optical fibre. To improve coupling in such waveguides either a high numerical aperture (NA) objective lens or special structures/fibres such as lensed or tapered [16, 17] need to be used and these are inconvenient and often costly options. Instead a rib waveguide geometry (Fig 4.15) can be used to maintain SM for larger dimensions [18, 19] improving coupling efficiency and relaxing fabrication tolerances.

For rib waveguides with large cross section (Fig 4.15), the SM condition is given by [20],

$$r > 0.5 \tag{4.2}$$

$$\frac{W}{H} \leq \frac{r}{\sqrt{1-r^2}} + C \tag{4.3}$$

where, C is a constant, $r = h/H$, where $h(=$ H-D) is the slab height, H is the rib height of the waveguide, D is the etch depth, and W is the width of the waveguide.

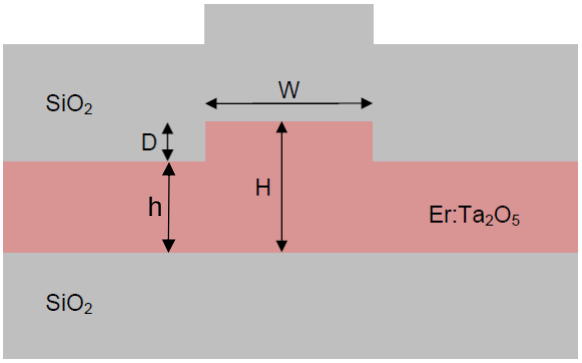

FIGURE 4.15: An erbium doped tantala rib waveguide cross-section where the dimensions of the waveguide are represented by W (width of the waveguide), H (rib height), D (etch depth), & h (slab height).

The constant C is a key parameter for the SM condition and has different values under different approximations. Soref et al obtained C =0.3 using mode matching [20], the effective index method (EIM) gives C =0 [21] and Pogossian et al [22] achieved C=-0.05 by fitting the experimental results published in [19] . Powell used the beam propagation method and obtained a value of C =0.3 [23] The exact SM condition is therefore under some dispute and an explicit condition in the region of r <0.5 has not been established. SM behavior in rib waveguides is achieved when higher order modes in the vertical direction are cut-off in the central rib section and get coupled to the fundamental mode of the slab section, which becomes leaky for r ≥0.5 This happens at r ≥0.5 , because the effective index of the fundamental slab mode (fig 1.15, region II) becomes higher than the effective index of any higher-order vertical mode in the central rib region (fig 1.15, region I) [20]. For our experiments, we adopted the Soref approach [20] as the starting point as it is most widely accepted.

4.3.2 Rib waveguide fabrication and optimisation

For making rib waveguides, an optimised thin film (as described in section 4.2) was used

as the starting material. Photolithography followed by etching yielded rib waveguides. For etching, argon ion beam milling (IBM) was employed. Based on Eq.(4.2, 4.3), the dimensions of the waveguide for SM operation at λ= 1550 nm were selected as the following: Rib height (H) = 2μm , etch depth ($d = H - h$) = 400 nm, and width (W) $\leq$3.2 μm.

For the fabrication, a photo-mask was designed in Olympios software where the narrowest waveguide was 1 μm wide and the widest was 10 μm wide on the photo-mask. Successive waveguides were separated by 100 μm spacing to ensure no cross-coupling between the waveguides when the light is coupled into one of the waveguides. The width of the waveguides increased with a constant value of 0.2 μm to fabricate few waveguides that would satisfy the SM conditions. The wider waveguides were designed for the experiments such as white light absorption measurements for erbium spectroscopy which requires higher coupling due to low power source.

4.3.2.1 Photolithography

- A thin film of Er:Ta_2O_5 ($\backsim 2\mu m$) was deposited on 4" Si/SiO_2 (2μm oxide layer) wafer using magnetron sputtering at 200^0C , 300 W of magnetron power and 5 sccm of O_2 flow. The wafer was heated in an oven at 120^0C for 15-20 minutes to remove any water vapour before spin coating the resist.
- For defining the channels on the substrate, a combination of S1813 positive resist (PR) and light field photo mask was used to make ribs (raised) structure. S1813 resists used were optimised for use at 405 nm (H-line of mercury emission spectrum).
- The substrate was cleaned and PR was spin coated on the substrate as follows. A ramp time of 2 s was used to reach 500 RPM and the dwell time was 5 s. This was followed by a ramp of 1.5 s to 3500 RPM and a dwell time of 1 minute. This yielded a minimum resist thickness of 1μm.
- The coated sample was covered and left for 5 minutes before soft baking in an oven for 30 minutes. The oven was maintained at 90^0C and care was taken to place the sample in the middle of the oven to maintain repeatability.
- After 30 minutes, the samples were taken out and left to cool down and get hydrated for about 12 mins. This is to ensure optimum performance upon exposure to UV light.
- The sample was placed in the substrate holder and sample was aligned with the photo-mask (notch in the 4" wafer was aligned parallel to the channels in the mask) to ensure that the waveguides could be cleaved perpendicular to the end facet. After several trial runs, the optimum exposure conditions were found to be

the following: Hard contact, 5.5 s exposure time at 15 W/cm^2 UV fluence using a mercury lamp emitting in the wavelength band 350-450 nm.

- For developing the sample, MF319 solution was used. The exposed sample was immersed in the developer solution for 40 s. During this time the sample was constantly shaken inside the solution and after 40s, the sample was cleaned in deionised (DI) water and blow dried in nitrogen.
- The sample was then placed in an oven maintained at 120^0C for 30 minutes for hard-bake.
- This formed the mask for the etching process. The above procedure yielded the best reproducible linewidth from the original photo-mask. In general, the PR mask was found to be 0.2-0.3 μm wider than the actual linewidth on the photo-mask.

4.3.2.2 Etching

Ion beam milling (IBM) was employed to realise erbium doped tantala rib waveguides. Milling involves bombardment of argon ions onto the substrate leading to physical removal of material where the argon ions impinge on the sample. Ar IBM was performed with the following optimised parameters: Ar gas flow 6 sccm, beam current 100 mA, beam voltage 500 V and RF power 500 W. It was also found that the milling done at the conventional 0^0 angle (ion beam w.r.t to the sample) led to resist sticking to the sidewalls leading to increased surface roughness. When the milling was done at 45^0 angle and rotated at 5 RPM, there was a significant reduction in the resist sticking to sidewall. This is clearly shown in Fig 4.16. This process lead to an average Er:Ta_2O_5 etch rate of $\sim$20 nm/min which was consistent over a range of samples for longer etch time as shown in Fig 4.17. But for shorter etch duration ($<$ 7 minutes) the etch rate was found to be higher ($\backsim$ 22 nm/min). After milling the sample was cleaned in acetone/IPA and ultrasonic bath to remove the resist scum following the etching process. It was found that this process alone was not effective in removing the scum completely. Therefore, O_2 plasma ashing was used to remove the resist scum. A 10 minute oxygen plasma treatment (pressure 50 mTorr, O_2 flow rate 10 sccm, power 100 W), followed by another acetone + ultrasonic bath + IPA wash, completely removed all the scum from the sidewalls and elsewhere. The etch depth was measured using stylus profilometer and for 20 minutes of etching the etch depth was found in the range 400 $\pm$ 25 nm across whole wafer.

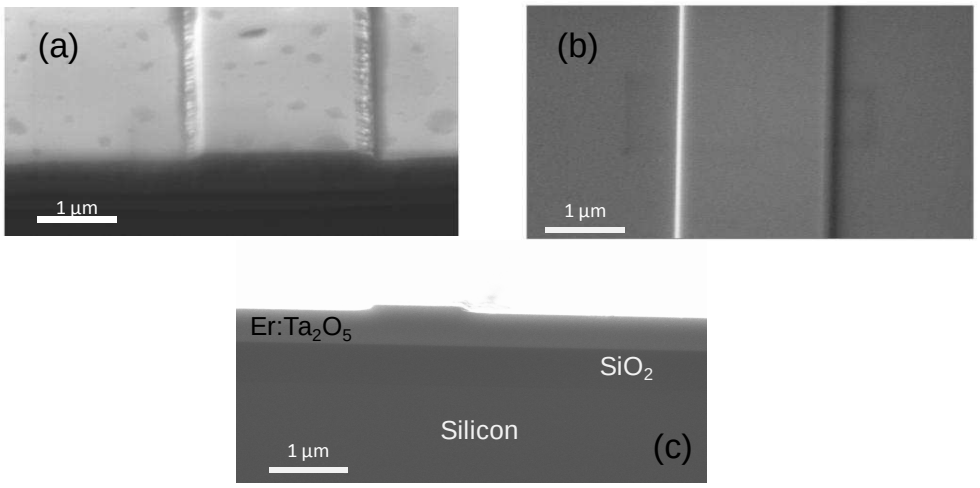

FIGURE 4.16: SEM pictures of rib waveguides fabricated by argon IBM at a) conventional 0^0 angle b) at 45^0 angle and c) end-on rib waveguide image. Note the reduction in the sidewall roughness/debris in the latter case (b).

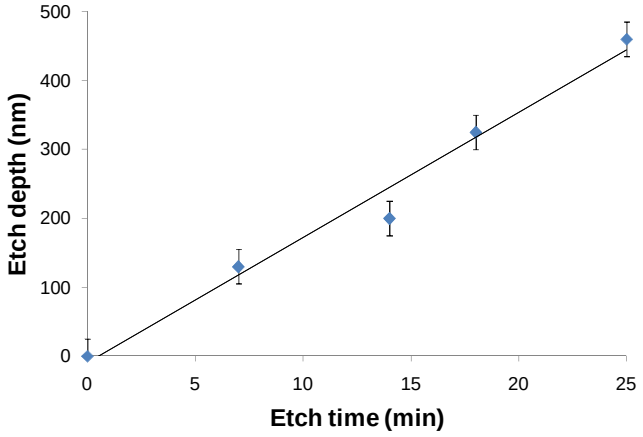

FIGURE 4.17: Etch rate of Er:Ta_2O_5using argon IBM at 45^0angle. The etching conditions were fixed at Ar gas flow 6 sccm, beam current 100 mA, beam voltage 500 V and RF power 500 W.

4.3.2.3 Annealing

After milling and cleaning, the sample was treated with aqueous potassium hydroxide (KOH) solution at 55^0C for 20 minutes and then thoroughly cleaned with de-ionized water. Lastly, this sample was annealed in O_2 at 600^0C for 2 hours in a tube furnace.

The annealing temperature and duration was based on the photoluminescence (PL) characterization results of Er:Ta_2O_5, where the maximum PL intensity and lifetime of erbium ions (2.4 ms) was achieved as discussed in section 4.2.6. The ramp time (up and down) was kept at 3^0C/min and the oxygen flow rate was fixed at 2 L/min. Annealing helps in maintaining the stoichiometry of the tantala by making up for any oxygen deficiency during the thin film deposition and reducing the absorptive losses. Annealing leads to a significant reduction in the waveguide propagation loss as will be shown in forthcoming section.

4.3.2.4 Cladding, dicing and polishing

The samples were then cladded with 2 μm thick silica using the same magnetron sputtering machine. The deposition rate for silica was found to be ∼3.3 nm/min. Post cladding the samples were re-annealed in oxygen at 600^0C for 2 hours to make up for any oxygen deficiency in silica during sputtering and to make the sputtered silica smooth. The final fabrication step was to dice the sample into smaller lengths to be used for optical characterisation. The diced samples were aligned and stacked to be end polished in the polishing machine. Care was taken that the all the diced samples were parallel to each other and to the sample holder during polishing to ensure perpendicularity of the waveguides to the end facets. However on few occasions waveguides were found to be at a greater angle ($< 2^o$) and it is expected that these waveguides might have higher mirror butting loss than the waveguides that are perpendicular to the end-facets.

4.3.3 Optical characterisation and erbium spectroscopy

4.3.3.1 Optical characterisation

Light from a tunable laser emitting between 1500-1580 nm was coupled into the monomode waveguides by end-fire coupling using a 40x lens objective and coupled out using a 40x objective and imaged onto a infrared (IR) camera and photodetector. Waveguides with width W between 1 μm and 3 μm were observed to be single mode at 1530 nm in accordance with the theoretical prediction of Eq.(4.2, 4.3). The mode intensity profile of a waveguide, both theoretical and experimental with width W= 1 μm and height H∼ 2.1 μm is shown in Fig 4.18. The modal spotsize for this waveguide was fitted to a Gaussian and the width was found to be ∼ 3.5 μm in the direction parallel to the surface and ∼ 2 μm in the direction normal to the surface as shown in Fig 4.18.

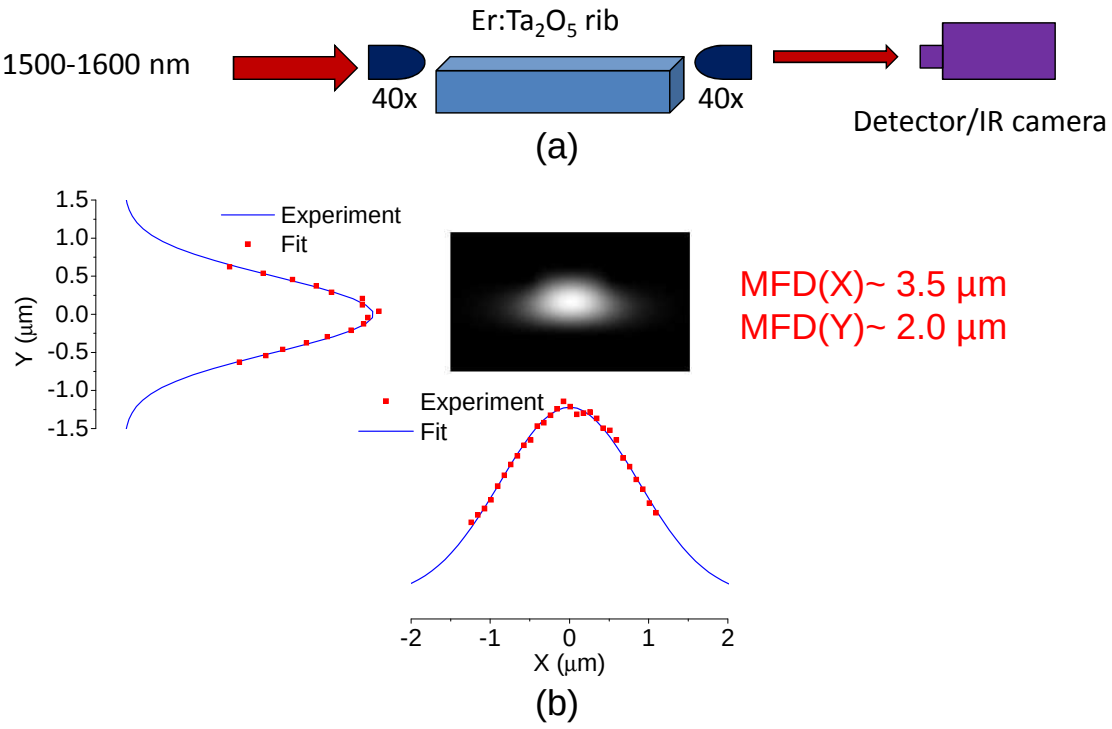

FIGURE 4.18: Mode intensity profile for a rib waveguide with width 1 μm and height 2.0 μm at 1530 nm. Red dots are the experimental points and the blue line is the Gaussian fit.

The propagation (waveguide) loss in the rib waveguides were measured at 1600-1620 nm, away from erbium absorption band using two techniques- cut-back [24] and FP method [25, 26]. In the cut-back method, the length of the sample to be used for loss measurements was measured followed by coupling light into the waveguide using 40x lens objective . Then the the input and output power from the waveguide at the desired wavelength was measured and the insertion loss (in dB) of the waveguide was calculated. The waveguide sample was then cleaved from the output end and whole process is repeated for 3-4 times each time measuring the loss for a shorter sample. Care was taken not to damage the input end and the loss was measured in the same set of 3-4 waveguides for every length of the sample. Finally, insertion loss vs. length of the sample was plotted and the experimental points were fitted to a straight line. The slope of the line fit yielded the value of the propagation loss while the intercept of the line on the y-axis (insertion loss) gave an estimate of the coupling loss. Fig 4.19 shows the result for an unannealed sample for different waveguides with different widths. The losses measured in the unannealed sample was in the range of 2.5-4 dB/cm. This method is quick and simple method to measure both the propagation and coupling loss in the waveguide but it is a destructive technique because the waveguide are physically cleaved into smaller lengths. Besides, there is some error in the experiments introduced due to

the change in the coupling conditions when the waveguide is taken out of the set up for cleaving and put back again for measuring loss. However the method is acceptable for estimating the coupling and propagation loss.

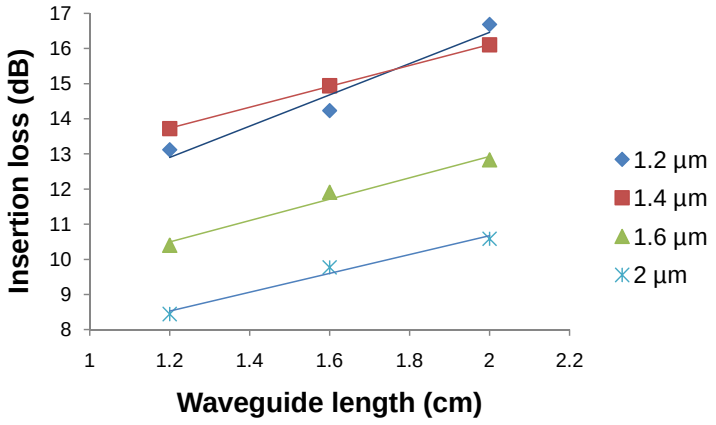

FIGURE 4.19: Insertion loss of Er:Ta_2O_5 rib waveguides of different widths in an unannealed sample

To reduce losses, monomode waveguide samples were treated with aqueous KOH solution at temperatures between 45^0C and 75^0C, for 5-30 minutes, to reduce roughness, thoroughly cleaned with deionized water and then annealed in oxygen at 600^0C between 2 and 10 hours. It was found that the waveguide loss was as high as 4.2 dB/cm for unannealed sample and decreased significantly to around 0.7 dB/cm for the sample that was treated with aqueous KOH at 55^0C for 20 minutes followed by annealing in O_2 for 2 hours. The optical loss remained similar (0.7 dB/cm) in the samples that were annealed for longer duration (4 & 10 hours).

The annealing temperature and initial duration were based on the previous PL results for Er:Ta_2O_5 slab waveguides, where the maximum PL intensity and erbium ion lifetime (2.4 ms) was achieved. The combination of KOH treatment and O_2 annealing dramatically reduced the waveguide propagation losses to $\sim$ 0.7 dB/cm. This was mainly due to the reduction in the absorptive loss and cleaner sidewalls. The annealing time did not have a major influence on the loss for dwell time longer than 2 hours and for all future devices the annealing time was fixed at 2 hours. (as shown in Fig 4.20)

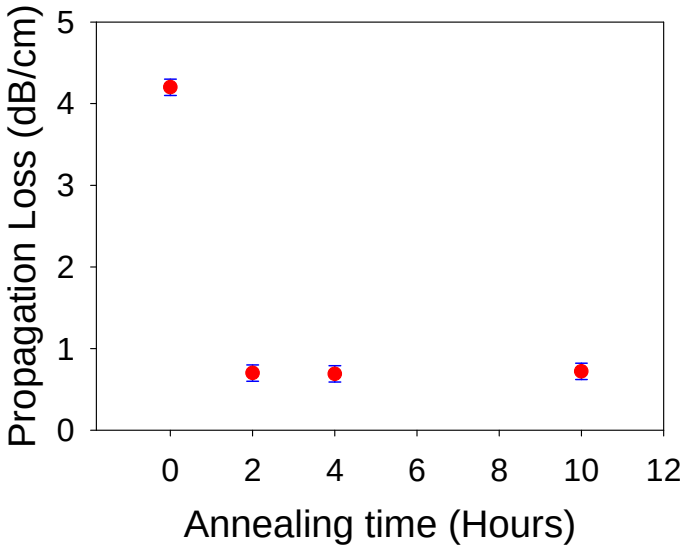

FIGURE 4.20: Effect of annealing on propagation loss of Er:Ta_2O_5 rib waveguide

A much better technique to measure losses, especially in the HIC material is the FP method. This method is based on the fact that the guided mode of the waveguide is partially reflected from the end facets of the waveguide due to the mismatch in the index between the air and and propagating mode. The reflected modes then interfere with each other to form a standing wave inside the waveguide cavity. When the transmitted power is spectrally scanned then oscillating intensity with respect to wavelength is obtained. The contrast of this pattern (γ), defined by

$$\gamma = \frac{(I_{max} - I_{min})}{(I_{max} + I_{min})} \tag{4.4}$$

where I_{max} & I_{min} corresponds to the maximum and minimum output intensities respectively. Assuming the waveguides are perpendicular to the end facets, the cavity loss (Λ) can be determined by the following relation [25]

$$\Lambda = 4.34 \left[ln\,(R) - ln \frac{1 - \sqrt{1 - \gamma^2}}{\gamma} \right] \tag{4.5}$$

where R is the end face Fresnel reflection coefficient between air and Er:Ta_2O_5 waveguide mode:

$$R = \frac{(n_{eff} - 1)^2}{(n_{eff} + 1)^2} \tag{4.6}$$

In Eq.(4.5), the second term in the square bracket represents the total waveguide loss (in dB) whereas the first term the loss due to Fresnel reflection. Contrast measurements were performed by tuning the wavelength of the light coupled into the waveguide and measuring the output intensity. The propagation loss in the waveguide was determined

by fitting and extracting the loss parameter α given by [27]

$$I_t = \frac{T^2 e^{-\alpha L}}{(1-R)^2 + 4R\sin^2(\phi/2)} I_0 \eta \tag{4.7}$$

where I_0 is the incident intensity, η is the coupling efficiency to the fundamental mode of the waveguide, T is the end-facet transmissivity, $\phi = 2\beta L$, is the internal phase difference with β being the propagation constant of the fundamental mode of the waveguide and R is given by Eq.(4.6).

This method is non-destructive, reliable and consistent technique to estimate the losses in the channel waveguides. But this method requires the waveguide to be single moded and to be perpendicular to the end facets. The end face quality is also important in obtaining good reflection from the end facets and hence consistent standing wave pattern. But because it is difficult to estimate the end face quality therefore there is always an error while calculating Fresnel coefficient using Eq.(4.6) and therefore, the losses estimated by the FP is the upper limit for the losses in the waveguide.

One such result is depicted in Fig 4.21for a waveguide of length 3.2 cm. The fit corresponds to a waveguide loss (α) equivalent to 0.65 $\pm$ 0.05 dB/cm. The losses were measured in many samples from different wafers and the measurements were repeatable for the optimised waveguide samples. The experimental set up remained similar to the one used for cut-back method except for the fact that single mode fibre (SMF 28) was used to couple light into the fibre. The wavelength was tuned using a tunable laser with a resolution of 1 pm. The contrast of the pattern shown in Fig 4.21 corresponds to the loss (0.65 dB/cm) while the free spectral range (FSR) yields the effective index of the mode (2.04).

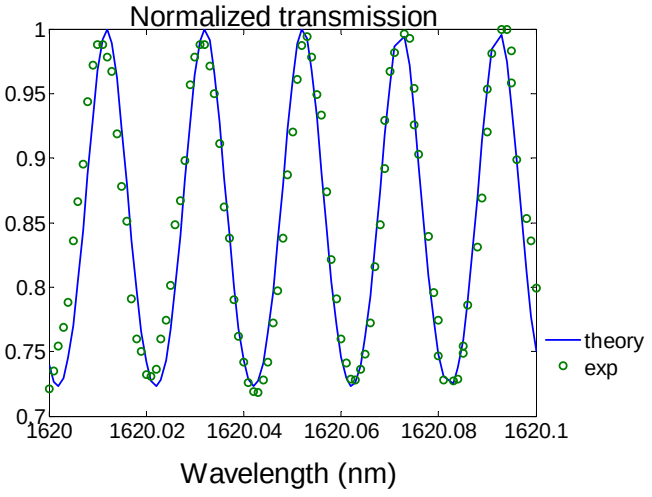

FIGURE 4.21: Propagation loss measurement in Er:Ta_2O_5 rib waveguide using the FP method.

4.3.3.2 Erbium absorption and emission cross sections

Measurement of the absorption spectra of monomode erbium-doped channel waveguides allows the precise determination of the erbium absorption cross sections at the pump (977 nm) and signal (1530 nm) wavelengths. The emission cross section at the signal wavelength was then be calculated from the absorption spectrum using McCumber theory [28].The absorption spectrum for Er:Ta_2O_5 was determined by broadband (700 nm to 1700 nm) white light measurements complemented by measurements using a tunable laser at wavelengths between 1500 nm and 1580 nm, where the total attenuation was high. In the former, light from a tungsten halogen lamp was coupled into a conventional optical fibre which was monomode at 1550 nm, which was butt-coupled to a one of the 4 μm high 1wt.% Er:Ta_2O_5 rib waveguide samples of length 2.5 cm. This waveguide design ensured that negligible power travelled in the cladding so that the absorption measurements were a true reflection of the Er:Ta_2O_5 material. Light was coupled out of the waveguide using a multimode fiber into an OSA. The resulting spectrum is shown in Fig 4.22a, where the prominent absorption bands of erbium (800, 980 and 1530 nm) are clearly visible. In the second experiment, a tunable laser (1500 nm to 1580 nm) was coupled into the same waveguide using a SMF and the output was collected by a multimode fiber and coupled into the OSA. The resulting spectrum is shown in Fig 4.22b. The peak absorption cross section for erbium ions in Ta_2O_5 in the pump band occurred at 977 nm and was calculated to be 2.10 $\pm$ 0.02 x 10^{-21}cm^2, using the estimated erbium concentration of 2.7 x 10^{20}ions/cm^3. This corresponded to a pump absorption of 2.40 $\pm$ 0.05 dB/cm.

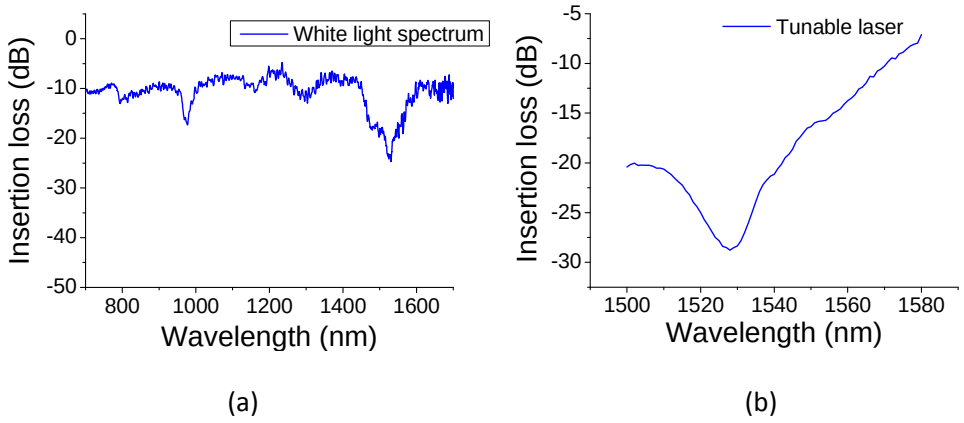

FIGURE 4.22: Absorption spectra of Er:Ta_2O_5 using a) White light spectrum b) tunable laser

The white light spectrum was noisy due to low input power and high coupling loss, and it was difficult to extract precise quantities especially in the 1500-1530 nm range

where the signal to noise ratio was poor. The tunable laser gave a smooth spectrum in the wavelength range of 1500-1580 nm. The two sets of measurements were stitched to obtain a high-quality absorption spectrum in the 1430-1600 nm range, which is shown in Fig 4.23. The peak absorption in the signal band occurred at a wavelength of 1527 nm and the peak cross section was calculated to be 4.8 $\pm$ 0.2 x 10^{-21}cm^2. This corresponded to an (unpumped) signal absorption of approximately 6.15 $\pm$ 0.25 dB/cm.

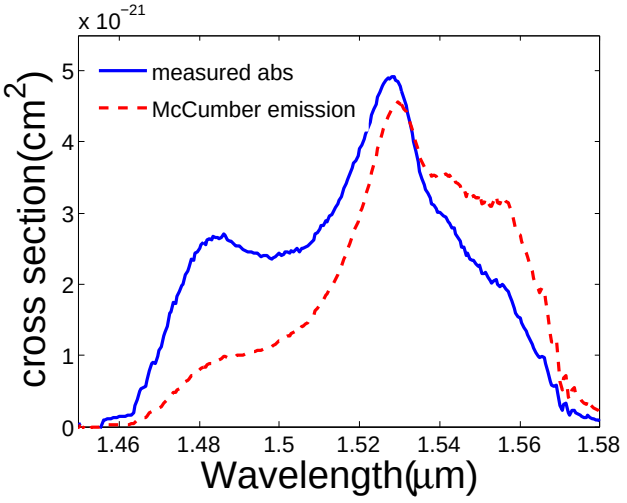

FIGURE 4.23: Absorption cross section, and emission cross section calculated by McCumber theory, of erbium ions in tantala host.

The emission cross section was calculated using McCumber theory [28]. According to this theory, the emission and absorption cross section of rare earth ions are related by the following equation [28]

$$\sigma_e(\nu) = \sigma_a(\nu)\, e^{-\frac{(\epsilon - h\nu)}{kT}} \tag{4.8}$$

Where ϵ is the net free energy required to excite one erbium ion from the $^4I_{15/2}$ to $^4I_{13/2}$ state at temperature T. Eq.(4.8) also indicates that the cross sections are equal at only one crossing frequency, ϵ/h. For higher frequencies, the emission cross section is smaller than absorption and vice versa for lower frequencies. Thus, for the calculation of the emission cross section, the knowledge of ϵ is very vital. The calculation of ϵ requires the knowledge of all the stark levels (8 ground levels and 7 excited first levels) and can be done in the following manner

$$\frac{N_1}{N_2} = e^{(\epsilon/kT)} \tag{4.9}$$

If the position of all the Stark levels is known then [28]

$$\frac{N_1}{N_2} = \frac{1 + \sum_j exp\left(-\frac{E_{1j}}{kT}\right)}{exp\left(-\frac{E_0}{kT}\right)\left[1 + \sum_j exp\left(-\frac{E_{2j}}{kT}\right)\right]} \tag{4.10}$$

In this expression E_0 is the separation between the lowest energy levels of the two manifolds $^4I_{15/2}$ and $^4I_{13/2}$ i.e. E_{21}-E_{11} and summation is over j sub-levels (1 to 8) for the numerator and from j=1 to j=7 for the denominator. This method has a practical difficulty for the material system where the sub-level energies (Stark levels) are unknown (e.g. Er:Ta_2O_5). Therefore, a modified version of McCumber theory [28] was used to calculate ϵ. This theory assumes the following [28]

- The manifold has stark levels equally spaced and is given by $E_{ij} = (j-1)E_i$. This assumption reduces the number of parameters from 14 to 3 in Eq.(4.10).
- The E_0 is the manifold spacing and taken as the average of the absorption (white light spectrum) and emission (photoluminescence spectrum) peaks.
- For the half widths of the spectrum, the separation between the peak and the energy at which the peak falls to its 5% value and then equate it to the spread of absorption (ΔE_1) and the emission manifold (ΔE_2) to find the approximate value of E_1 and E_2 such that

  $$\Delta E_1 = 7E_1 \,\&\, \Delta E_2 = 6E_2 \tag{4.11}$$

  Then finally using above assumptions, Eq.(4.9-4.11), ϵ can be evaluated as the following

  $$e^{(\epsilon/kT)} = Ke^{(E_0/kT)} \tag{4.12}$$

  Where K is the normalization constant with which the absorption cross section must be multiplied to obtain the absolute emission cross section. Based on this theory, ΔE_1 and ΔE_2 were calculated from the white light spectrum Fig 4.22a and PL spectrum Fig 4.12 and then using Eq. (4.8, 4.10, 4.11) emission cross section for wavelengths were calculated. The calculated emission spectrum is shown superimposed on the absorption spectrum in Fig 4.23 and the value of the peak emission cross section was found to be 4.4 ± 0.2 $\times 10^{-21}$cm^2. This cross-section and concentration corresponds to a maximum gain obtainable, for a propagation loss of 0.65 dB/cm and assuming perfect spectroscopic behavior and complete inversion, of 3.1 ± 0.1 dB/cm as discussed in chapter 3 and 5. The peak absorption and emission cross sections of Er:Ta_2O_5 near 1530 nm are compared with those of other HIC host materials in Table 4.4. The absorption cross-section is comparable to other HIC materials but the emission cross section value is slightly on the lower

side and the expected behavior for a high index material is high emission cross-section. Low emission cross-section would yield lower gain in the material system. The emission cross-section could be further improved by alternative deposition techniques as discussed in chapter 7.

Host	Refractive index	Absorption cross section (10^{-21}cm^2)	Emission cross section (10^{-21}cm^2)
Phosphate [29]	1.51	5.4	5.3
Alumina [10]	1.64	5.6	4.2
ZSG [14]	1.75	6.0	-
Tellurite [9]	2.05	6.8	6.9
Zirconia [12]	2.08	5.6	-
Tantala [this thesis]	2.10	4.8	4.4

TABLE 4.4: Comparison of erbium cross sections in different host materials

4.4 Conclusions

The entire fabrication process of Er:Ta_2O_5 waveguides on silicon was optimised for yielding low loss, single mode slab/rib waveguides at 1500-1550 nm. The thin film was deposited on oxidised silicon using magnetron sputtering and channels were defined using photolithography. The maximum losses measured in the optimised cladded rib waveguides was 0.60 dB/cm at 1600 nm where the losses were measured using cut-back and FP method. The refractive index of the waveguides was measured to be 2.105 at 1530 nm using ellipsometry. PL and lifetime experiments were performed on the optimised thin film and that yielded a metastable lifetime of 2.3 ms and a bandwidth of 50 nm that was comparable to other HIC materials. The peak absorption cross-section for $^4I_{13/2}$ manifold was measured to be 4.8 $\times$ 10^{-21}cm^2 that was comparable to other materials but the emission cross-section that was measured to be 4.4 $\times$ 10^{-21} cm^2 using McCumber theory was slightly on the lower side when compared to other high index materials. The optical characterisation and erbium spectroscopy results on Er:Ta_2O_5 waveguides are promising for making amplifiers and lasers in the 1550-1550 nm wavelength band.

Bibliography

[1] P. K. Tien. *Light Waves in Thin Films and Integrated Optics. Appl Opt*, **10**:2395, 1971.

[2] A. Kahn, Y. Kuzminykh, H. Scheife, and G. Huber. *Nondestructive measurement of the propagation losses in active planar waveguides. J Opt Soc Am B*, **24**:1571, 2007.

[3] Y. Okamura, S. Yoshinaka, and S. Yamamoto. *Measuring Mode Propagation Losses of Integrated Optical-Waveguides - a Simple Method. Appl Opt*, **22**:3892, 1983.

[4] H.G. Tompkins. A User's guide to ellipsometry. Academic press Inc., San Diego, 1993.

[5] K. Postava, M. Aoyama, T. Yamaguchi, and H. Oda. *Spectroellipsometric characterization of materials for multilayer coatings. Appl Surf Sci*, **175**:276, 2001.

[6] S. Musa, H. J. van Weerden, T. H. Yau, and P. V. Lambeck. *Characteristics of Er-doped Al_2O_3 thin films deposited by reactive co-sputtering. J Quant Electron*, **36**:1089, 2000.

[7] P. C. Joshi and M. W. Cole. *Influence of postdeposition annealing on the enhanced structural and electrical properties of amorphous and crystalline Ta_2O_5 thin films for dynamic random access memory applications. J Appl Phys*, **86**:871, 1999.

[8] P. M. Peters, D. S. Funk, A. P. Peskin, D. L. Veasey, N. A. Sanford, S. N. Houde-Walter, and J. S. Hayden. *Ion-exchanged waveguide lasers in Er^{3+}/Yb^{3+} codoped silicate glass. Appl Opt*, **38**:6879, 1999.

[9] R. Rolli, M. Montagna, S. Chaussedent, A. Monteil, V. K. Tikhomirov, and M. Ferrari. *Erbium-doped tellurite glasses with high quantum efficiency and broadband stimulated emission cross section at 1.5 μm. Opt Mater*, **21**:743, 2003.

[10] J. D. B. Bradley, L. Agazzi, D. Geskus, F. Ay, K. Worhoff, and M. Pollnau. *Gain bandwidth of 80 nm and 2 dB/cm peak gain in Al_2O_3:Er^{3+} optical amplifiers on silicon. J Opt Soc Am B*, **27**:187, 2010.

[11] K. Vu and S. Madden. *Tellurium dioxide Erbium doped planar rib waveguide amplifiers with net gain and 2.8dB/cm internal gain. Opt Exp*, **18**:19192, 2010.

[12] R. Schermer, W. Berglund, C. Ford, R. Ramberg, and A. Gopinath. *Optical amplification at 1534 nm in erbium-doped zirconia waveguides. J Quant Electron*, **39**: 154, 2003.

[13] R. R. Goncalves, G. Carturan, M. Montagna, M. Ferrari, L. Zampedri, S. Pelli, G. C. Righini, S. J. L. Ribeiro, and Y. Messaddeq. *Erbium-activated HfO_2-based waveguides for photonics. Opt Mater*, **25**:131, 2004.

[14] C. C. Baker, J. Heikenfeld, Z. Yu, and A. J. Steckl. *Optical amplification and electroluminescence at 1.54 μm in Er-doped zinc silicate germanate on silicon. Appl Phys Lett*, **84**:1462, 2004.

[15] A. V. Chelnokov, J. M. Lourtioz, P. Boucaud, K. Bernas, J. Chaumont, and T. Plowman. *Deep Erbium-Ytterbium Implantation Codoping of Low-Loss Silicon Oxynitride Wave-Guides. Electron Lett*, **31**:636, 1995.

[16] L. O. Lierstuen and A. S. Sudbo. *Coupling Losses between Standard Single-Made Fibers and Rectangular Wave-Guides for Integrated-Optics. Appl Optics*, **34**:1024, 1995.

[17] D. Van Thourhout, G. Roelkens, R. Baets, W. Bogaerts, J. Brouckaert, P. Debackere, P. Dumon, S. Scheerlinck, J. Schrauwen, D. Taillaert, F. Van Laere, and J. Van Campenhout. *Coupling mechanisms for a heterogeneous silicon nanowire platform. Semicond Sci Tech*, **23**, 2008.

[18] B. Jalali, P. D. Trinh, S. Yegnanarayanan, and F. Coppinger. *Guided-wave optics in silicon-on-insulator technology. IEE P-Optoelectron*, **143**:307, 1996.

[19] A. G. Rickman, G. T. Reed, and F. Namavar. *silicon-on-insulator optical rib waveguide loss and mode characteristics. J Lightwave Technol*, **12**, 1994.

[20] R. A. Soref, J. Schmidtchen, and K. Petermann. *Large Single-Mode Rib Wave-Guides in Gesi-Si and Si-on-SiO_2. J Quant Electron*, **27**:1971, 1991.

[21] Ramaswamy.V. *Strip-Loaded Film Waveguide. AT & T Tech J*, **53**:697, 1974.

[22] S. P. Pogossian, L. Vescan, and A. Vonsovici. *The single-mode condition for semiconductor rib waveguides with large cross section. J Lightwave Technol*, **16**:1851, 1998.

[23] O Powell. *single-mode condition for silicon rib waveguides. J Lightwave Technol*, **20**, 2002.

[24] I. P. Kaminow and L. W. Stulz. *Loss in Cleaved Ti-Diffused $LiNbO_3$ Waveguides. Appl Phys Lett*, **33**:62, 1978.

[25] D. Castaldini, P. Bassi, S. Tascu, G. Sauder, P. Aschieri, M. De Micheli, P. Baldi, K. Thyagarajan, and M. R. Shenoy. *All-in-one measurement setup for fast and accurate linear characterization of guided-wave optical devices. Opt Eng*, **46**, 2007.

[26] S. Taebi, M. Khorasaninejad, and S. S. Saini. *Modified Fabry-Perot interferometric method for waveguide loss measurement. Appl Opt*, **47**:6625, 2008.

[27] R. Regener and W. Sohler. *Loss in Low-Finesse Ti-$LiNbO_3$ Optical Wave-Guide Resonators. Appl Phys B*, **36**:143, 1985.

[28] W. J. Miniscalco and R. S. Quimby. *General Procedure for the Analysis of Er^{3+} Cross-Sections. Opt Lett*, **16**:258, 1991.

[29] J. A. Valles, M. A. Rebolledo, and J. Cortes. *Full characterization of packaged Er-Yb-codoped phosphate glass waveguides. J Quant Electron*, **42**:152, 2006.

Chapter 5

Er:Ta_2O_5 Waveguide Amplifier and Laser

EDWAs are key integrated optical devices potentially providing gain in the telecommunications C-band window (1525-1565nm) for metro networks [1]. Ideally, an EDWA should be compact and provide high gain at low pump power to compensate for the loss in passive devices in a network. Gain in waveguides has been demonstrated in several dielectric waveguide materials [2–9] but recently there has been significant growth in interest in HIC materials systems for compact, low power amplifiers [10–12]. HIC between waveguide core and cladding allows strong confinement of optical modes and small bend radii with low loss, enabling ultra small devices for dense lightwave circuits. The tight mode confinement results in low pump power threshold for amplification and, where desired, low-power nonlinear devices. Among HIC materials, alumina [12] (n=1.64) has exhibited a net gain of 2 dB/cm with a pump threshold of 4 mW ($I_{th}\sim$ 1.75 x 10^5 W/cm^2) but has insufficiently high refractive index for ultra-compact devices such as photonic crystals, zirconia [11] (n=2.08) and zinc-silicate-germanate [10] (n=1.75) exhibited much lower gain (< 1dB/cm) with pump thresholds at 36 mW ($I_{th}\sim$ 3.43 x 10^5 W/cm^2) and 12 mW ($I_{th}\sim$ 4 x 10^5 W/cm^2) respectively while the high-index glasses such tellurite [13] have shown on-chip net gain of 2.2 dB/cm but have higher threshold ($P_{th}\sim$25 mW, $I_{th}\sim$ 9.26 x 10^5 W/cm^2) and lower lifetime whereas other HIC glasses have lower compatibility with silicon processing. Tantalum pentoxide has been used as a host for erbium ions [14, 15], but to date gain and lasing has only been reported in Nd-doped tantalum pentoxide [16] . In this chapter, the net gain and laser action is demonstrated for the first time in waveguides fabricated in Er:Ta_2O_5. The lasing was achieved by attaching mirrors to the ends of the rib waveguides, and pumped using a 977 nm laser diode and gain was measured by coupling pump and signal simultaneously using a fibre WDM.

5.1 Gain measurements in Er:Ta_2O_5waveguides

For gain measurements, rib waveguides of nominal widths ranging from 1 μm – 10 μm with etched depths of approximately 400 ± 25 nm, were fabricated under optimised conditions as discussed in chapter 4. The waveguides formed were measured to be typically 0.3 μm wider than the nominal width (i.e. the original mask width). A 2-μm-thick silica cladding was deposited on top of these waveguides to further reduce the losses and improve the symmetry of the modes. The clad waveguides were re-annealed as above to reduce absorptive losses in the cladding. The wafers were then diced and end-polished to provide 2.3-cm-long waveguides, which were then characterised for propagation loss and for erbium absorption at the pump and signal wavelengths. The refractive index of an Er:Ta_2O_5 film deposited and annealed as above was measured by spectroscopic ellipsometry to be n = 2.10 at a wavelength of 1530 nm. The waveguide propagation loss was measured at wavelengths near 1620 nm, where the erbium absorption is weak, using the FP method [17] with end-fire coupling from a tunable semiconductor laser, and found to be α = 0.65 ± 0.05 dB/cm. White light was coupled into a nominally 2 μm wide waveguide to measure the absorption spectra, and the peak erbium absorption was found to be 5.7 ± 0.2 dB/cm at 1527 nm and 2.50 ± 0.02 dB/cm at 977 nm, yielding peak absorption cross-sections of σ_a = 4.8 ± 0.2 × 10^{-21} cm^2 at 1527 nm and 2.10 ± 0.02 × 10^{-21} cm^2 at 977 nm. The emission cross-section was then calculated to be σ_e = 4.4 ± 0.2 × 10^{-21} cm^2 using modified McCumber theory [18] , and the excited-state ($^4I_{13/2}$ level) lifetime was measured to be τ = 2.3 ± 0.1 ms. All the above parameters (σ_a, σ_e & τ) were calculated using the methods described in detail in chapter 4.

Gain measurements were performed by coupling pump and signal simultaneously into waveguides using a fibre WDM. The output was collected using a multimode fibre and analysed using an OSA as shown in Fig 5.1 . The waveguide was pumped using a laser diode at 977 nm and the signal was provided by a tunable laser source, tuned from 1500 nm to 1550 nm. The launched pump power was estimated by measuring the output pump power at very low pump power levels (to prevent significant depletion of the ground state) and calculating the launched pump power by taking into account the absorption and propagation losses.

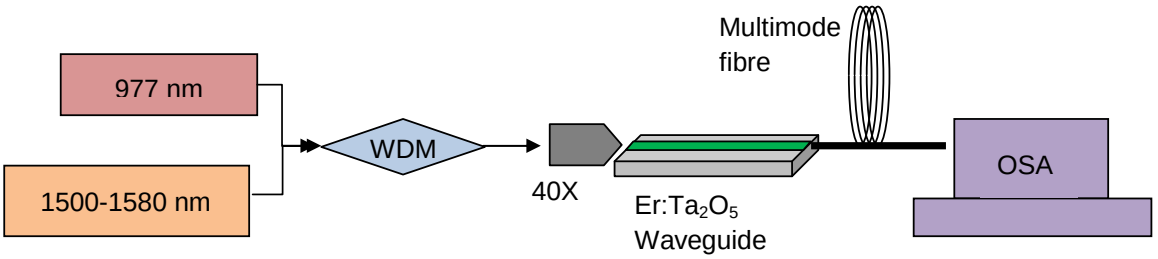

FIGURE 5.1: Schematic set-up for performing gain measurements

Measurements of the signal spectrum were made for launched pump powers of 1.2 mW and 20 mW and with the pump off, and with a launched signal power of 100 nW. Measurements of the ASE spectrum were made with the pump on and the signal off. The net optical gain coefficient (above the absorption and propagation losses), G_{dB}, was calculated by correcting the measured power enhancement at the signal wavelength for the ASE, erbium absorption and propagation loss as shown below:

$$G_{dB} = 10Log_{10}\left[\frac{(P_{sig+ase} - P_{ase})}{P_0}\right] - (\alpha + 4.34\sigma_a N)L \tag{5.1}$$

where $P_{sig+ase}$ and P_{ase} are the measured output powers at the signal wavelength with the signal on and off, respectively, P_0 is the measured signal output power with the pump off, L is the waveguide length (2.3 cm) and α, σ_a and N are the propagation loss (in dB/cm), absorption cross-section and dopant density. Fig 5.2 shows the experimentally-measured signal enhancement spectrum (the first term in Eq. (5.1)) and Fig 5.3 shows the net gain spectrum G_{dB}, both for a 2 μm wide waveguide. Zero "net" gain corresponds to the amplifier gain exactly compensating the waveguide propagation loss. The maximum net on-chip optical gain of 5.2 ± 0.1 dB (2.25 ± 0.05 dB/cm) was achieved at a signal wavelength of 1531.5 nm with a launched pump power of 20 mW (maximum power delivered by the diode). This corresponds to an internal gain (achievable if the propagation loss were reduced to near zero) of 2.9 ± 0.05 dB/cm.

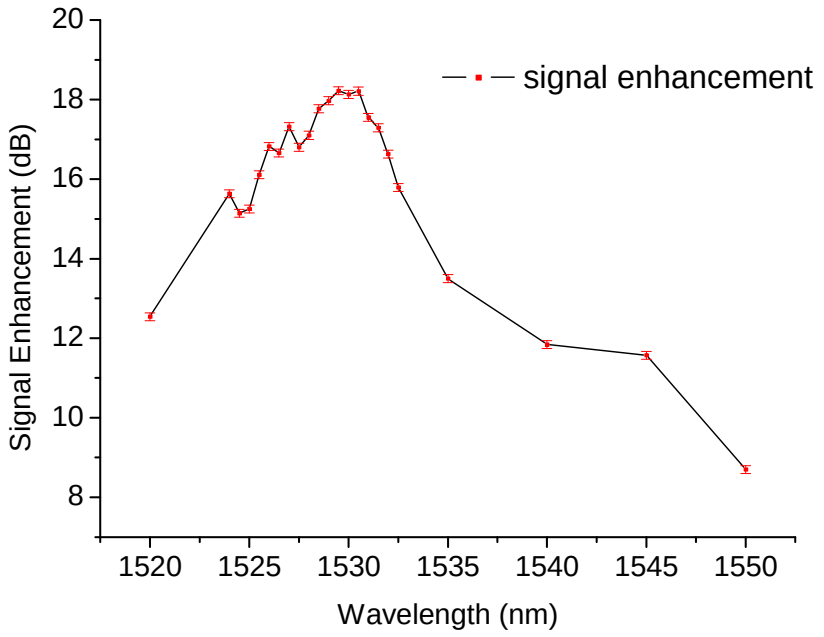

FIGURE 5.2: Signal enhancement for 2.3 cm long Er:Ta_2O_5 waveguide amplifier vs. wavelength for 20 mW of launched pump power at 977 nm. The line joining the experimental points is simply a guideline to the eye.

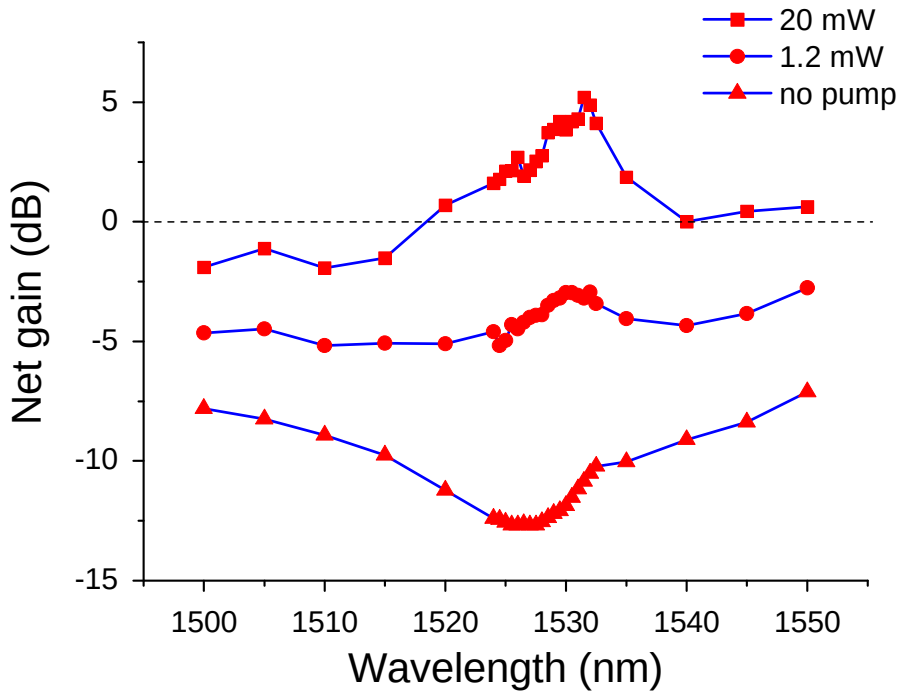

FIGURE 5.3: Net gain at different pump powers versus wavelength at a constant signal power of 0.1 µW. The line joining the experimental points are simply the guideline to eye.

Fig 5.4 shows the experimentally measured net gain for a nominally 2.6 μm wide waveguide at the maximum gain wavelength of 1531.5 nm as a function of launched pump power together with a theoretical curve assuming zero upconversion and a theoretical fit where the upconversion coefficient was the free parameter. The theoretical calculations were performed by solving the rate equations for erbium ions by numerical integration along the waveguide cavity as discussed in chapter 3. The experimental results show that positive net gain is achieved at a launched pump power of $\sim$ 4.5 mW, with the low value of gain threshold being due to the HIC between the waveguide core and cladding leading to a small modal spot-size (FWHM) of $\sim$ 2.0 $\times$ 4.05 μm^2 at $\lambda \approx$ 1530 nm as discussed in chapter 4. The experimentally measured maximum gain was 4.83 $\pm$ 0.11 dB corresponding to 2.1 $\pm$ 0.05 dB/cm, slightly lower than that in Fig 5.3 due to the lower pump intensity in this larger waveguide. The theoretical curves show that in the ideal case, with no upconversion or ESA, a maximum gain of 3.75 dB/cm would be expected, reduced to 3.1 dB/cm due to the waveguide loss, and that net gain would be achieved at a pump power of 0.5 mW. The theoretical curve including upconversion fits the experimental data well using a co-operative upconversion coefficient of 10^{-17} cm^3 s^{-1}, comparable to that in alumina doped with 3 $\times$ 10^{20} ions/cm^3 erbium ions [10] and confirming that this is the major limiting factor in high-concentration amplifier performance [19].

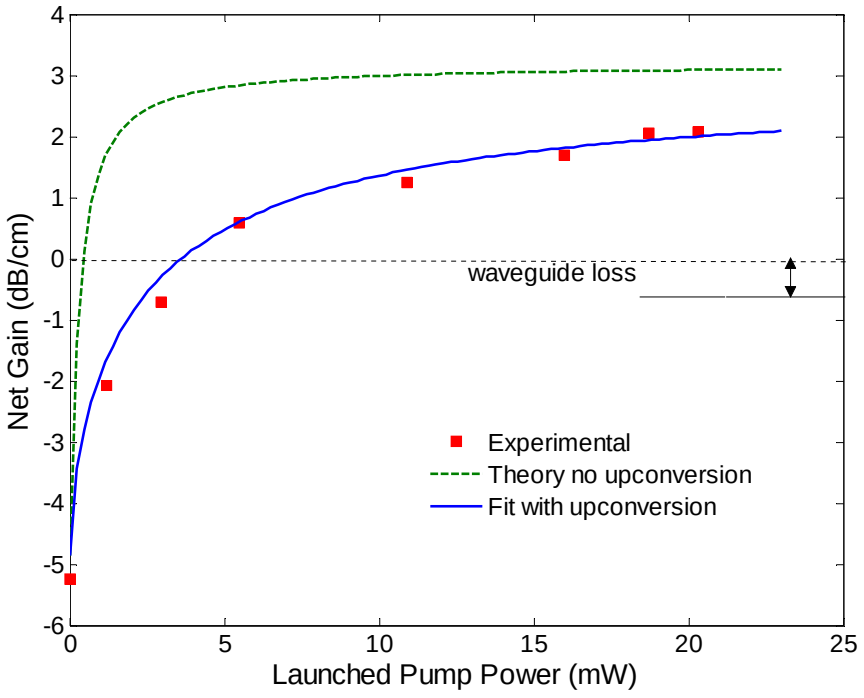

FIGURE 5.4: Net gain coefficient vs. launched pump power for a signal at 1531.5 nm wavelength. Net gain was achieved at a pump power of about 4.5 mW.

Amplifier performance could be further improved by (i) improving or using alternative waveguide fabrication to further reduce the losses and upconversion, (ii) optimising the erbium ion concentration for upconversion and gain coefficient and (iii) adjusting the length of the amplifier to yield the maximum gain for the available pump power and erbium concentration. Using the numerical model discussed in chapter 3, for the available pump power (200 mW) and calculated C_{up} (10^{-17} cm^3/s), a maximum gain of 10.81 dB can be extracted from the amplifier of length 5.2 cm with erbium concentration of 4.3 $\times$ 10^{20} ions/cm^3. A 20 dB gain for a 5 cm waveguide could readily be achieved, with a HIC waveguides on a 1 mm^2 chip, offering great potential for low-cost amplifiers.

5.2 Er:Ta_2O_5 waveguide laser

5.2.1 Lasing cavity characterisation

The waveguide sample used to make an EDWA was also used to demonstrate lasing action in erbium doped tantala film. A laser cavity was formed by affixing mirrors to both waveguide end facets with the aid of index matching oil. Both mirrors had $\sim$ 92% reflectivity in the 1500-1600 nm wavelength range and $>$ 95% transmission at 977 nm. The lasing cavity was characterised for losses using the FP method before the after fixing each mirror. The FP fringes before and after introduction of mirrors is shown in Fig 5.5a. The fringe contrast increases with the mirrors at the ends due to reduction in the cavity losses. Fig 5.5b is the theoretical prediction of the fringe contrast fitted to the experimental results of the change in the transmission through the waveguide with two mirrors at the ends. The total fractional round-trip loss measured by the FP measurements near 1620 nm was found to be $\Lambda = 0.86 \pm 0.03$, corresponding to approximately 8.4 dB. The cavity loss per trip was calculated from the fringe contrast (γ) using Eq. (4.5) in chapter 4

$$\Lambda = 4.34 \left[ln \frac{1 - \left(1 - \gamma^2\right)^{1/2}}{\gamma} \right] \tag{5.2}$$

$$\gamma = \frac{I_{max} - I_{min}}{I_{max} + I_{min}} \tag{5.3}$$

The known values of propagation loss (0.65 dB/cm) and attenuation due to mirror transmission (2 $\times$ 0.4 dB) yields an excess loss of approximately 2.3 dB/mirror.

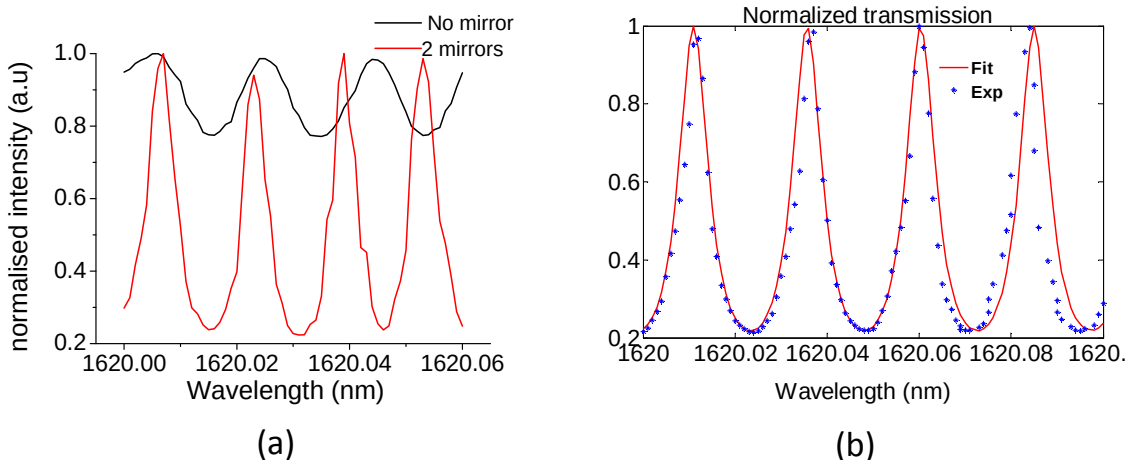

FIGURE 5.5: Laser cavity characterisation results a) FP oscillations with and without mirrors & b) theoretical fit to the FP experimental points in (a) with 2 mirrors

5.2.2 Lasing results

Pump light from a laser diode emitting at 977 nm was coupled into the waveguide using a ×40 objective (0.45 NA), as shown in Fig 5.6. With the output mirror removed and at maximum incident pump power, where the bleaching of erbium ions (inversion) is highest, the launched pump power was estimated from the output pump power by correcting for the measured propagation loss. With the output mirror re-attached, light emerging from the waveguide was collected using a multimode fibre and observed on an OSA in order to characterise laser action.

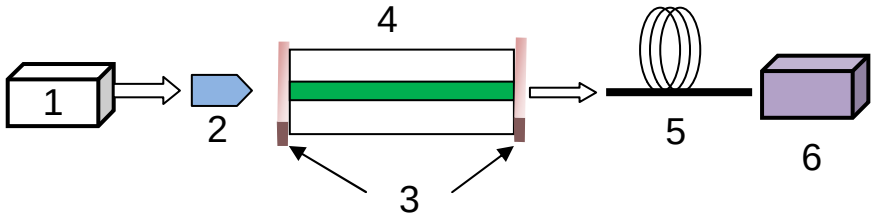

FIGURE 5.6: Schematic of the laser configuration. 1 (977 nm laser diode), 2 (× 40 objective), 3 (92% reflectivity mirrors), 4 (Er:Ta_2O_5 waveguide), 5 (multimode fibre), and 6 (OSA).

Fig 5.7 shows the lasing output power plotted against launched pump power for a waveguide of nominal width 2.4 µm. The maximum single-end output power at the lasing

wavelengths was ∼ 2.35 µW. It should be noted that a similar output power would also be available from the input mirror as it has the same reflectivity. The line of best fit to the data yields a pump threshold for lasing of approximately 14 mW and single end slope efficiency with respect to the launched pump power of ∼0.3%.

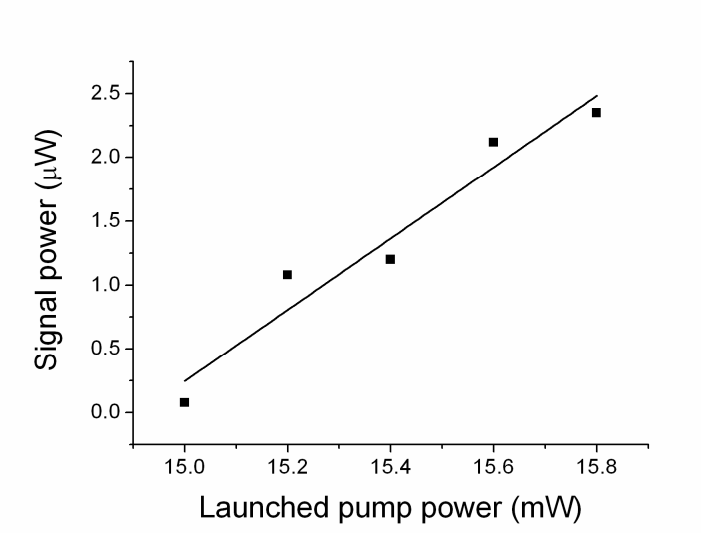

FIGURE 5.7: Laser output power vs. launched pump power with line of best fit.

The expected slope efficiency η_s with respect to the launched pump power can be written as follows [20]:

$$\eta_s = \frac{\lambda_p}{\lambda_s} \frac{ln\,(1-T)}{ln\,(1-\Lambda)} \eta_a \eta_q \eta_o \tag{5.4}$$

The first term gives the ratio of the signal and pump photon energies, T is the transmission of the output coupler (0.08), Λ is the total round trip loss of the waveguide cavity (∼0.86), η_a is the pump absorption efficiency, η_q is the quantum efficiency and η_o is an effective overlap factor between the pump and signal mode. Determination of η_a requires estimation of the degree of population inversion above threshold. Threshold is achieved when the round-trip gain equals the cavity loss, i.e.

$$(1-\Lambda)\, exp\,[2\,(n_2\sigma_e - n_1\sigma_a)\,L] = 1 \tag{5.5}$$

where Λ is the cavity round-trip loss, n_2 and n_1 are the excited-state and ground-state populations, respectively, σ_e and σ_a are the emission and signal absorption cross-sections at lasing wavelength, and L is the length of the cavity. Using $n_1 + n_2 = N$, the average inversion level (n_2/N) above threshold is estimated to be 0.72 therefore fraction of ions in the ground state (n_1/N) will be 0.28. The pump absorption in the sample with no pump was calculated to be 2.5 dB/cm so with 72% inversion, the pump absorption in the sample of 2.3 cm length is calculated to be 1.61 dB, and the corresponding pump absorption efficiency is $\eta_a = 0.31$. Taking the known cavity losses, and calculated overlap factor

(0.95) and using idealized values of the quantum efficiency, the maximum single-end slope efficiency w.r.t. launched pump power is predicted to be 0.78%. The discrepancy between this and the experimental value of 0.3% is most likely to be due to (i) reduced quantum efficiency due to non-radiative quenching sites and co-operative upconversion from the $^4I_{11/2}$ level [19] and (ii) an underestimate of the population inversion required for threshold due to upconversion processes reducing the gain for a given inversion, which then results in an overestimate of pump absorption.

Fig 5.8 shows the lasing spectrum for a 2.4 μm wide waveguide at several values of launched pump powers above threshold. Lasing was observed in a single longitudinal and transverse mode at 1558.8 nm for the highest available pump power. The calculated longitudinal mode spacing for the 2.3 cm cavity length and estimated modal effective index of 2.01 is $\sim$ 26 pm at wavelengths near 1559 nm. As the measurements were recorded with 20 pm resolution, if lasing had been on more than one longitudinal mode it would have been observable. No lasing was observed for waveguides of width less than 2 μm, probably due to imperfections during fabrication and hence higher loss, and for widths greater than 3.4 μm, due to reduced pump intensity inside the waveguide.

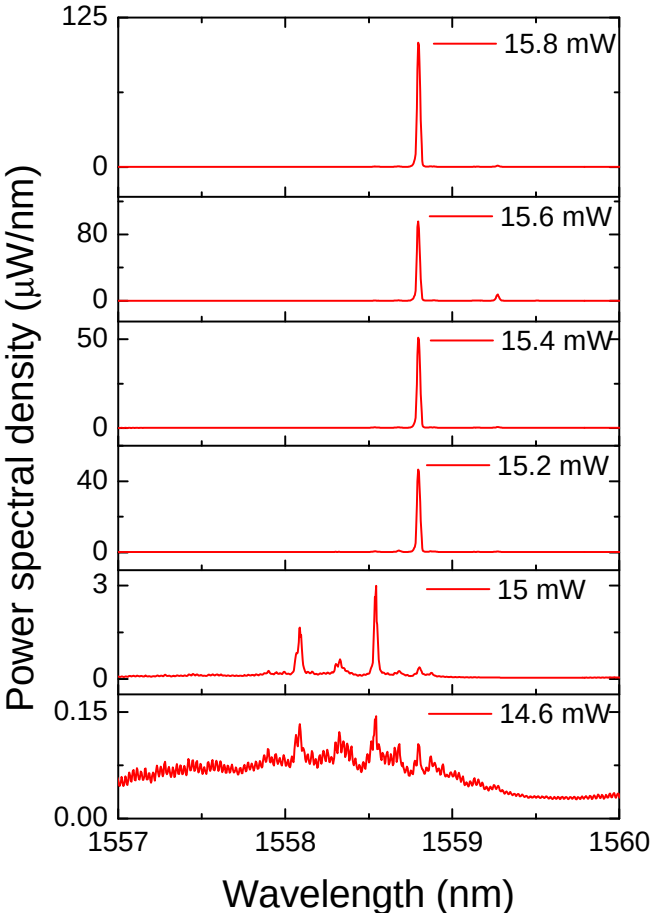

FIGURE 5.8: Laser output spectrum for various launched pump powers

5.2.3 Discussion

Comparison of the estimates of theoretical and experimental slope efficiency shows that tantala is a promising host for compact erbium-doped lasers and amplifiers. The experimental absorbed pump power threshold and slope efficiency may be estimated to be 4.3 mW and 1%, respectively. The absolute value of the slope efficiency is low primarily due to high cavity losses and due to double-ended emission from the cavity, and not due to fundamental limitations of the material. The high cavity losses can be attributed to the excess loss at the mirrors due to non-optimum polishing and possible non-perpendicularity of the waveguide channels and facets. Therefore, fabrication process improvements to further reduce propagation and mirror loss, and integration of grating or ring mirrors [12], is expected to improve the efficiency significantly. The pump absorption efficiency is estimated to be less than 31%, resulting in a significantly elevated threshold and reduced slope efficiency with respect to launched pump power. This may be improved by optimization of the cavity length and potentially by introducing a sensitizer such as Yb. Measurements of gain and optimization of erbium concentration with respect to effects such as upconversion are to be undertaken. The output power and the measured slope efficiency of the laser were also limited by the available pump power which yielded a very small range of experimental points (laser output power) just above threshold resulting in the low slope efficiency. The problem can be addressed by the combination of much powerful source and efficient pump coupling (e.g. lensed fibre).

5.3 Conclusions

Er:Ta_2O_5 waveguides were prepared by RF magnetron sputtering on oxidised silicon wafer. A net on-chip optical gain of 2.25 dB/cm at 1531.5 nm was achieved for the first time in Er:Ta_2O_5 waveguide amplifier doped with 2.7×10^{20} ions/cm^3 erbium ions. The 2.3 cm long waveguide was pumped at 977 nm and net gain was achieved at $\sim$ 4.5 mW of launched pump power, which is among the lowest threshold values yet achieved. The HIC ($\Delta n \approx 0.66$) between the core ($\Delta n \approx 2.10$) and cladding ($n \approx 1.45$) leads to tight confinement of the optical mode and efficient use of the pump leading to a low pump threshold. There is significant scope for improvement for the gain achieved in terms of optimising the length of the waveguide and concentration of the erbium ions in the waveguide. The combination of HIC and gain demonstrates a great potential for ultra-compact integrated photonic devices.

The same waveguides were also used to demonstrate an Er:Ta_2O_5 waveguide laser. The waveguide laser was pumped at 977 nm with a laser diode and lasing was observed between 1556 nm and 1560 nm. The launched pump power threshold and slope efficiency were measured to be $\sim$14 mW and 0.3%, respectively. The threshold and slope efficiency with respect to absorbed pump power are estimated to be 4.3 mW and 1%, respectively.

Lasing in this high-index waveguide offers significant potential for low cost miniature devices in optical systems.

Bibliography

[1] K. Ennser, S. Taccheo, T. Rogowski, and J. Shmulovich. *Efficient Erbium-doped waveguide amplifier insensitive to power fluctuations. Opt Exp*, **14**:10307, 2006.

[2] R. N. Ghosh, J. Shmulovich, C. F. Kane, M. R. X. deBarros, G. Nykolak, A. J. Bruce, and P. C. Becker. *8-mW threshold Er^{3+}-doped planar waveguide amplifier. Photon Tech Lett*, **8**:518, 1996.

[3] T. Kitagawa, K. Hattori, K. Shuto, M. Yasu, M. Kobayashi, and M. Horiguchi. *Amplification in Erbium-Doped Silica-Based Planar Lightwave Circuits. Electron Lett*, **28**:1818, 1992.

[4] K. Hattori, T. Kitagawa, M. Oguma, Y. Ohmori, and M. Horiguchi. *Erbium-Doped Silica-Based Wave-Guide Amplifier Integrated with a 980/1530nm WDM Coupler. Electron Lett*, **30**:856, 1994.

[5] W. Huang and R. R. A. Syms. *Sol-gel silica-on-silicon buried-channel EDWAs. J Lightwave Technol*, **21**:1339, 2003.

[6] Y. C. Yan, A. J. Faber, H. deWaal, P. G. Kik, and A. Polman. *Erbium-doped phosphate glass waveguide on silicon with 4.1 dB/cm gain at 1.535 μm. Appl Phys Lett*, **71**:2922, 1997.

[7] J. Zyss I. Ledoux. G. Cusmai R. Costa. A. Barberis A.Q.L. Quang, R. Hierle and S.M. Piertralunga. *Demonstration of net gain at 1550 nm in an erbium doped polymer single mode rib waveguide. Appl Phys Lett*, **89**:141124, 2006.

[8] W. H. Wong, E. Y. B. Pun, and K. S. Chan. *Er^{3+}-Yb^{3+} codoped polymeric optical waveguide amplifiers. Appl Phys Lett*, **84**:176, 2004.

[9] S. Kogahara, S. Shinada, S. Nakajima, T. Kawanishi, H. Nakajima, and M. Izutsu. *Optical amplification characteristics of Ti-diffused waveguides on Erbium-doped $LiNbO_3$ crystal. Ieice Electron Expr*, **4**:134, 2007.

[10] C. C. Baker, J. Heikenfeld, Z. Yu, and A. J. Steckl. *Optical amplification and electroluminescence at 1.54 μm in Er-doped zinc silicate germanate on silicon. Appl Phys Lett*, **84**:1462, 2004.

[11] R. Schermer, W. Berglund, C. Ford, R. Ramberg, and A. Gopinath. *Optical amplification at 1534 nm in erbium-doped zirconia waveguides. J Quant Electron*, **39**: 154, 2003.

[12] J. D. B. Bradley, L. Agazzi, D. Geskus, F. Ay, K. Worhoff, and M. Pollnau. *Gain bandwidth of 80 nm and 2 dB/cm peak gain in Al_2O_3:Er^{3+} optical amplifiers on silicon. J Opt Soc Am B*, **27**:187, 2010.

[13] S. J. Madden and K. T. Vu. *Tellurium dioxide Erbium doped planar rib waveguide amplifiers with net gain and 2.8dB/cm internal gain. Opt Exp*, **18**:19192, 2010.

[14] H. Rigneault, F. Flory, S. Monneret, S. Robert, and L. Roux. *Fluorescence of Ta_2O_5 thin films doped by kilo-electron-volt Er implantation: Application to microcavities. Appl Opt*, **35**:5005, 1996.

[15] N. Maeda, N. Wada, H. Onoda, A. Maegawa, and K. Kojima. *Preparation and optical properties of sol-gel derived Er^{3+}-doped Al_2O_3-Ta_2O_5 films. Opt Mater*, **27**: 1851, 2005.

[16] B. Unal, M. C. Netti, M. A. Hassan, P. J. Ayliffe, M. D. B. Charlton, F. Lahoz, N. M. B. Perney, D. P. Shepherd, C. Y. Tai, J. S. Wilkinson, and G. J. Parker. *Neodymium-doped tantalum pentoxide waveguide lasers. J Quant Electron*, **41**:1565, 2005.

[17] T. Feuchter and C. Thristrup. *High-Precision Planar Wave-Guide Propagation Loss Measurement Technique Using a Fabry-Perot Cavity. Photon Tech Lett*, **6**: 1244, 1994.

[18] W. J. Miniscalco and R. S. Quimby. *General Procedure for the Analysis of Er^{3+} Cross-Sections. Opt Lett*, **16**:258, 1991.

[19] P. G. Kik and A. Polman. *Cooperative upconversion as the gain-limiting factor in Er doped miniature Al_2O_3 optical waveguide amplifiers. J Appl Phys*, **93**:5008, 2003.

[20] W. P. Risk. *Modeling of Longitudinally Pumped Solid-State Lasers Exhibiting Reabsorption Losses. J Opt Soc Am B*, **5**:1412, 1988.

Chapter 6

Sub-Micron Period Gratings in Er:Ta_2O_5 Waveguides

Sub-micron relief structures inscribed in the optical waveguides provide an attractive route for numerous applications such as sensing of chemical [1] and biological substances [2], wavelength filters [3], and as mirrors for waveguide lasers [4]. Tantala is already in use as a sensing material in both chemical and biological environment [5], and relief gratings have already been inscribed in tantala waveguides [6] for potential use as reflectors but so far such structures have not been studied tantala waveguides with gain. Fabrication and characterisation of such structures in Er:Ta_2O_5waveguides would enable realisation of integrated line narrowed lasers at 1530 nm and filters for compact multifunctional PLCs. In this chapter, the feasibility of inscribing such sub-micron structures using two different techniques- interferometric ablation and photolithography is presented.

6.1 Sub-micron structures in Ta_2O_5waveguides using interferometric ablation

In an interferometric ablation method, Ta_2O_5 waveguides are exposed to pulsed ultraviolet (UV) high power source to different energy densities in an interferometric set-up at Institute of Electronic Structure and Laser, FORTH, Crete, Greece as shown in Fig 6.1. For the experiment, output of a pulsed quintupled Nd:YAG laser emitting 213 nm , 150 ps radiation was used to irradiate the sample. The laser beam was split into several diffraction orders using a fused silica phase mask, and the ± 1 orders were made to interfere on the sample using two high reflectivity mirrors. The angle between the interfering beams on the sample defines the periodic intensity pattern on the sample which leads to the formation of grating structures on the waveguides. The process of irradiating the material with the interfering high power beams also leads to physical damage/removal of the material or ablation and therefore this technique is called interferometric ablation method. But the ablation phenomenon is dependent on many factors such as material, wavelength, pulse duration and surface topology and a generalised ablation theory for all the materials is elusive. Therefore, to have well defined structures proper calibration of the experimental set-up is required to have a controlled ablation. Determination of the exact physical processes involved in ablation in tantala waveguides is outside the scope of this thesis. Here, this technique is used as a tool to establish the feasibility and conditions for writing sub-micron period grating structures in thin film erbium doped tantala waveguides, and use those gratings as output couplers (reflectivity $\sim$10 dB) for lasing applications in the 1520-1550 nm wavelength band.

The first challenge to inscribe such structures in tantala waveguide is the period of the gratings which is $\sim$400 nm for the wavelength range of 1530-1550 nm. Such structures can be fabricated using standard UV photolithography but it would be difficult to achieve the required resolution in one step and would require multi-steps which increases the complexity of the process. E-beam lithography and focused ion beam (FIB) can easily make such structures but they are costly and slow processes. The fabrication of grating structures using interferometric ablation [7–11] offers many advantages due to its simplicity, the tuneability of the grating period, and the capacity to produce different kinds of gratings (photosensitive, relief and volume damage) by simply tuning the exposure dose conditions. Besides this technique can be applied to the majority of the optoelectronic materials to produce high quality relief structures of different resolution and shapes and effectively done in a single step pattering on the thin film or any other photonic structure. The relief gratings are specially robust and remain active and efficient for a long time.

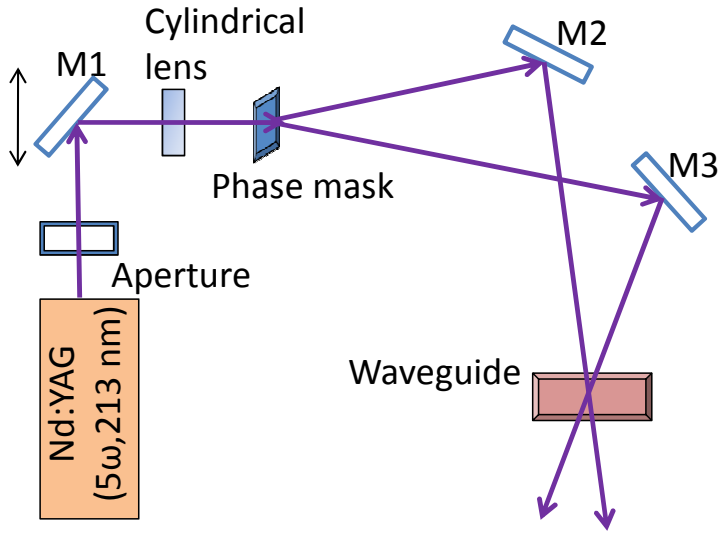

FIGURE 6.1: Frequency quintupled Nd:YAG laser ablation interferometer. M1 is the moveable mirror, M2, M3 are fixed mirrors.

6.1.1 Optimisation of the writing conditions

Before exposing samples to the high power pulses, the interferometer was calibrated to write gratings with desired period. To achieve that the interferometer was first adjusted to write gratings on a silicate optical fibre of known effective index. An ASE source was used to couple light into the fibre and its transmission spectra was recorded on an OSA. The energy density of the exposure was adjusted using the cylindrical lens placed just before the phase mask as shown in Fig 6.1. Another motorised mirror (M1) was placed just after the laser capable of producing constant jitter to the mirror to achieve spatial homogenisation of the beam and hence uniform beam at the sample. The whole set-up was enclosed in a box to avoid the effects of air currents. The fibre was placed on the sample holder and the fibre was exposed to the laser pulses to inscribe the grating structures on it. The fibre was then removed from the set- up and the transmission spectra was recorded after the exposure to check for the Bragg peak wavelength. The angle of the beam was then adjusted to alter the period of the grating followed by the exposure and recording of transmission spectra. This process was repeated until Bragg wavelength peaked at 1531 nm, which was the wavelength of maximum gain of erbium in Er:Ta_2O_5 sample as discussed in chapter 4. Then using the known value of n_{eff} of the fibre and Bragg wavelength (1530 nm) in the Bragg equation, the period of the grating was calculated as shown in Eq. (6.1),

$$\Lambda = \lambda_B / 2n_{eff} \tag{6.1}$$

where Λ is the period of the grating and λ_B is the Bragg wavelength which in this case was 1530 nm. After calibrating the set-up for the angle between the interfering

beams (period of the grating), the waveguide test sample (Er:Ta_2O_5 slab waveguide) was placed on the waveguide holder and exposed to the interfering beams. Erbium doped tantala thin films 1.4 μm thick were deposited on silica glass substrates using RF magnetron sputtering. Channel waveguides of width 1-10 μm were patterned using standard photolithography and ribs realised by Ar ion milling with etch depth 160 nm. The samples were then end polished beforehand to couple light into the waveguide. For the waveguide used the n_{eff} of fundamental mode was calculated to be ~2.04. The exposure area was measured to be ~2×1 mm^2. The exposure was carried out under different conditions of energy density and number of pulses on the slab waveguides. The exposed region due to high energy pulses and repeated exposure causes significant changes in morphological characteristics of the surface of the waveguide due to material evaporation, remelting or debris deposition on the exposed area. The ablation effects take place when the energy density of the exposure surpasses a minimum threshold energy density, which is the characteristic for each material. When the ablation threshold is surpassed, material expulsion is triggered [12]. Now, when the exposed area is observed under the microscope it scatters light and depending on the exposure conditions the number of scattering centres and the intensity will change. Above threshold, surface damage is maximum and therefore scattering area and intensity is also maximum. Below threshold the debris and surface damage is minimum or absent leading to less scattered light when observed under the microscope. Based on this technique, the optimum energy density for unablated gratings was found to be 10-11 mJ/cm^2 and an exposure time of 2 hours (72000 pulses). After that the rib waveguide samples were placed on the sample holder the gratings were written both above (23 mJ/cm^2) and just below (9.85 mJ/cm^2) ablation threshold with different exposure time that are summarised below in Table 6.1.

Sample#1 (1.4 μm rib)		Sample#2 (1.4 μm rib)	
Energy density	no. of pulses	Energy density	no. of pulses
23	1000	9.85	36000
	3000		72000
	5000		

TABLE 6.1: Exposure conditions used for inscribing grating structures on Er:Ta_2O_5 rib waveguides

6.1.2 SEM and AFM characterisation of the grating structures

Post exposure the samples were characterised using SEM and atomic force microscopy (AFM) methods to determine the period of the grating. AFM was also used to study the morphology of the exposed region. Firstly, to determine the period the gratings were

imaged in an SEM. Fig 6.2 shows the SEM picture of gratings written with 23 mJ/cm^2 and 1000 pulses. The figure shows the gratings written on top of the rib waveguide and the measured period of the grating was ∼368 nm. The SEM images of the other samples were similar.

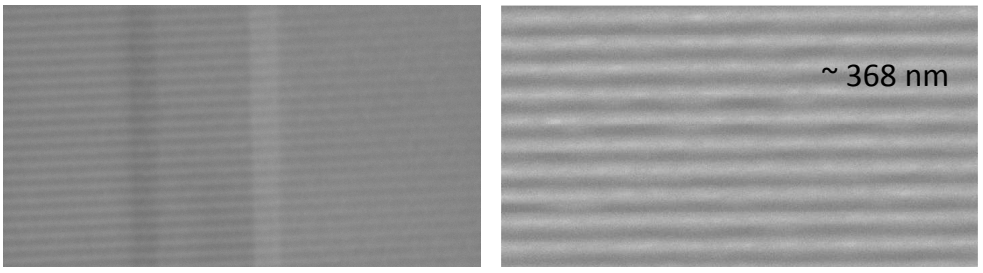

FIGURE 6.2: SEM image a) grating written on top of 1.42 μm rib waveguide b) zoomed in image of the grating showing the average period of the grating (∼368 nm)

In order to understand the effect of different energy density and number of pulses on the grating structure, transmission measurements (1500-1580 nm) and AFM were carried out on the gratings. Fig 6.3 shows the AFM scan that reveals the surface topology of the exposed area i.e. gratings written on sample#1 (above threshold) as illustrated in Fig 6.1. The AFM scan revealed the damage suffered by the exposed area at this energy density (23 mJ/cm^2). This can be gauged from the physical appearance of the scan as shown in Fig 6.3. For example, for the grating inscribed with 23 mJ/cm^2 and 1000 pulses, the profile scan (Fig 6.3a) looks very flat and uniform as compared to the surface scan of grating inscribed with 23 mJ/cm^2 but 3000 pulses (Fig 6.3b), which shows the presence of non-uniform surface profile and reduction in the flatness. This can be attributed to the thermal damage suffered by the exposed area due to the exposure above ablation threshold energy density that causes material melting and resolidification resulting in a surface damage rather than purely etched structures. The average grating depth also increases with increase in the number of pulses from about 14±5 nm to 400±30 nm. It is difficult to ascertain the exact depth of the grating due to the presence of debris and redeposited material that is seen as tall structures in the profile of the gratings written with a higher number of pulses. The grating period more or less remains same around 369 ± 2 nm as shown by the line scan in Fig 6.3d. The line scan represents a 1-D scan at a particular location of the surface profile obtained earlier with AFM. This scan was performed at different locations to obtain the average value/variation of the period of the grating.

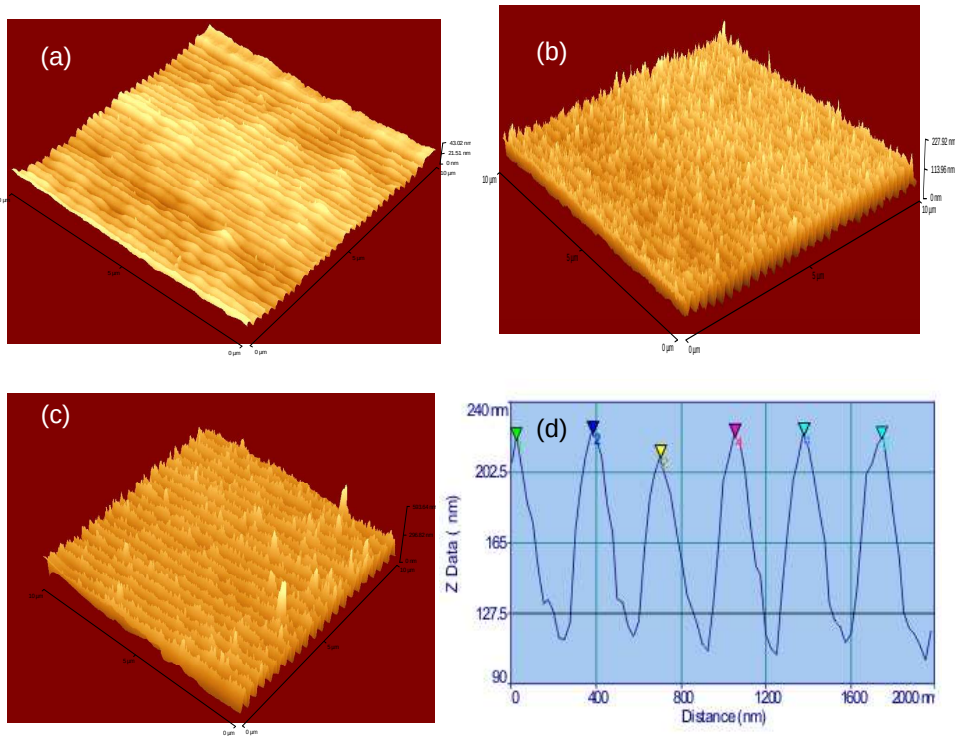

FIGURE 6.3: AFM microscan of grating ablated with energy density 23 mJ/cm^{2}and a)1000 pulses, b) 3000 pulses, c) 5000 pulses & d) line scan of AFM microscan for sample #1, condition (a).

6.1.3 Optical transmission measurements of the waveguide inscribed with grating

The experimental set up for performing the optical transmission measurement through the waveguide inscribed with grating is shown in Fig 6.4. The main aim of this experiment was to determine the grating strength and the peak Bragg wavelength. The source used was a tuneable fibre coupled 1500-1580 nm laser with a maximum power of 2 mW at 1580 nm. The light was coupled into the waveguide with an objective lens of 40x magnification. A Similar lens was used to collect the output from the waveguide and was imaged onto a Hamamatsu IR camera to ascertain that the light was coupled into the right waveguide. The TM component of polarisation was obtained using a polariser set at 120^0 while the TE component was selected by using a half wave plate before the polariser and setting the polariser at 30^0 (Brewster angle).

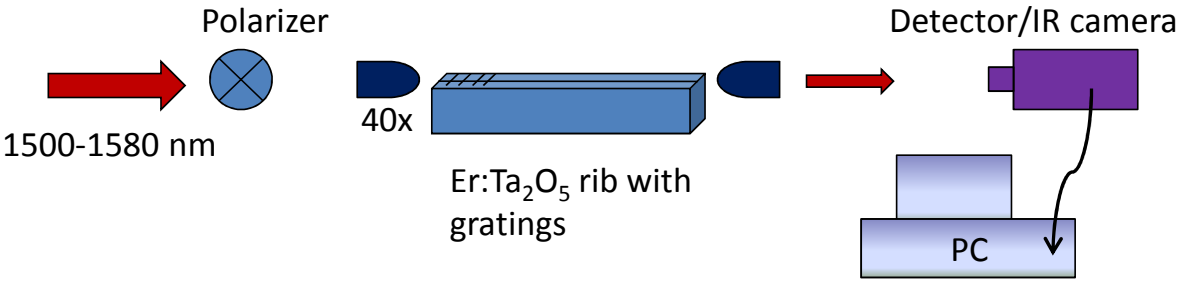

FIGURE 6.4: Experimental set up for spectral characterisation of waveguide grating sample

The grating characterisation was performed by tuning the wavelength in the step of 0.1 nm from 1500 nm to 1580 nm, and collecting the transmitted power using the detector. Both the laser source and detector was controlled by the PC through LabView interface. The data was collected and averaged for 1 second for each wavelength and recorded on the PC. Fig 6.5 shows the transmission spectra of the waveguide grating normalised to the waveguide without any grating. Transmission measurements yielded a spectral notch of spectral depth 11 dB for a 2 mm long grating written with an energy density of 23 mJ/cm^2 (above threshold) and 1000 pulses for TE polarisation. The strength of the grating decreases from about 11 dB (Fig 6.5a) for shorter duration grating (1000 pulses) to about 5 dB for longer duration (5000 pulses) grating (Fig 6.5b). This can be attributed to poor surface quality and higher density of accumulated particles in the ablated area of the exposed region leading to higher loss and lower grating strength. Secondly, the grating peak wavelength shifts towards shorter wavelength- from 1504.8 nm for a grating written with 1000 pulses to 1501.6 nm for 5000 pulses grating. Unfortunately, the measurement for the grating written with 3000 pulses could not be conducted due to poor coupling (bad facet) into the respective waveguide. This shift in the peak wavelength can be attributed to the greater amount of material ablated from the waveguide written with 5000 pulses leading to reduction in the waveguide thickness and hence effective index. The Bragg wavelength is directly related to effective index and hence the shift towards shorter wavelength. The gratings exhibited substantially lower extinction for the TM polarization (Fig 6.5c), due to significantly lower overlap [11] with the grating corrugation than the TE polarisation in the wavelength range 1500-1580 nm. This results in the increased interaction of the guided mode (TE) with the surface modifications (grating) and hence the strong transmission dip as shown in Fig 6.5. Due to lack of an appropriate source this experiment could not be performed for shorter wavelengths.

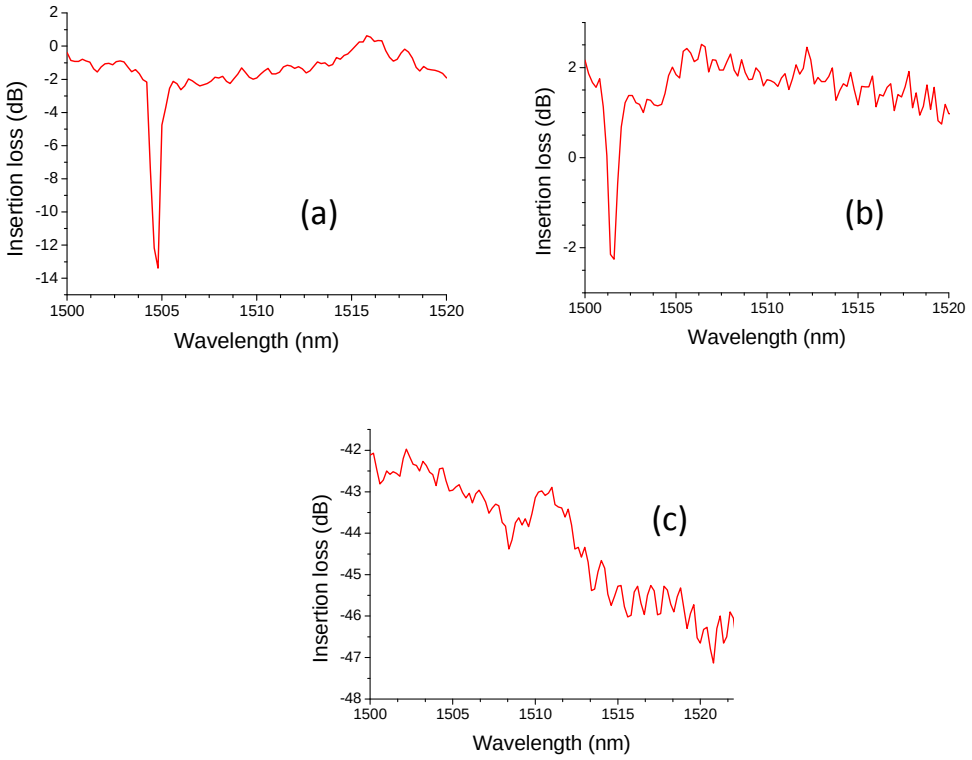

FIGURE 6.5: TE Waveguide transmission spectra for grating ablated with energy density 23 mJ/cm^2 (sample#2) and a) 1000 pulses, b) 5000 pulses & c) TM spectra for 1000 pulses

In sample #2, two gratings with the same average energy density 9.85 mJ/cm^2 but different writing time (36000 and 72000 pulses) were written on waveguides with different widths. However, due to the combination of bad end facets and high losses, transmission measurements could be performed only on two waveguides. The shorter duration grating was written on a $\sim$ 7- 8 μm wide waveguide (multimode at 1550 nm) and the longer duration grating written on a $\sim$2.5-3 μm wide waveguide (multimode at 1550 nm). Fig 6.6(a, b) shows the AFM scans for these two gratings. Now, since these gratings are written at 9.85 mJ/cm^2 (below ablation threshold) therefore the surface morphology of the inscribed structure is much flatter and more uniform than those for ablated gratings (Fig 6.3). At this exposure level uniform relief gratings without much thermal damage or redeposition are formed. The difference between gratings shown in Fig 6.6 can be attributed the accumulated damage on the exposed area that occurs due to repetitive exposure of the material (increase in the number of pulses), this is known as incubation [12]. At lower number of pulses, volume damage gratings are formed which are areas with overexposed material. These areas might contain color centres that can act as absorption centres and less excavated exposed region as shown in Fig 6.6a. Incubation affects leads to gradual decrease in the material ablation threshold and subsequent exposure to pulses at this energy can lead to the removal of volume damage areas leading to pure surface

relief structures [11]. This explains the change in the appearance of the surface profile with the number of pulses as illustrated in Fig 6.6(a,b). The surface profile is very uniform with less surface damage than that seen in sample#1 due to much reduced energy density. The average grating depth was measured to 16 ± 5 nm (36000 pulses) and 25 ± 5 nm (72000) pulses and period was found to be 368 ± 3 nm.

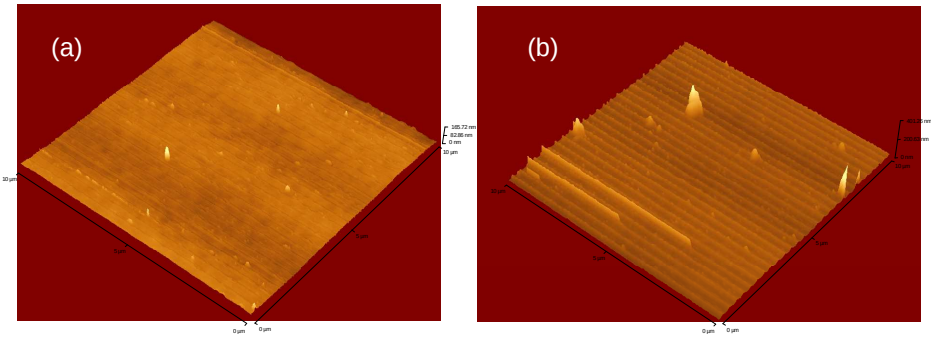

FIGURE 6.6: AFM microscan of grating ablated with energy density 9.8 mJ/cm^{2}and a)36000 pulses, b) 72000 pulses on a 1.42 μm thick Er:Ta_2O_5 rib waveguides

Fig 6.7 shows the transmission spectra of the waveguide grating written with 9.8 mJ/cm^2 energy density. Transmission measurements yielded a notch of spectral depth of ∼5.5 dB (Fig 6.7a) for TE polarisation peaking at 1511 nm and 1512 nm for shorter write time (36000 pulses) and the strength of the grating increases to about 7 dB (Fig 6.7b) for longer duration grating peaking at 1510.4 nm. With the increase in the exposure time the diffraction efficiency of the relief pattern formed increases. The shift in the wavelength can again be explained by the amount of material removed at longer exposure. The second lobe appearing in the spectral curves could be explained by the higher order modes supported by the waveguide or from scattering from some spurious modes. As with the earlier sample, these gratings also exhibited substantially lower extinction for the TM polarization due to significantly lower overlap with the grating corrugation than TE in the 1500-1580 nm wavelength range.

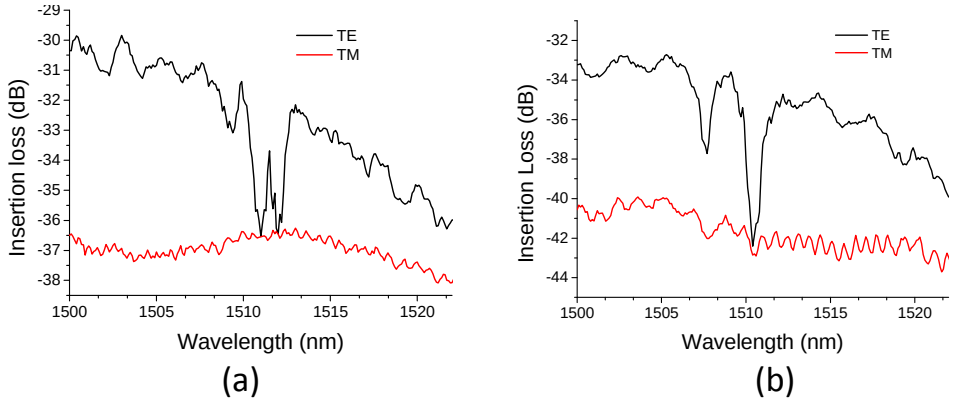

FIGURE 6.7: TE & TM waveguide transmission spectra for grating ablated with energy density 9.8 mJ/cm^2 and a) 36000 pulses & b) 72000 pulses

6.1.3.1 Bragg wavelength shift using oil overlay method

The Bragg peak wavelength was found to peak well short of the desired 1530 nm wavelength where the gain of the erbium is maximum in erbium doped tantala waveguides. In order to red-shift the Bragg peak and to remove any spurious modes, an oil overlay method was employed. In this method, index matching oil of various refractive indices (up to 1.64) were put on top of the gratings (exposed area) to change the effective index of the mode. The n_{eff} increases with the increase in the cladding index on top of the grating. The higher n_{eff} then in turn leads to red-shifting of the Bragg wavelength and therefore the observed shift in the Bragg wavelength.

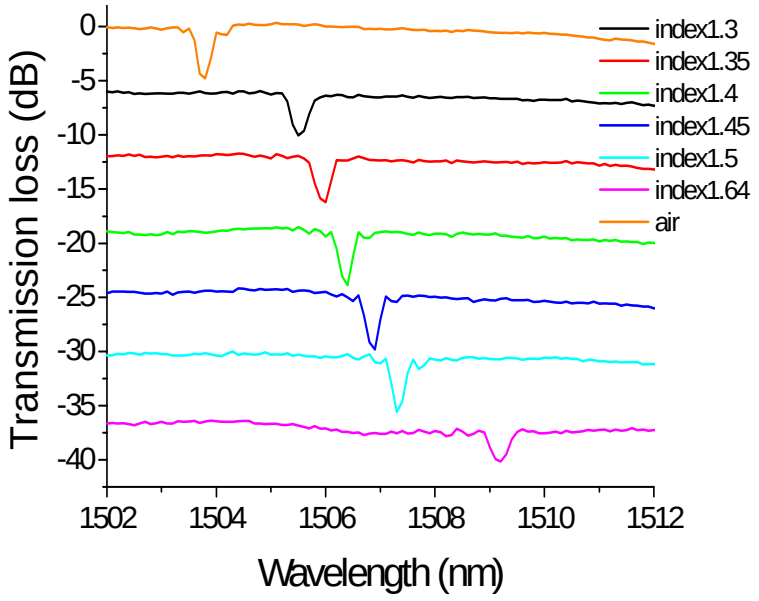

FIGURE 6.8: TE waveguide transmission spectra and wavelength shift using oil overlay method for grating ablated with energy density 23 mJ/cm^2 & 1000 pulses

For this experiment, ablated gratings written with 1000 pulses and 23 mJ/cm^2 was used. Fig 6.8 shows the spectral response of the gratings to the index matching oil on top. The oil on top leads to progressive red-shift of Bragg wavelength $\sim$ 6nm with the increase in the index of the oil.This variation is shown in Fig 6.9 and is also fitted to the theoretical prediction for the Bragg wavelength. The change in the Bragg wavelength was calculated from Eq. (6.1) using the following relation:

$$\frac{\Delta n_{eff}}{n_{eff}} = \frac{\Delta \lambda_B}{\lambda_B} \tag{6.2}$$

where Δn is the change in the effective index and $\Delta \lambda_B$ is the change in the Bragg wavelength. This normalisation is done to take care of the error in the calculation of the actual effective indices of the waveguide. To get the best fit of the theory to the data the theoretical thickness of the waveguide was varied because during exposure the material was physically removed/ablated that would have lead to the reduction in the material thickness. No such shift was found for TM polarisation in the 1500-1580 nm range. Overall a good match between the theoretical prediction and experimental results were obtained.

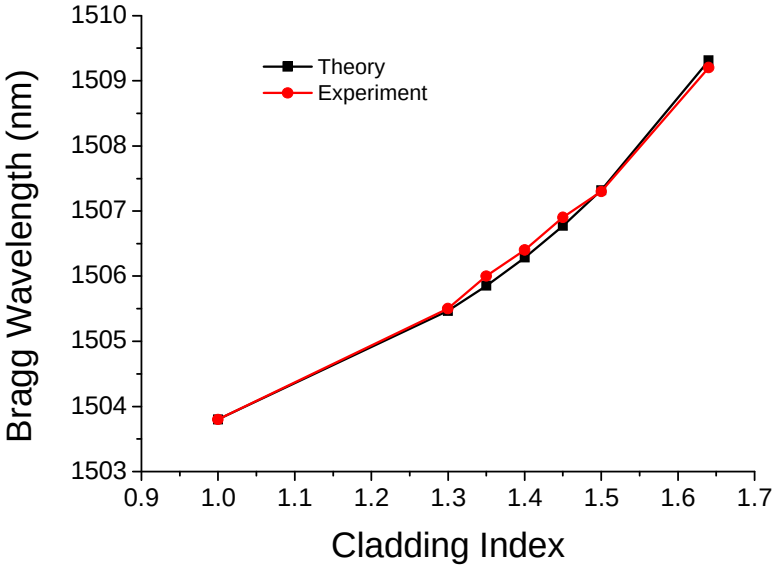

FIGURE 6.9: Effect of overlay oil on effective index and Bragg wavelength

Although the strength of the grating achieved in one of the samples 11 dB is good enough to act as a mirror for lasing, the reflection wavelength was still far away from the desired 1530 nm. The main reason for the large blue shift in the wavelength from the target wavelength of 1530 nm was can be attributed to the achieved grating period of 368 $\pm$3 nm instead of 376 nm. It was found later that the n_{eff} of the fibre that was used to

calibrate the period of the grating had been incorrectly specified leading to improper setting of the interfering beam and hence slightly shorter period of the grating.

6.2 Waveguide grating fabrication using photolithography

In this section, waveguide grating fabrication using photolithography will be discussed. Although the interferometric ablation method of recording gratings is convenient way and essentially a single step pattering process on the thin films, it does require a complex set-up, absence of air currents, and fine tuning of the mirrors for the correct angle. It also requires the samples to be prepared and end-polished beforehand and sometimes also requires post processing such as wet etching to make the gratings smooth and less lossy. Therefore, there is a scope for a less cumbersome technique that could avoid all these extra steps for writing gratings. Photolithography provides one such avenue that potentially allows the patterning of the whole device, in this case, both the waveguides and gratings, on the thin film in one step. During mask design there is a flexibility of including different parameters that can be patterned on to the thin film in one step and that makes it cost effective and saves lot of time. A Mask was designed in *Olympios* and Fig 6.10 shows the typical design of waveguide gratings made for the mask. For optimisation, a 4 μm period grating was also designed to optimise fabrication. The length of the grating was varied from about 10 mm to 30 mm while the amplitude of the grating was varied from as small as 100 nm to 1 μm.

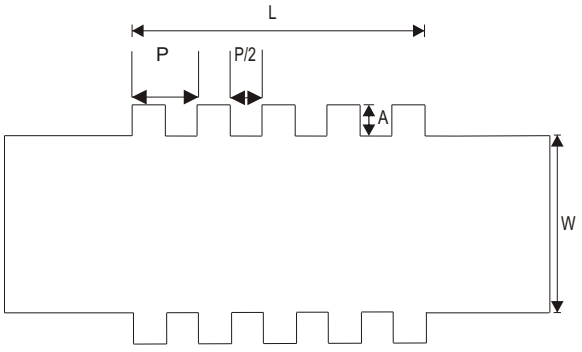

FIGURE 6.10: Typical design of waveguide grating. P is the grating period, A the amplitude of the grating, L the length of the grating and W the width of the waveguide

However, there is an inherent difficulty in achieving sub-micron dimensions using the standard UV photolithography set-up as they are generally designed to provide at best an optical resolution of 0.8 μm. But for a reflection grating at 1530 nm, a period of 375 nm is required. However, even if the mask aligner is not able to resolve 375 nm structure

completely but the process is well optimised then a small component at the spatial frequency of the grating may be transmitted through the mask into the photoresist. As the amplitude of the grating required is only a few nanometres, substantial suppression of the grating frequency may still result in a grating with suitable reflection strength. Besides, there were also designs of grating with period that were multiples 375 nm (1125 nm) with a possibility of achieving a third harmonic grating that resembles the grating that is required to operate at 1530 nm in erbium doped tantala waveguides. Fig 6.11 shows the SEM images of the actual mask. Already it can seen that the perfect square wave of grating in the design has become sinusoidal and upon exposure under perfect conditions would lead to sinusoidal pattern being replicated faithfully on the resist.

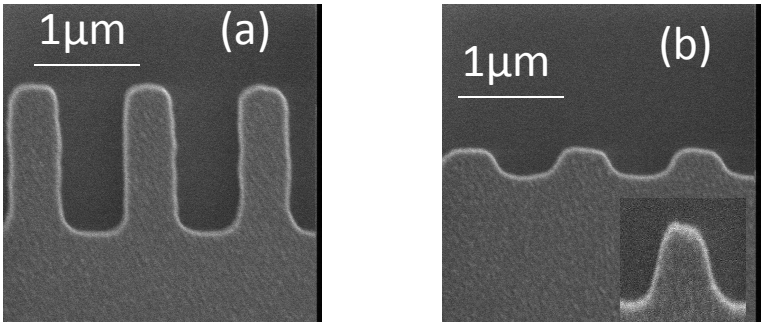

FIGURE 6.11: SEM picture of actual optical mask features. a) $1\mu m$ period and 500 nm amplitude & b) $1\mu m$ period and 100 nm amplitude. Inset shows the zoomed in picture of (b)

6.2.1 Optimisation and fabrication of gratings

Undoped and erbium doped tantala films (1 wt%, 2 wt%) were sputtered onto oxidised silicon wafers under the optimum conditions as discussed in earlier chapters. Before photolithography, sputtered sample was thoroughly cleaned in acetone, IPA and water and blow dried. To replicate sub-micron features S1805 positive photoresist was used instead of S1813 used earlier for photolithography. S1805 is a very dilute resist and it is possible to coat a thin layer (500 nm) of resist on the substrate as opposed to around 900 nm thick layer with S1813 resist. This was important since we were expecting very weak light to go through the mask and in order to have a complete exposure of the resist it was imperative to use a thin layer. Besides that the resist was applied on the substrate using a syringe and filter (200 nm) to ensure all dirt particulate bigger than 200 nm were filtered off so that they do not interfere in the photolithography process.

Resist was spun coated on the substrate at 3000 RPM and then it was covered and kept separate for 5 minutes before placing it in the oven at 90^0C for 18 minutes to evaporate any excess solvent. After that the sample was kept at room temperature for 15 minutes so that the resist could absorb some moisture from air which would in turn help in

absorbing UV more efficiently upon exposure. The mask was placed in the mask holder and the mask aligner was prepared for exposure. In order to have best possible result in terms of resolution and reproducibility, high vacuum contact exposure with contact time as high as 15 seconds was used. The contact time was increased to remove any stress in the sample when it comes in contact with the mask and also to make the contact uniform across the sample. A quick squirt of the compressed air was used to remove any dirt on the sample and the sample was then exposed to UV for 5 seconds in the hard vacuum contact mode. The exposed sample was then developed in MF314 solution for 30 seconds and was cleaned in DI water and blow dried. The sample was then hard baked at 120^0C for 25 minutes before taking it out of the yellow room for etching. The sample was then etched down by ∼360 nm using IBM using the recipe developed for normal rib waveguides and as discussed in chapter 4. The sample was ultrasonicated in acetone and IPA followed by plasma ashing to remove any resist/ organic residue sticking to the walls of the device. Finally it was then annealed in the tube furnace in oxygen for 2 hours at 600^0C.

6.2.2 SEM characterisation of the gratings

To have a closer look at the outcome of the fabrication and to measure the dimensions of the features on the device SEM images were taken of the samples. 6.12 shows few SEM images of different waveguide gratings fabricated.

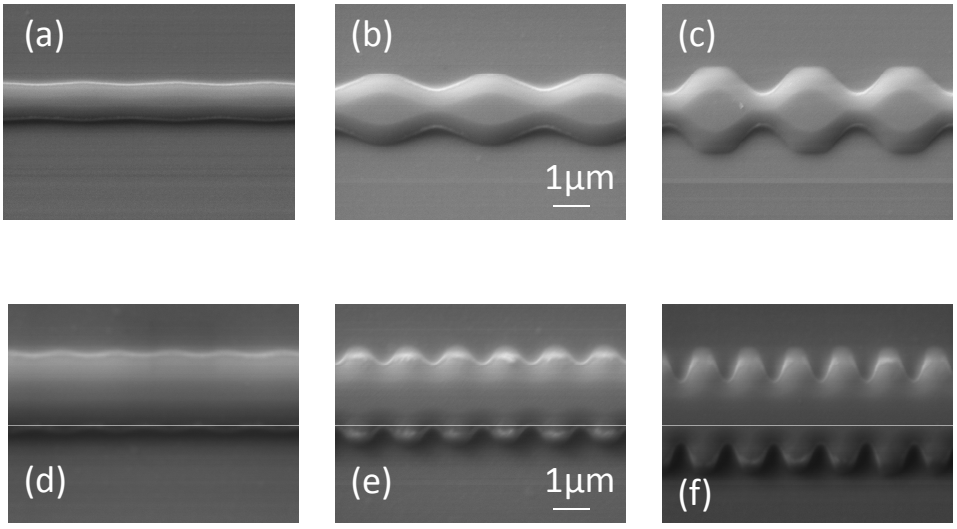

FIGURE 6.12: SEM images of the waveguide gratings a) P=4μm, A=100 nm, b)P=4μm, A=500 nm, c)P=4μm, A=1 μm, d)P=1.1μm, A=100 nm, e)P=1.1μm, A=500 nm & (f) P=1.1μm, A=1 μm

The quality of the images in Fig 6.12 suggests the successful optimisation of the fabrication process of the gratings. The period of the grating for 1.125 μm and 4 μm gratings were as desired in the design. However, the analysis of the SEM image of 375 nm period grating was inconclusive as no periodicity could be detected in the image. Fig 6.13 shows the SEM image of such a device and it definitely shows deposition of resist on top of waveguide at the right place but SEM could not detect any visible periodicity of the grating.

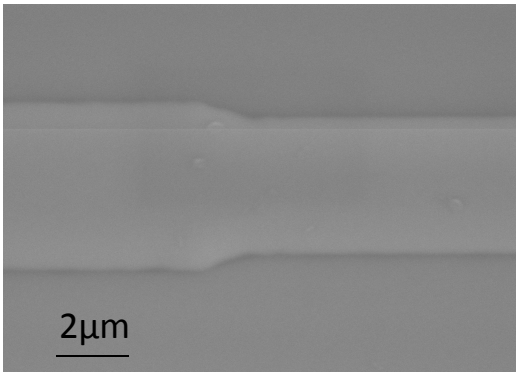

FIGURE 6.13: SEM image of the waveguide grating with 375 nm period and 500 nm amplitude

6.2.2.1 Fourier analysis of the gratings

To determine the presence of any periodicity in-situ Fourier analysis of the SEM images was carried out. This method is based on the fast Fourier transformation (FFT) of the SEM images and gives the spatial frequency distribution of the image. If there was any periodicity then the FFT spectrum would have revealed it. Fig 6.14 shows the spatial frequency of the periodic structure (4 μm period and different amplitude) is well spotted by the FFT technique and is presented as the the horizontal separation between the two vertical lines and is also shown as the circle that covers it. The spatial period calculated was $0.25/\mu m$ that corresponds exactly with the period of the grating (4 μm). However, no such result was obtained when the experiment was done on the waveguides with 375 nm gratings, and more detailed analysis is necessary.

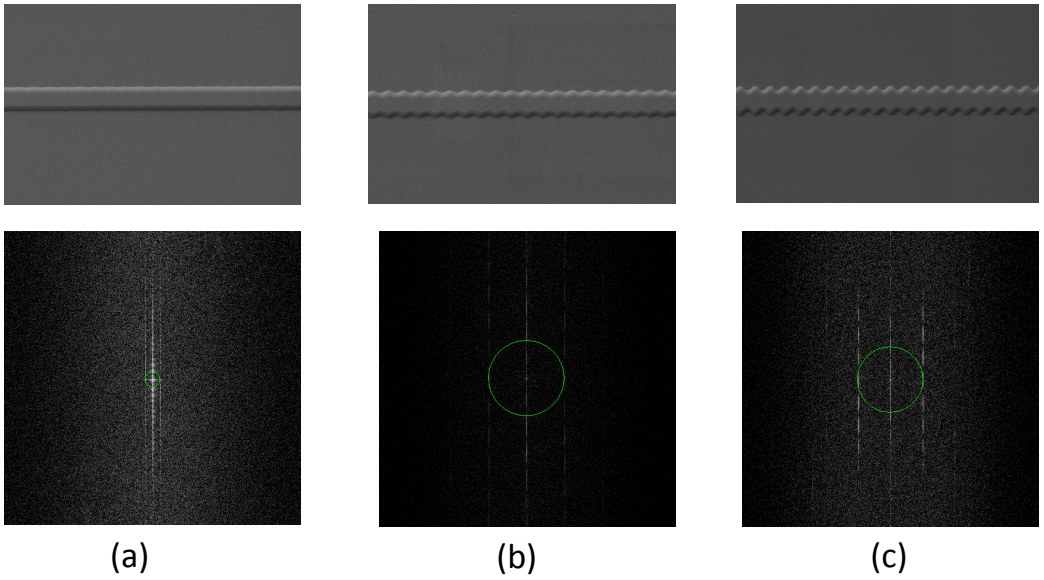

FIGURE 6.14: (Top) SEM image of gratings of 4 μm period & amplitude a)100 nm, b)500 nm & c)1μm. Bottom image shows the FFT spectrum of the 4 μm gratings with a spatial period of 0.25/μm for all the three images.

6.3 Conclusions

The feasibility study of inscribing sub-micron grating structures in erbium doped tantala waveguides was successfully carried out and established using two different techniques-interferometric ablation and photolithography. Using interferometric ablation method, relief grating structures were written for two different energy densities (9.8 mJ/cm^2 & 23 mJ/cm^2) at different writing time. The best result was achieved for ablated grating written with 23 mJ/cm^2 and 1000 pulses, in which the transmission measurements yielded a spectra depth of 11 dB for TE polarisation peaking at between 1505 nm. It was also found that the both the quality and spectral strength of the grating deteriorated with the increase in the writing time. Gratings written below ablation threshold were not as strong and at best a spectral depth of 7 dB was achieved that peaked at 1510.4 nm . Oil overlay method was used to shift the Bragg peak wavelength by about 6 nm but was still far away from the required wavelength of 1527 nm. The main reason for the discrepancy in the Bragg wavelength was the mismatch in the targeted (375 nm) and achieved (368 nm) period of the grating. A better way of negotiating this problem would be to do an in-situ measurement of the transmission and reflection spectra while the grating is being written to avoid any errors in the grating strength and period. The angle of the beam can be adjusted while the grating is being written and the Bragg wavelength shift can be monitored to peak it at the right wavelength. Also the reflection/transmission spectra can be monitored for the writing time of the grating. When the required grating strength, for example as lasing mirror, is achieved the writing can be stopped. Thus it

will allow grating pitch selection for these waveguides. This technique is therefore applicable to erbium doped tantala waveguides to form integrated laser cavities and realise a line narrowed waveguide laser system.

Secondly, fabrication conditions of grating and waveguides using photolithography was optimised. The SEM and FFT scan of the gratings looked promising for gratings up to 1 μm period. But for gratings with period 375 nm, no periodicity was seen through SEM or FFT scan. Spectral characterisation of the gratings could not be performed at this stage. An increased contact time between mask and sample could also help in improving the exposure and resolution of the gratings fabricated. A theoretical study of these structures for example by comparing the spatial frequency spectrum on the resist and on the etched waveguide, with the ideal frequency spectrum would show the attenuation behavior of the higher harmonics and thus could shed light on the feasibility of reproducing the 375 nm pattern on the resist using photolithography and steps to improve it.

Bibliography

[1] K. Tiefenthaler and W. Lukosz. *Grating Couplers as Integrated Optical Humidity and Gas Sensors. Thin Solid Films*, **126**:205, 1985.

[2] G. L. Duveneck, A. P. Abel, M. A. Bopp, G. M. Kresbach, and M. Ehrat. *Planar waveguides for ultra-high sensitivity of the analysis of nucleic acids. Anal Chim Acta*, **469**:49, 2002.

[3] S. Pissadakis, L. Reekie, M. N. Zervas, J. S. Wilkinson, and G. Kiriakidis. *Gratings in indium oxide film overlayers on ion-exchanged waveguides by excimer laser micromachining. Appl Phys Lett*, **78**:694, 2001.

[4] J. Kim, K. A. Winick, C. Florea, and M. McCoy. *Design and fabrication of low-loss hydrogenated amorphous silicon overlay DBR for glass waveguide devices. J Sel Top Quant Electron*, **8**:1307, 2002.

[5] K. Schmitt, K. Oehse, G. Sulz, and C. Hoffmann. *Evanescent field sensors based on tantalum pentoxide waveguides - A review. Sensors-Basel*, **8**:711, 2008.

[6] S. Pissadakis, A. Ikiades, C. Y. Tai, N. P. Sessions, and J. S. Wilkinson. *Sub-micron period grating structures in Ta_2O_5 thin oxide films patterned using UV laser post-exposure chemically assisted selective etching. Thin Solid Films*, **453-54**:458, 2004.

[7] S. Pissadakis, S. Mailis, L. Reekie, J. S. Wilkinson, R. W. Eason, N. A. Vainos, K. Moschovis, and G. Kiriakidis. *Permanent holographic recording in indium oxide thin films using 193 nm excimer laser radiation. Appl Phys a-Mater*, **69**:333, 1999.

[8] S. Pissadakis, L. Reekie, M. Hempstead, M. N. Zervas, and J. S. Wilkinson. *Ablated gratings on borosilicate glass by 193-nm excimer laser radiation. Appl Phys a-Mater*, **69**:S739, 1999.

[9] S. Pissadakis, L. Reekie, M. Hempstead, M. N. Zervas, and J. S. Wilkinson. *Relief gratings on Er/Yb-doped borosilicate glasses and waveguides by excimer laser ablation. Appl Surf Sci*, **153**:200, 2000.

[10] S. Pissadakis, L. Reekie, M. N. Zervas, and J. S. Wilkinson. *Excimer laser inscribed submicron period relief gratings in InO_x films and overlaid waveguides. J Appl Phys*, **95**:1634, 2004.

[11] S. Pissadakis, M. N. Zervas, L. Reekie, and J. S. Wilkinson. *High-reflectivity Bragg gratings fabricated by 248-nm excimer laser holographic ablation in thin Ta_2O_5 films overlaid on glass waveguides. Appl Phys a-Mater*, **79**:1093, 2004.

[12] S. Pissadakis. Bragg gratings in optical waveguides,glasses and thin oxide films induced by excimer laser radiation. PhD thesis, University of Southampton, UK, 2000.

Chapter 7

Conclusions & Suggestions For Future work

7.1 Conclusions

This thesis presents a i) comprehensive optimisation and fabrication of high index contrast erbium doped tantala waveguides on Si/SiO_2 substrates, ii) theoretical study of EDWA based on those waveguides, iii) experimental demonstration of net optical gain and lasing action in $Er:Ta_2O_5$ waveguides for the first time, and finally iv) a feasibility study on the fabrication of grating structures using two different mechanisms- interferometric ablation and photolithography assisted etching with potential use as integrated mirrors for lasing and filters.

Tantalum pentoxide waveguides were fabricated, optimised and characterised to achieve net optical gain and lasing from the material system. The erbium doped tantala thin film was deposited using magnetron sputtering on oxidised silicon substrates. The optimum conditions for sputtering low loss thin film were established as 200^0C substrate temperature, 300 W magnetron power and, 5 sccm and 20 sccm of oxygen and argon flow rate to yield low loss (0.4 dB/cm) slab waveguides. The optimum conditions for realising rib waveguides were then established using photolithography and argon IBM to yield rib waveguides of dimensions $\sim$ 2 μm high, etched down by $\sim$400 nm and widths ranging from 1.2 μm - 10 μm. To reduce the losses, the waveguides were first treated with aqueous KOH solution for 20 minutes followed by annealing in a tube furnace in an oxygen atmosphere for 2 hours at 600^0C. The waveguide loss was measured at 1600 nm to avoid the erbium absorption band and a maximum waveguide loss of 0.60 $\pm$ 0.05 dB/cm at 1600 nm was measured using FP technique. The annealing treatment yielded low loss amorphous waveguides and this was confirmed by the XRD measurements that revealed no evidence of crystallinity for the annealed samples. The refractive index of

the erbium doped tantala material system was measured to be 2.105 at 1530 nm using ellipsometry. The waveguides were designed to be SM for widths $\leq$3.2 μm at 1550 nm and experimentally they matched the design very well as they were observed to be SM for widths $\leq$3 μm in the wavelength range of 1500-1620 nm. Thereafter, a complete erbium spectroscopy study was performed on the Er:Ta_2O_5 waveguides doped with 2.7 $\times$ 10^{20} ions/cm^3 erbium ions concentration. The luminescence bandwidth and lifetime of the erbium ions were found to be 50 nm and 2.3 ms respectively. The peak absorption cross-section of the erbium ions in tantala was measured to be 4.8 $\pm$ 0.2 $\times$ 10^{-21}cm^2 at 1527 nm. The emission cross-section was calculated using McCumber theory and that yielded a peak emission cross-section of 4.4 $\pm$ 0.2 $\times$ 10^{-21}cm^2.

A numerical model to study the gain dynamics in the tantala waveguides was also successfully developed. The model was based on the three level rate equations of the erbium ions and only included homogeneous upconversion effects. The rate equations were solved numerically in the steady state by evaluating the evolution of pump and signal along the length of the waveguide The model was used to calculate the small signal gain ($<$ 20 dB) only and therefore, ASE effects were not included in the model. The signal gain was analysed as a function of erbium concentration, pump power, length of the waveguide and upconversion coefficient. Based on this model, it was found that the net optical gain in the material was limited by the upconversion in the material and accordingly length and pump power needed to be altered. Based on the numerical model developed it is predicted that the maximum gain attainable in this material with $C_{up}\leq$ 5 $\times$ 10^{-18} cm^3/s is as high as 22 dB for a 5.5 cm long sample (4 dB/cm) with an erbium concentration of 5.4 $\times$$10^{20}$ ions/cm^3 at 200 mW of pump power. Whereas for an erbium concentration of 2.7 $\times$$10^{20}$ ions/cm^3 used in the samples prepared, a maximum gain of 3.1 dB/cm is predicted for a 2.5 cm long sample without any upconversion effects.

This thesis, for the first time presented net optical gain in the Er:Ta_2O_5 material system. The net gain obtained in erbium doped tantala was found to be comparable to recently published tellurite glass [1] and best among any other HIC material system [2–4] reported so far. A net optical gain as high as 2.25 dB/cm was obtained in an 2.3 cm long Er:Ta_2O_5 doped with 2.7 $\times$$10^{20}$ ions/cm^3 erbium ions. The maximum gain was achieved when 200 mW of pump (977 nm) and 1 μW of signal (1500-1580 nm) was launched into the waveguide simultaneously using WDM. The launch pump threshold was found to be as low as $\sim$ 4.5 mW. When the experimental result was fitted with the numerical model it was found that the gain was severely limited by the upconversion coefficient that was found to be as high as 10^{-17} cm^3/s . While this is comparable to other prominently reported material [5–7] it also suggests that there is a large scope for improvement in the maximum gain that can be achieved from this material through the reduction of upconversion coefficient and possible clustering of erbium ions in the material using different deposition techniques as discussed in the next section.

This thesis presents for the first time, laser action in Er:Ta_2O_5 waveguide. The lasing cavity was formed by affixing mirror (92% reflection at 1500-1580 nm) at both ends of the end-polished waveguides using index matching oil. The waveguide was pumped at 977 nm. The pump threshold for lasing was found to be as low as $\sim$ 4.3 mW with respect to absorbed pump power. The efficiency for the laser was found to be 0.78% and 1 % with respect to launched and absorbed pump power respectively. The lasing was into fundamental mode and had a peak wavelength between 1558-1559 nm. The lasing result was limited mainly because of the high mirror butting loss (2.3 dB/mirror) and double sided emission from the cavity and not due to any fundamental limitations in the material.

In an effort towards realising line narrowed integrated laser and filters, a feasibility study for writing grating structures in the erbium doped waveguides based on interferometric ablation and photolithography was undertaken. In the first technique, sub-micron grating structures ($\sim$ 370 nm) in erbium doped waveguides were inscribed in an elliptical interferometer set-up using frequency quintupled pulsed Nd:YAG laser. Relief grating structures were inscribed on rib waveguides for two different energy densities (9.8 mJ/cm^2 & 23 mJ/cm^2) at different writing times. The best result was achieved for ablated grating written with 23 mJ/cm^2 and 1000 pulses, where transmission measurements yielded spectral depth of $\sim$ 11 dB peaking at 1504 nm for TE polarisation. It was also found that the both the quality and spectral strength of the grating deteriorated with the increase in the writing time. Gratings written below ablation threshold were not as strong and at best a spectral depth of 7 dB was achieved that peaked at 1510.4 nm . The wavelength of reflection was shifted towards 1530 nm by putting oil of different refractive indices on top of the inscribed region and measuring the transmission spectra from the waveguide. A shift of more than 6 nm was observed but it remained shorter than the desired wavelength of 1527.5 nm where the erbium absorption is maximum in tantala. In the second method, a mask for the gratings and waveguides was designed, and they were realised on the oxidised silicon substrates under the optimised conditions using photolithography assisted dry etching. The SEM and FFT of the gratings down to 1 μm structure corresponded well with the dimensions on the original mask. But for gratings with period of 375 nm, SEM and FFT did not reveal any information on the periodicity. The spectral characterisation of these gratings could not be carried out at this stage but the results obtained looks promising to establish a simple one step process to obtain waveguide and grating for lasing and filtering applications.

The work presented in this thesis is an effort towards establishing the versatility of tantalum pentoxide as an all-purpose material for different photonic devices and applications. The work presented in this thesis focuses on the clear advantage of HIC of tantala and with the demonstration of net optical on-chip gain in Er:Ta_2O_5 , it paves the path for realising more complex optical devices in a compact way on a single platform. The work

presented in this thesis takes tantalum pentoxide one step closer towards realising low power, compact PLC.

7.2 Suggestions and future endeavours

This thesis presented the fabrication and characterisation of Er:Ta_2O_5 waveguides for achieving low waveguide loss and net optical gain. There exists further room for improvement in the fabrication and design aspect to further improve the results. Some of them are listed below

- **Alternative deposition technique:** Sputtering can deposit thin films low temperatures, multiple targets (different materials) can be used simultaneously and is relatively cheap process. But sputtered tantala films were rough (with pinholes in the film), low yield (one sample/run), and had low deposition rate ($<$ 2 nm/min) with non-uniform thickness ($\sim$5-10 %) and refractive index ($\sim$0.9-1.0$\times10^{-3}$). In this context, films grown by using PECVD provides uniform, conformal and adherent layer of thin films. PECVD has been reported [8] to give higher deposition rate ($\sim$40-50 nm/min or higher), excellent control over thickness ($\sim$1%) and refractive index ($\sim5\times10^{-4}$) uniformity and repeatability. It is a batch process that would also increase the yield and reduce the cost/wafer. It has been shown the tantala thin film grown by CVD are superior to sputtered films [9] and it has also been used for other material [8, 10] in the past with great success. CVD is the standard method for silicon based microelectronic devices as well and from a future perspective, CVD deposition perhaps would also help in monolithic integration of microelectronics with tantala based optical interconnects and PLCs while maintaining the thermal budget of the electronics and the overall quality and cost of the device. For the same reasons, CVD could also be used for depositing the cladding with superior quality on top of the waveguide.

- **Alternative etching technique:** One of the main reasons for the high propagation loss in the rib waveguides can be attributed to the quality of sidewalls achieved after argon IBM etching process. Argon IBM effectiveness was limited to features $>$ 2 μm and etch depth to $<$ 350 nm as it lead to redeposition of material, non-vertical rough sidewalls leading to higher loss. Reactive ion etching (RIE) uses reactive gases (CHF_3, SF_6 etc.) to combine both physical and chemical etching in the same ion beam resulting in lower surface damage and no redeposition. RIE and its variants such as inductively coupled RIE (ICP-RIE) therefore has been used extensively by many groups [11–13] and found to yield better selectivity and anisotropic etching leading to much smoother vertical sidewalls and lower loss even for narrower waveguides and deeper etch depths.

- **Alternative waveguide design for smaller footprint and better coupling**: Shallow etch (rib) waveguides are better for large dimension SM waveguides but the low lateral confinement means the bend radius remains relatively large. Completely etched (strip) waveguides can lead to HIC in both directions and also very tight bends leading to extremely small footprint ($\sim mm^2$) of devices. It would also lead to much lower threshold for EDWA and lasing. In order to commercialise an integrated waveguide device, the device needs to be mode matched to a standard telecom optical fibre for coupling light in and out of the device to ensure easier packaging and alignment for measurements. In the current work, large mismatch in the mode dimensions of waveguide and optical fibre led to huge coupling loss ($\sim$8-10 dB) and a strip geometry would lead to even higher loss. Inverse taper design with very short taper length and large misalignment tolerance [14] has been used for low coupling and back-reflection loss. A combination of shallow etch (used in this thesis) and deep etch also has been shown to be very effective in reducing the loss and cross-talk in the silicon based HIC photonic wires [15] that can be extended to tantala waveguides as well.

- **Ion implantation of rare-earths:** The gain obtained in Er:Ta_2O_5 was limited by the upconversion and higher gain could be achieved by reducing the upconversion coefficient. Sputtering is known to produce non-homogeneous distribution of erbium ions in the material leading to regions of high and low erbium concentration leading to higher upconversion value [6]. Ion implantation is known to produce homogeneous distribution of erbium ions and it also provides with an accurate knowledge of the depth and concentration of ions. This would help in better pump utilisation, lower upconversion and therefore higher signal gain in the material system.

- **Using Yb as sensitizer:** It has been shown many times in the past, both theoretically and experimentally [16] that use of Yb increases the gain of the amplifier and laser significantly due to much better pump absorption, and ability to dope higher erbium concentration without PIQ [17]. The moderate phonon energy of tantala [18] would be helpful in the reducing back-transfer of energy from Er to Yb.. There is a tremendous potential and opportunity to improve upon the results of Er:Ta_2O_5 waveguide amplifier and laser.

- **Co-doping alumina and phosphorus:** Both alumina [19] and phosphorus [20] are considered as modifiers as they help in reducing the clustering of erbium ions and help in achieving higher erbium concentration than otherwise. Extended X-ray absorption fine structure (EXAFS) [19] of Er:Ta_2O_5 with and without modifiers would reveal both qualitative and quantitative information about the clustering of erbium ions in tantala and help in reducing the upconversion in the material to low values.

- **Nonlinear effects:** There is growing demand for compact, low power high speed switching devices that could be used as on-chip WDM or add-drop filters in a PLC. This requires material like Ta_2O_5, with large nonlinear refractive index and high thermal, and mechanical stability. The large nonlinear refractive index of Ta_2O_5 [21, 22] in conjunction with the lasing demonstrated in this thesis can be used for the applications such as mode-locking and Q-switching for producing high energy ultra-short pulses. The high nonlinear refractive index in tantala can be utilised in realising on-chip super continuum generation [23] and low power fast optical switches for the telecommunications spectral window.

Bibliography

[1] S. J. Madden and K. T. Vu. *Tellurium dioxide Erbium doped planar rib waveguide amplifiers with net gain and 2.8dB/cm internal gain. Opt Exp*, **18**:19192, 2010.

[2] J. D. B. Bradley, L. Agazzi, D. Geskus, F. Ay, K. Worhoff, and M. Pollnau. *Gain bandwidth of 80 nm and 2 dB/cm peak gain in Al_2O_3:Er^{3+} optical amplifiers on silicon. J Opt Soc Am B*, **27**:187, 2010.

[3] C. C. Baker, J. Heikenfeld, Z. Yu, and A. J. Steckl. *Optical amplification and electroluminescence at 1.54 μm in Er-doped zinc silicate germanate on silicon. Appl Phys Lett*, **84**:1462, 2004.

[4] R. Schermer, W. Berglund, C. Ford, R. Ramberg, and A. Gopinath. *Optical amplification at 1534 nm in erbium-doped zirconia waveguides. J Quant Electron*, **39**: 154, 2003.

[5] Y. D. Hu, S. B. Jiang, G. Sorbello, T. Luo, Y. Ding, B. C. Hwang, J. H. Kim, H. J. Seo, and N. Peyghambarian. *Numerical analyses of the population dynamics and determination of the upconversion coefficients in a new high erbium-doped tellurite glass. J Opt Soc Am B*, **18**:1928, 2001.

[6] P. G. Kik and A. Polman. *Cooperative upconversion as the gain-limiting factor in Er doped miniature Al_2O_3 optical waveguide amplifiers. J Appl Phys*, **93**:5008, 2003.

[7] E. Snoeks, G. N. Vandenhoven, A. Polman, B. Hendriksen, M. B. J. Diemeer, and F. Priolo. *Cooperative up-Conversion in Erbium-Implanted Soda-Lime Silicate Glass Optical Wave-Guides. J Opt Soc Am B*, **12**:1468, 1995.

[8] K. Worhoff, L. T. H. Hilderink, A. Driessen, and P. V. Lambeck. *Silicon oxynitride - A versatile material for integrated optics applications. J Electrochem Soc*, **149**: F85, 2002.

[9] C. Chaneliere, J. L. Autran, R. A. B. Devine, and B. Balland. *Tantalum pentoxide (Ta_2O_5) thin films for advanced dielectric applications. Mat Sci Eng R*, **22**:269, 1998.

[10] G. L. Bona, R. Germann, and B. J. Offrein. *SiON high-refractive-index waveguide and planar lightwave circuits. IBM J Res and Dev*, **47**:239, 2003.

[11] B. Unal, M. C. Netti, M. A. Hassan, P. J. Ayliffe, M. D. B. Charlton, F. Lahoz, N. M. B. Perney, D. P. Shepherd, C. Y. Tai, J. S. Wilkinson, and G. J. Parker. *Neodymium-doped tantalum pentoxide waveguide lasers. J Quant Electron*, **41**:1565, 2005.

[12] J. D. B. Bradley, F. Ay, K. Worhoff, and M. Pollnau. *Fabrication of low-loss channel waveguides in Al_2O_3 and Y_2O_3 layers by inductively coupled plasma reactive ion etching. Appl Phys B-Lasers O*, **89**:311, 2007.

[13] K. P. Lee, K. B. Jung, R. K. Singh, S. J. Pearton, C. Hobbs, and P. Tobin. *Comparison of plasma chemistries for dry etching of Ta_2O_5. J Vac Sci Technol A*, **18**: 1169, 2000.

[14] V. R. Almeida, R. R. Panepucci, and M. Lipson. *Nanotaper for compact mode conversion. Opt Lett*, **28**:1302, 2003.

[15] W. Bogaerts, P. Dumon, D. Van Thourhout, and R. Baets. *Low-loss, low-cross-talk crossings for silicon-on-insulator nanophotonic waveguides. Opt Lett*, **32**:2801, 2007.

[16] C. Strohhofer and A. Polman. *Relationship between gain and Yb^{3+} concentration in Er^{3+}-Yb^{3+} doped waveguide amplifiers. J Appl Phys*, **90**:4314, 2001.

[17] M. Federighi and F. Dipasquale. *The Effect of Pair-Induced Energy-Transfer on the Performance of Silica Wave-Guide Amplifiers with High Er^{3+}/Yb^{3+} Concentrations. Photon Tech Lett*, **7**:303, 1995.

[18] P. S. Dobal, R. S. Katiyar, Y. Jiang, R. Guo, and A. S. Bhalla. *Raman scattering study of a phase transition in tantalum pentoxide. J Raman Spectrosc*, **31**:1061, 2000.

[19] F. Rocca, M. Ferrari, A. Kuzmin, N. Daldosso, C. Duverger, and F. Monti. *EXAFS studies of the local structure of Er^{3+} ions in silica xerogels co-doped with aluminium. J Non-Cryst Solids*, **293**:112, 2001.

[20] K. Hattori, T. Kitagawa, M. Oguma, H. Okazaki, and Y. Ohmori. *Optical amplification in Er^{3+}-doped P_2O_5-SiO_2 planar waveguides. J Appl Phys*, **80**:5301, 1996.

[21] C. Y. Tai, J. S. Wilkinson, N. M. B. Perney, M. C. Netti, F. Cattaneo, C. E. Finlayson, and J. J. Baumberg. *Determination of nonlinear refractive index in a Ta_2O_5 rib waveguide using self-phase modulation. Opt Exp*, **12**:5110, 2004.

[22] R. Y. Chen, M. D. B. Charlton, and P. G. Lagoudakis. *Chi 3 dispersion in planar tantalum pentoxide waveguides in the telecommunications window. Opt Lett*, **34**: 1135, 2009.

[23] R. Y. Chen, M. D. B. Charlton, and P. G. lagoudakis. *Experimental demonstration of on-chip optical parametric oscillation in planar tantalum pentoxide waveguides. P Soc Photo-Opt Inst*, **7781**:778108, 2010.

List of Publications

Journals

1. **A.Z. Subramanian**, C.J. Oton, R. Greef and J.S. Wilkinson, "Waveguiding and photoluminescence in Er^{3+} doped Ta_2O_5 planar waveguides," J Lumin., **129**, 812 (2009).

2. B.S. Ahluwalia, **A.Z. Subramanian**, O.G. Hellesø, N.M.B. Perney, N.P. Sessions, and J.S. Wilkinson, "Fabrication of submicrometer high refractive index tantalum pentoxide waveguides for optical propulsion of microparticles," Photon Technol Lett., **21**, 1408 (2009).

3. **A.Z. Subramanian**, C.J. Oton, D.P. Shepherd, and J.S. Wilkinson, "Erbium doped tantalum pentoxide waveguide laser," Photon Technol Lett., **22**, 1571 (2010).

4. **A.Z. Subramanian**, G.S. Murugan, M.N. Zervas, and J.S. Wilkinson, "High index contrast Er:Ta_2O_5 waveguide amplifier on silicon," Opt Commun., Submitted (2010).

5. J.J. Carvajal, W. Bolanos, X. Mateos, S.M. Ganapathy, **A.Z. Subramanian**, J.S. Wilkinson, E. Cantelar, D. Jaque, G. Lifante, M. Aquila, and F. Diaz, "Mirrorless buried waveguide laser in monoclinic double tungstates fabricated by a novel combination of ion milling and liquid phase epitaxy," Opt Exp, **18**, 26937 (2010).

6. K.S. Kaur, **A.Z. Subramanian**, D.P. Banks, C.L. Sones, S. Mailis, and R.W. Eason, "Waveguide mode filters fabricated using laser-induced forward transfer," Opt. Exp., Submitted (2011)

Under preparation

1. **A.Z. Subramanian,** C.J. Oton, G.S. Murugan, and J.S. Wilkinson, "Fabrication and numerical modelling of Er:Ta_2O_5 waveguide amplifier and laser," Optics Express.

International Conferences

1. **A.Z. Subramanian**, C.J. Oton, R. Greef and J.S. Wilkinson, "Er:Ta_2O_5 waveguide optimization & spectroscopy," ECIO, Eindhoven (2008).

2. B.S. Ahluwalia, O.G. Hellesø, **A.Z. Subramanian**, and J.S. Wilkinson, "High index contrast waveguides for micro-particle guidance," Photonics, New Delhi (2008).

3. **A.Z. Subramanian**, S. Pissadakis, C.J. Oton, and J.S. Wilkinson, "Sub-micron period relief grating structures inscribed on erbium doped Ta_2O_5 waveguides using 213 nm, 150 ps laser radiation," CLEO-EU, Munich (2009).

4. B.S. Ahluwalia, O.G. Hellesø, **A.Z. Subramanian**, N.M.B. Perney, N.P. Sessions, and J.S. Wilkinson, "Fabrication and optimisation of tantalum pentoxide waveguides for optical micropropulsion," Photonics West, San Francisco (2010).

5. B.S. Ahluwalia, O.G. Hellesø, **A.Z. Subramanian**, J.S. Wilkinson, J. Chen, and X. Chen, "Integrated platform based on high refractive index contrast waveguide for optical guiding and sorting," Photonics West, San Francisco (2010).

6. W. Bolanos, J.J. Carvajal, X. Mateos, M. Aquila, F. Diaz, G.S. Murugan, H.C. Hunt, **A.Z. Subramanian**, and J.S. Wilkinson, "Er- doped $KY_{1-x-y}Gd_xLu_y(WO_4)_2$ surface channel waveguides," ECIO, Cambridge (2010).

7. K. Kaur, **A.Z. Subramanian**, D.P Banks, M. Feinaeugle, C.Y.J. Ying, C.L. Sones, S. Mailis, R.W. Eason, "Waveguide Mode Filter Fabricated Using Laser-Induced Forward Transfer," CLEO-US, Baltimore (2011).

Research Proposals

1. *Young Guest and Doctoral Researcher's Annual Scholarships for Investigation and Learning* (YGGDRASIL) *International Scholarship* 2009-10 (ref 195598/V11) submitted to Norwegian Research Council on "**High-Index Contrast Tantalum Pentoxide Waveguides for Optical Propulsion**"